Aalto-yliopisto
Aalto-universitetet
Aalto University

Master's Programme in Advanced Energy Solutions

Techno-Economic Analysis of Battery Energy Storage Systems in Wind Power Plants and Reserve Markets

---

Juho Laine-Ylijoki

Master's thesis
2024

Aalto-yliopisto
Aalto-universitetet
Aalto University

Author Juho Laine-Ylijoki

Title of thesis Techno-Economic Analysis of Battery Energy Storage Systems in Wind Power Plants and Reserve Markets

Programme Advanced Energy Solutions

Major Energy Systems and Markets

Thesis supervisor Assistant Prof. Mahdi Pourakbari Kasmaei

Thesis advisor(s) M.Sc. Risto Ant-Wuorinen

Collaborative partner Eolus Finland Oy

Date 18.07.2024 **Number of pages** 140 + 2 **Language** English

Abstract

The increased share of renewable energy sources causes issues in the power system, which must be able to balance energy production and consumption at all times. These operational challenges can be addressed by utilizing battery energy storage systems. The recent fluctuations in electricity market prices have, however, made it more difficult for companies to evaluate the profitability of these systems, both in conjunction with existing wind power plants and as standalone systems.

This thesis investigates the operation and annually generated revenues of a lithium-ion battery energy storage system in wind power balance error management and in Finnish electricity reserve markets by formulating two optimization models. First, a Mixed-Integer Linear Programming (MILP) model is formulated to analyze the utilization of a battery energy storage system in wind power balance error management. After that, the utilization of a standalone battery energy storage system in the Finnish reserve markets is researched by formulating a Mixed-Integer Nonlinear Programming (MINLP) model, which is further recast into an equivalent MILP model. Both models are simulated for one year using data from 2023. Finally, profitability analyses based on the simulated annual revenues are conducted using the two models to examine the long-term profitability outlook of the investments.

Based on the research, the utilization of a battery energy storage system decreases the wind power balance error. However, the low revenues combined with high investment costs do not support the battery energy storage system investment solely for wind power balance error management, with a payback period of over 20 years. The research also shows that the operation of a standalone battery energy storage system in the Finnish reserve markets is profitable, with a net present value of 8.6 million euros and a payback period of under five years.

Keywords BESS, battery, battery energy storage, battery operation, battery profitability, wind power plant, reserve markets, imbalance management

Aalto-yliopisto
Aalto-universitetet
Aalto University

Tekijä Juho Laine-Ylijoki

Työn nimi Teknis-taloudellinen analyysi akkusähkövarastojärjestelmien hyödyntämisestä tuulivoimassa ja sähkön reservimarkkinoilla

Koulutusohjelma Advanced Energy Solutions

Pääaine Energy Systems and Markets

Vastuuopettaja/valvoja Assistant Prof. Mahdi Pourakbari Kasmaei

Työn ohjaaja(t) DI Risto Ant-Wuorinen

Yhteistyötaho Eolus Finland Oy

Päivämäärä 18.07.2024 **Sivumäärä** 140 + 2 **Kieli** Englanti

Tiivistelmä

Uusiutuvien energialähteiden määrän kasvu aiheuttaa ongelmia sähköjärjestelmässä, jonka on tasapainotettava energiantuotantoa ja -kulutusta jatkuvasti. Nämä toiminnalliset haasteet voidaan ratkaista hyödyntämällä akkuvarastoja. Viimeaikaiset sähkönhinnan vaihtelut ovat kuitenkin vaikeuttaneet näiden järjestelmien kannattavuuden arviointia, sekä osana olemassa olevia tuulivoimaloita että itsenäisinä järjestelminä.

Tässä diplomityössä on tutkittu litiumioniakkuvaraston toimintaa ja sen mahdollisia vuosituottoja tuulivoiman tasehallinnassa sekä Suomen sähkön reservimarkkinoilla. Tutkimus on toteutettu muodostamalla kaksi erillistä optimointimallia. Akkuvaraston toimintaa tuulivoiman tasehallinnassa on tutkittu ensin muotoilemalla Mixed-Integer Linear Programming (MILP) -malli. Tämän jälkeen akkuvaraston toimintaa Suomen reservimarkkinoilla on tutkittu muotoilemalla Mixed-Integer Nonlinear Programming (MINLP) -malli, josta on muotoiltu vastaava MILP-malli. Molempia malleja on simuloitu yhden vuoden ajan käyttämällä vuoden 2023 tietoja. Lopuksi simuloinneista saatuja vuosittaisia tuottoja on hyödynnetty kannattavuusanalyysien tekemisessä investointien pitkän aikavälin kannattavuuden tutkimiseksi.

Tutkimuksen perusteella akkuvarasto pystyy vähentämään tuulivoiman tasevirhettä. Kuitenkin alhaiset vuosittain tuotetut tulot yhdistettynä korkeisiin investointikustannuksiin eivät tue pelkästään tuulivoiman tasehallintaan tarkoitetun akkuinvestoinnin kannattavuutta, sillä investoinnin takaisinmaksuaika on yli 20 vuotta. Tutkimus osoittaa myös, että erillisen akkuvaraston toiminta Suomen reservimarkkinoilla on kannattavaa, investoinnin nettonykyarvon ollessa 8.6 miljoonaa euroa ja takaisinmaksuajan ollessa alle viisi vuotta.

Avainsanat BESS, akku, akkuvarasto, akun toiminta, akun kannattavuus, tuulivoimala, reservimarkkinat, tasehallinta

Table of Contents

Preface and acknowledgements

This thesis concludes my four-year long journey at Aalto University, which has undoubtedly provided me with the best years of my life thus far.

First of all, I want to thank my supervisor Assistant Professor Mahdi Pourakbari Kasmaei for his invaluable support in formulating the models used in this thesis. Without his encouragement this thesis would not have turned out the way it did. I also want to thank my advisor Risto Ant-Wuorinen for his guidance throughout this journey. A big thank you also goes to Eolus Finland Oy, which has provided me with the opportunity to do a master's thesis on a subject which interests me greatly.

I also want to extend special thanks to all my friends who have supported me throughout these years and made these years very special to me.

Finally, I want to thank my parents for supporting me for all my life as well as Elma and Antti for always having my back no matter the situation. Last but certainly not least, I would like to thank my dear wife Julia for her constant support over the years.

Helsinki, 18 July 2024
Juho Laine-Ylijoki

Symbols and abbreviations

Symbols

$P_{W,T}$	Theoretical maximum wind power production
ρ	Air density
A	Area swept by a wind turbine rotor
V	Wind speed
P_{turb}	Output power of a wind turbine
C_p	Power coefficient of a wind turbine
P_{cap}	Electricity price in a price area with no available transmission capacity
P_H, P_L	Electricity price in a price area with full trading capacity
$\gamma^{idling}\ (SOC_{j_3,k_3})$	Capacity degradation rate from idling
$\gamma^{cycling}\ (DOD_{j_3,k_3,n_3})$	Capacity degradation rate from cycling
SOC_{j_3,k_3}	Average daily state of charge
DOD_{j_3,k_3,n_3}	Depth of an arbitrary discharge cycle
${A_{j_3}}^{idle}, {B_{j_3}}^{idle}, {C_{j_3}}^{idle}$	Fitting parameters for capacity degradation rate from idling
${A_{j_3}}^{cycle}, {B_{j_3}}^{cycle}$	Fitting parameters for capacity degradation rate from cycling
j_3	Set of energy storage technologies
k_3	Set of transmission grid nodes
n_3	Set of charge/discharge cycles
C_{f_cyc}	Capacity fade from cycling degradation
C_{f_cal}	Capacity fade from calendar degradation
SOC_{av}	Average state of charge during a cycle
SOC_l	Battery storage state of charge level
cd	Depth of a charge or discharge cycle
nc	Number of cycles for a given cycle depth
t_s	Storage time (months)
$Q_{loss,cyc}$	Cycling performance loss
Ah	Current throughput of the battery
$\gamma_1, \gamma_1, \gamma_1$	Constant fitting parameters
c^{deg}	Degradation cost coefficient
$c^{battery}$	Battery replacement cost coefficient
E^{let}	Lifetime energy throughput
N^c	Total number of cycles
E^s	Battery energy capacity (MWh)
DOD^{avg}	Average depth of discharge

P_t^{charge}	Battery charging power at hour t
$P_t^{discharge}$	Battery discharging power at hour t
t	Index for an hour
J, T	Time period (hours)
r	Discount rate
n	Lifetime of an investment
t_1	Operation year
FCF	Free cash flow
$f(x)$	Arbitrary function
$g_i(x)$	All inequality constraints
$h_j(x)$	All equality constraints
i	Index of inequality constraints
m	Number of equality constraints
j	Index of equality constraints
j_1	Set of all less-than-or-equal-to constraints
j_2	All equality constraints
L	Number of equality constraints
r^U, u	Explicit upper bounds for arbitrary variables
$r^L, -l$	Explicit lower bounds for arbitrary variables
$c_0, c_k, A^e_{j,k}, A^g_{j_1,k}, A^l_{j_2,k}$, $b^e_j, b^g_{j_1}\ b^l_{j_2}$	Constants
n_1	Set of variables
r, r_k	Arbitrary decision variable
k	Index of variables
m_e	Number of equal-to constraints
m_g	Number of greater-than-or-equal-to constraints
m_l	Number of less-than-or-equal-to constraints
$\mathbb{Z}$	Set of all integers
$\mathbb{R}$	Set of all real numbers
d	Arbitrary real variable
$y, y_1, y_2, w, C, \delta 1_t,$ $\delta 2_t, v1_t, v2_t, u1_t, u2_t,$ $u3_t, z_t, x_t, r1_t, r2_t$	Binary variables
q, D	Product of a real and a binary variable
s	Variable, which acts as a slack variable
B	Continuous and bounded variable
$\bar{B}$	Upper bound for variable B
$\underline{B}$	Lower bound for variable B
$a_{1,k}, a_{2,k}, b_1, b_2$	Parameters
$M1, M2, M3, M4$	Large constants
λ_t^{DA}	Day-ahead market price at hour t

λ^{output}	Transmission fee from the main grid
λ^{input}	Transmission fee to the main grid
P_t^F	Forecasted wind power production at hour *t*
P_t^W	Realized wind power production at hour *t*
λ_t^-	Upregulation price in the balancing market at hour *t*
λ_t^+	Downregulation price in the balancing market at hour *t*
$P_t^{up,r}$	Remaining underproduction from a wind power plant at hour *t*
$P_t^{op,r}$	Remaining overproduction from a wind power plant at hour *t*
λ^{BA}	Imbalance fee
OM^s	Operation and maintenance cost coefficient
η^c	Battery charging efficiency
η^d	Battery discharging efficiency
P_t^{ch}	Transferred energy from a wind power plant to a battery at hour *t*
P_t^{dch}	Discharged energy from the battery to the grid at hour *t*
SOC_t	Battery state of charge level during hour *t*
SOC_0	Battery state of charge level in the beginning of a simulation
SOC^{min}	Battery minimum state of charge level
SOC^{max}	Battery maximum state of charge level
P^{bess}	Battery power capacity (MW)
Δf	Frequency deviation from the nominal system frequency
f_n	Nominal system frequency (50 Hz)
f_{i_1}	Frequency measurement of a three-minute interval i_1
i_1	Index of three-minute intervals
P_t^{reg}	Required FCR-N up- or downregulation power at hour *t*
P_t^{FCR}	Bid capacity to the FCR-N market at hour *t*
Δf_t^{avg}	Average frequency deviation at hour *t*
$R_t^{FCR,CU}$	Capacity fees paid to the FCR-N reserve provider at hour *t* for upregulation power
$R_t^{FCR,CD}$	Capacity fees paid to the FCR-N reserve provider at hour *t* for downregulation power
$R_t^{FCR,E}$	Energy fees for the transmitted energy between the main grid and the battery at hour *t*

S_t^{FCR}	Sanction paid by the reserve provider at hour t for operating in the FCR-N market with a too high or low state of charge level
P_t^{down}	Provided FCR-N downregulation power from the battery at hour t
P_t^{up}	Provided FCR-N upregulation power from the battery at hour t
P^{FFR}	Bid capacity to the FFR market
λ_t^{FFR}	Price of procured FFR at hour t
P_FCRU	Maximum FCR-N bid capacity
$SOC^{bid,min}$	Desired minimum bidding state of charge level
$SOC^{bid,max}$	Desired maximum bidding state of charge level
λ_t^{FCR}	FCR-N market price at hour t

Operators

Σ_i	sum over index i

Abbreviations

AC	Alternating Current
AEM	Alert State Energy Management
aFRR	Automatic Frequency Restoration Reserve
BESS	Battery Energy Storage System
BMS	Battery Management System
BRP	Balance Responsible Party
BSP	Balancing Service Providers
B-TMS	Battery Thermal Management System
CAPEX	Investment Costs
CET	Central European Time
DA	Day-ahead
DC	Direct Current
DOD	Depth of Discharge
EET	Eastern European Time
EMS	Energy Management System
EoL	End of Life
FCR-D	Frequency Containment Reserve for Disturbances
FCR-N	Frequency Containment Reserve for Normal Operation
FFR	Fast Frequency Reserve
HVDC	High Voltage Direct Current
ID	Intraday

ILP	Integer Linear Programming
IRR	Internal Rate of Return
LER	Limited Energy Reservoir
LFP	Lithium Iron Phosphate
LIB	Lithium-ion Battery
LMO	Lithium Manganese Oxide
LP	Linear Programming
LTO	Lithium Titanate
mFRR	Manual Frequency Restoration Reserve
M	Million
MILP	Mixed Integer Linear Programming
MINLP	Mixed-Integer Nonlinear Linear Programming
MPPT	Maximum Power Point Tracking
NCA	Lithium Nickel Cobalt Aluminium
NEM	Normal State Energy Management
NLP	Nonlinear Programming
NMC	Lithium Nickel Manganese Cobalt Oxide
NPV	Net Present Value
OPEX	Operation and Maintenance Costs
OTC	Over-The-Counter
POC	Point of Connection
QP	Quadratic Programming
RES	Renewable Energy Sources
RV	Residual Value
SCADA	Supervisory Control and Data Acquisition
SEI	Solid Electrolyte Interphase
SOC	State of Charge
SOH	State of Health
S-TMS	System Thermal Management System
TSO	Transmission System Operator
YoY	Year-on-Year
VRE	Variable Renewable Energy
WFO	Wind Farm Operator

1 Introduction

Reducing emissions from energy production by integrating more Renewable Energy Sources (RES) is one of the most essential ways to mitigate climate change and achieve carbon neutrality by 2050. In 2022 RES accounted for 30 % of the world's total electricity production (IEA 2023a, p. 126). A significant share of the overall renewable energy is produced by wind power. In 2022, a total of 77.6 GW of new wind power capacity was added globally, bringing the total installed capacity to 906 GW (Global Wind Energy Council 2023, p. 8). Majority of the new wind power capacity was onshore wind power, with a Year-on-Year (YoY) growth of 8.8 % (Global Wind Energy Council 2023, p. 92-93). Although, the wind power capacity has grown rapidly in recent years, reaching the carbon emission goals requires even stronger annual growth. Achieving the goal would require increasing the annual capacity additions to about 350 GW in 2030 (IEA 2023b).

However, there are challenges associated with wind power production. The most significant issue is the poor predictability and instability of production, which is caused by the variation of wind speed. This inherent variability of production causes problems in the power system, which must be able to balance energy generation and demand at all times. These problems can be solved using large-scale energy storages, which can store energy when production exceeds demand and release it back into the grid, when demand again exceeds production (Mitali et al. 2022). One of the most promising energy storage methods is battery energy storage. In Finland, several Battery Energy Storage System (BESS) projects have been initiated and their ability to shift production and consumption to the most profitable hours has raised interest among companies. However, the recent fluctuations in electricity market prices have made it more difficult for companies to predict the possible revenues generated by these systems and evaluate their profitability.

In this thesis the utilization of a BESS in conjunction with a wind farm in Finland is investigated. The aim of the study is to analyze the operation of the BESS and the revenues it could generate in terms of wind power balance error management in the Day-ahead (DA) market and Finnish reserve markets. Also, the optimal capacity of the battery is analyzed based on the size of the wind farm. This study formulates two optimization problems to assess the operation and potential revenue streams of battery energy storages in these markets. First a Mixed-Integer Linear Programming (MILP) model is created to research the utilization of a BESS in wind power balance error management. After that a separate Mixed-Integer Nonlinear Programming (MINLP) model, which is further recast into an equivalent MILP model, is formulated to analyze the utilization of a standalone BESS in the Finnish reserve markets. To narrow down the research topic, in terms of the Finnish reserve

markets, only the operation and the cash flows generated by a battery in the Frequency Containment Reserve for Normal Operation (FCR-N) and Fast Frequency Reserve (FFR) markets are analyzed, as they are considered particularly suitable marketplaces for BESSs. This study primarily investigates the operation of battery energy storages and their associated annual cash flows in the different scenarios, while considering battery degradation and Operation and Maintenance Costs (OPEX) and other network related fees. Additionally, this study evaluates the financial viability of BESS investments. The study focuses on the economic viability and operation strategy of a lithium-ion battery energy storage without a further investigation of other battery technologies.

This thesis begins with a literature review, where existing studies analyzing BESS profitability and capacity optimization in different situations are reviewed. After this, the operating principle of wind power and its current state in Finland are examined, as well as the problems associated with its production. In Section 4, a broader inspection of the electricity markets in Finland is conducted. This includes the DA and Intraday (ID) markets operated by Nord Pool and the Finnish reserve markets operated by Fingrid. In Section 5, BESSs are researched in further detail. The study focuses on different lithium-ion battery technologies, their structure and characteristics. Also, the degradation of lithium-ion batteries and the overall BESS components are studied. The section is concluded with a life cycle cost analysis of BESSs, focusing on Investment Costs (CAPEX) and OPEX.

In Section 6, three different investment calculation methods are introduced, including the Net Present Value (NPV), the Internal Rate of Return (IRR) and the payback period methods. Section 7 gives an overview of optimization problem modelling and solving, including a deeper look into MILP models and how to formulate and solve them. Section 8 investigates the utilization of a BESS to balance wind power forecast errors and decrease the wind power related imbalance costs. In Section **Error! Reference source not found.**, t he operation and profitability of a standalone BESS in the Finnish FCR-N and FFR markets is researched. Lastly, the final conclusions of this thesis are given in Section 10.

2 Literature review

The utilization of BESSs has been recently studied extensively in literature. This literature review will approach the topics of BESS profitability and capacity optimization from different perspectives. First, several studies which utilize a BESS to increase the profitability of wind and solar power plants are reviewed. Existing research on BESS capacity optimization in different situations is then analyzed. Then, the existing literature on utilization of standalone BESS in energy, ancillary and reserve markets is examined. Concluding the literature review, the importance of this study is presented.

Several studies have focused on the aspect of utilizing a BESS to increase the profitability of Variable Renewable Energy (VRE) power production such as wind and solar power production from the asset owners' point of view. Some of the studies consider only the use of BESSs in energy markets while some also consider the additional participation in ancillary markets. Kordkheili et al. (2021) proposed a joint operation-planning model, which utilises a BESS and a gas storage to optimize the Wind Farm Operator's (WFO's) bids in both the DA electricity market and the gas market. The purpose of the study was to enhance wind power production flexibility by decreasing over- and under-production. A similar study was conducted by Moghaddam et al. (2018), where a BESS control scheme was proposed to manage the net energy exchange between the electricity market and a wind farm to increase daily profits. In the study short-term wind and price forecasts were used to obtain the best times to discharge or charge batteries or purchase electricity from the DA market. He et al. (2016) in turn proposed a co-operation scheme between a wind farm and a BESS to find an optimal bidding strategy for joint energy and regulation markets. The study focused on optimizing, for example, battery cost, lifetime and availability of wind turbines and minimizing the curtailed wind power. Li et al. (2023a) used a novel deep reinforcement learning-based approach to maximize operational revenues for a joint-market bidding strategy of a co-located wind-battery system. The bidding strategy was optimized for spot and ancillary service markets. The study showed that BESS utilization could increase revenues and decrease wind power curtailment significantly. Khojasteh et al. (2021) also presented a model for optimal joint energy and reserve market bidding for a BESS and wind power resource based on market prices, ramp rates, marginal costs and other technical constraints. Naemi et al. (2022) examined the optimal performance of a wind farm integrated with a BESS in a wholesale electricity market. The NPV of the wind farm was maximized by participating in both the energy and frequency control ancillary services, while different market conditions and technical constraints were considered. Graça Gomes et al. (2023) investigated the use of a BESS to schedule the DA operation of a renewable energy power plant consisting of a wind farm and a solar power plant in two liberalised

power markets. The study considered the Italian and Iberian power markets and concluded that coupling a BESS with wind power generates higher revenues than coupling with solar power.

Literature survey also suggests that studies have been conducted to determine the optimal size of a BESS in different situations. Dui et al. (2017) presented a two-stage method to determine the optimal power characteristics and capacity for a BESS connected with a wind farm and thermal generators. Paul et al. (2019) presented a novel multi-objective planning framework to determine an optimal capacity for a BESS in connection with a large wind farm. Khajeh et al. (2023) developed a two-stage model to optimize the sizing and siting of their lithium-ion BESS to provide flexibility services for system operators. In the first stage the minimum capacity and location of the storage system is determined based on local network security and in the second stage the profit of the BESS is maximized by providing FCR-N services. Ahlawat & Das (2023) presented a model to optimize the sizing and scheduling of a BESS with distributed generators consisting of wind and solar power plants under seasonal load variations. The optimal sizing and scheduling were determined by minimizing voltage deviation and real power loss in a distribution network. Also, a techno-economic analysis was conducted to determine the energy savings in the system. Yaldiz et al. (2021) investigated the optimal sizing of an integrated solar power and BESS hybrid power plant in the context of peer-to-peer energy trading together with the grid. The optimal sizing of the system for prosumers is obtained through a MILP-based algorithm structure. Fallahifar & Kalantar (2023) proposed a MILP model for optimal lithium-ion battery energy storage capacity for microgrid applications. The model included a comprehensive analysis of the effects of battery degradation and different battery cycles to battery capacity optimization.

There are also studies which investigate the use of a standalone BESS in the energy, ancillary and reserve markets. Mohamed et al. (2023) examined the opportunity for a BESS to participate in multiple energy markets by determining the optimal stack of services to maximize annual revenues. The markets considered included DA and ID markets, frequency regulation, reserve markets and capacity markets. Alizadeh (2017, p. 82-90) developed a bidding model for a BESS for the Nord Pool DA, ID markets and Fingrid's frequency containment reserve markets. In the model the capacity of the storage system was allocated to different markets and the total expected value of the system's profit was maximized. Hameed et al. (2023) investigated the operation strategies for BESS owners in the Nordic ancillary markets from a business viewpoint. In the study the revenue streams and hourly price patterns of different ancillary markets were analyzed to identify the optimal bidding hours in these markets. Also, the different system and market requirements were discussed. Pusceddu et al. (2021) analyzed synergies between fast frequency

response and energy arbitrage for a BESS. The study found that the system could increase its profitability considerably by alternating between the two services. Li et al. (2023b) in turn researched the use of a BESS in grid peak and frequency regulation. In the study a model was produced to find the optimal configuration and control strategy for the storage to provide short-term frequency regulation and long-term peak and valley filling.

Various aspects of BESSs have been studied extensively. However, their operation, profitability and sizing in the context of wind power balance error management and reserve markets in Finland remain underexplored. This thesis aims to fill this existing research gap. Paasolainen (2023, p. 74-101) proposed a model to optimize BESS operation in imbalance management, reserve markets and energy arbitrage in connection with a Finnish hybrid power plant, consisting of wind and solar power. Korhonen (2022, p. 56-65) in turn studied the use of BESS in connection with a solar power plant in Finland. Furthermore, this thesis aims to introduce new modelling for the use of BESSs in frequency regulation and for the simultaneous use of batteries in different reserve markets in Finland.

3 Wind power

In this chapter, wind power as a form of energy production is examined at a general level. First, the operation principle of wind power production is given, after which the use of wind power in Finland and how it has developed over the past decades is described. Later, the chapter focuses on the instability of wind power and its effects on the electricity grid more broadly. Finally, this chapter concludes with an overview of the Nordic balancing model and how it affects individual wind power producers.

3.1 Operating principle of a wind turbine

The operating principle of a wind turbine is based on the lift generated by the airfoil-shaped turbine blades which rotate the turbine's rotor (Allamehzadeh 2016). The kinetic energy of the wind is transformed into rotational kinetic energy of the rotor. The rotational kinetic energy of the rotor drives the gearbox of the turbine through a low-speed shaft, which in turn drives the generator through a high-speed shaft. The gearbox increases the rotational speed (Allamehzadeh 2016). The sizes of wind turbines have grown significantly in recent decades. Currently, the typical hub height of an onshore wind turbine in Finland is 150-175 meters, whereas in 2010 the maximum hub height was 100 meters (Finnish Wind Power Association 2023a). Also, the nominal power of these turbines has increased from 3 MW in 2010 to 6.2 MW in 2022.

The main factors which affect the wind turbine output power are the wind speed and its variability, intensity of turbulence and the air density (Xiaoming et al. 2018). The available wind speed directly dictates the amount of kinetic energy the rotor can capture. The amount of turbulence affects the wind energy absorption through an effect called "hysteresis", which means that the behaviour of the turbine under the external conditions differ over time (Nouriani & Moradi 2020). The energy density also has a significant impact on the wind power output. Xiaoming et al. (2018) point out that an increase in energy density also increases the power output under the same wind speed. Also, the rotor diameter significantly affects the overall output of the wind turbine (Abdelghafar et al. 2023). The bigger the area is swept by the rotor, the more kinetic energy of the wind can be captured.

The theoretical maximum amount of power that can be extracted from the kinetic energy of the wind by the wind turbine is given in (1) (Mathew & Philip 2012).

$$P_{W,T} = \frac{1}{2}\rho A V^3, \tag{1}$$

where $P_{W,T}$ is the theoretical maximum wind power production, ρ is the air density, A is the area swept by the rotor and V is the wind speed. However, the rotor of the turbine can only extract a fraction of this theoretical maximum power (Mathew & Philip 2012). The efficiency at which the rotor can extract power from the wind is known as the power coefficient of the rotor C_P. When considering C_P, the power extracted from wind is given in (2) (Mathew & Philip 2012).

$$P_{turb} = \frac{1}{2}\rho C_P A V^3 \,, \tag{2}$$

Where P_{turb} is the output power of the turbine. In theory a maximum of 59 % of the total kinetic energy of the wind can be utilized by the wind turbine (De Lellis et al. 2018). Different turbines have different power output characteristics which can be modelled with a power curve. The power curve gives the relationship between the wind speed and the turbine's mechanical power (Allamehzadeh 2016). Figure 1 depicts a power curve for a Vestas 7 MW wind turbine.

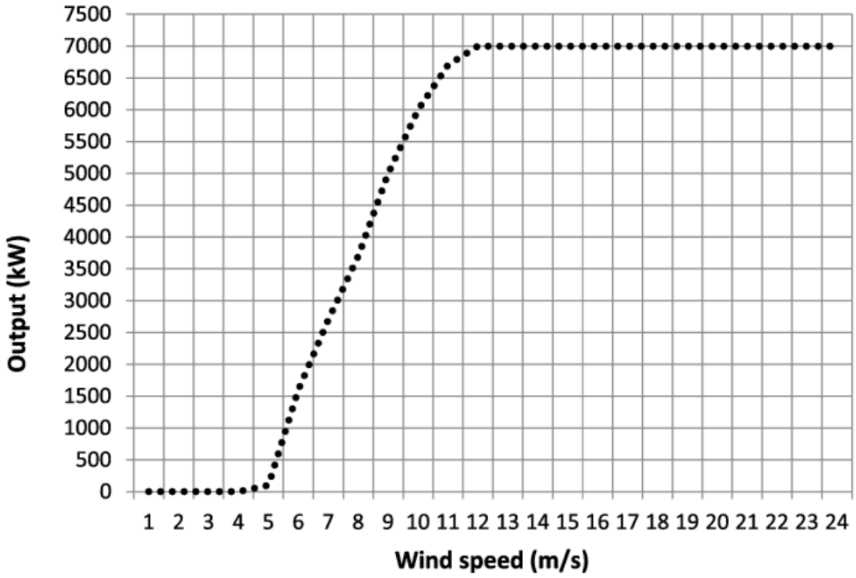

Figure 1: Power curve for Vestas 7 MW wind turbine (Abdelhady et al. 2017).

The power curve is typically characterized by three different sections, which are the cut-in wind speed, cut-out wind speed and the rated wind speed (Allamehzadeh 2016). The cut-in wind speed is the lowest wind speed at which the turbine still operates. The rated wind speed is the wind speed at which the generator produces its rated output power. The cut-out wind speed

indicates the highest wind speed at which the turbine is allowed to operate. If the turbine would be allowed to operate after the cut-out wind speed, excessive damage could occur (Allamehzadeh 2016).

3.2 Wind power production in Finland

The wind power capacity in Finland has increased rapidly during the last decades. At the end of 2010 the wind power capacity in Finland was 197 MW with a total annual energy generation of 294 GWh, which was approximately 0.3 % of the overall Finnish energy consumption during that year (Stenberg & Holttinen 2011, p. 4). Also, 2010 saw the then highest annual increase in wind power capacity in Finland's history, as the capacity increased by 52.3 MW (Finnish Wind Power Association 2023b). By the end of 2022 the wind power capacity had increased to 5 677 MW with an annual energy generation of 11.5 GWh (Finnish Energy 2023, p.15-16). This accounted for 14.1 % of the overall energy consumption in Finland in 2022. The capacity also increased by 76 % compared to the previous year. Figure 2 depicts the annual increase in wind power capacity in Finland from 1997 to 2022.

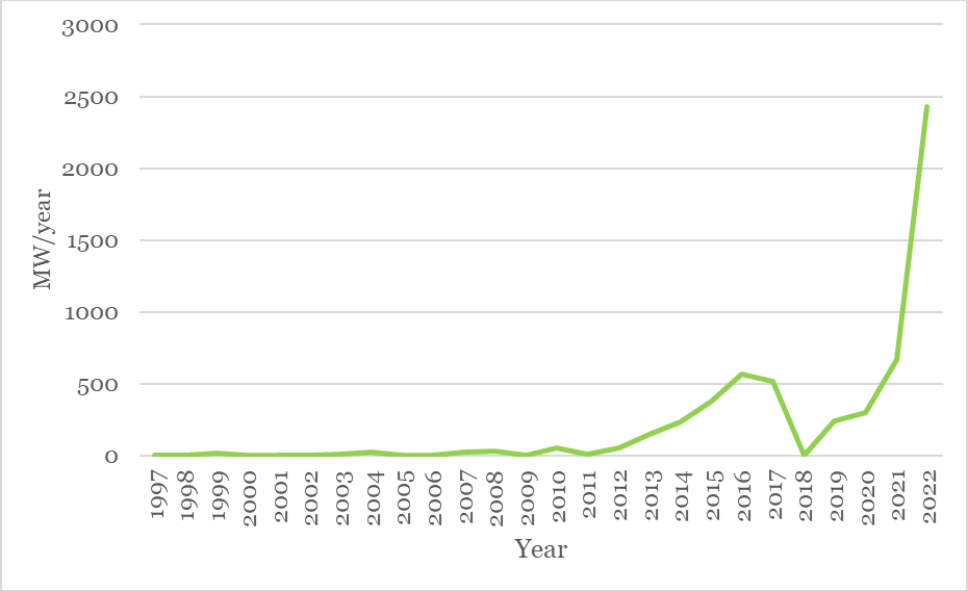

Figure 2: Annual increase in wind power capacity in Finland. Modified from Finnish Wind Power Association (2023b).

As Figure 2 shows, the increase in wind power capacity has been rapid from 2010 onwards. Figure 3 depicts the cumulative increase in wind power generation capacity in Finland from 2010 to 2022.

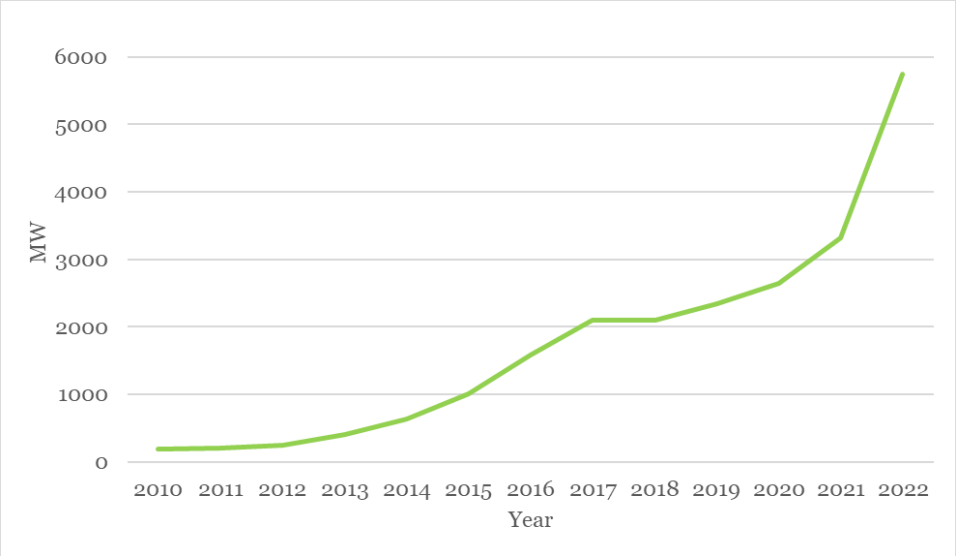

Figure 3: The increase in cumulative wind power capacity. Modified from Finnish Wind Power Association (2023b).

The above figures illustrate the rapid surge in both annual and cumulative wind power capacity. Notably, the most rapid increase in new capacity has occurred over the last three years. This trend is expected to persist as numerous projects are underway, with Finland witnessing a substantial influx of investments in new wind power infrastructure. According to the Finnish Wind Power Association, new wind power projects worth around 120 GW had been announced by May 2023 (Finnish Wind Power Association 2023c). Currently, the overall capacity of announced onshore wind power projects is approximately 63 GW, of which 3 GW are already fully permitted and 3.4 GW are under construction (Finnish Wind Power Association 2023c).

In response to the growing significance of wind power in Finland's energy landscape, Fingrid (2023a, p. 14-23) has outlined four different scenarios for wind power development in Finland:

- Power to Products
- Hydrogen from Wind
- Windy Seas
- Local Power,

which represent different possible trends in electricity consumption, production and storage. These scenarios were prepared for both 2035 and 2045. In all these scenarios the wind power capacity, both onshore and offshore, will significantly increase in the future (Fingrid 2023a, p. 14-23). This is also supported by the fact that by early June of 2023 Fingrid, the Transmission System Operator (TSO) of Finland, had received preliminary connection inquiries for both offshore and onshore wind projects amounting to over 210 GW

(Jyrinsalo 2023, p. 3). Figure 4 illustrates the development of wind power generation capacity in the different scenarios.

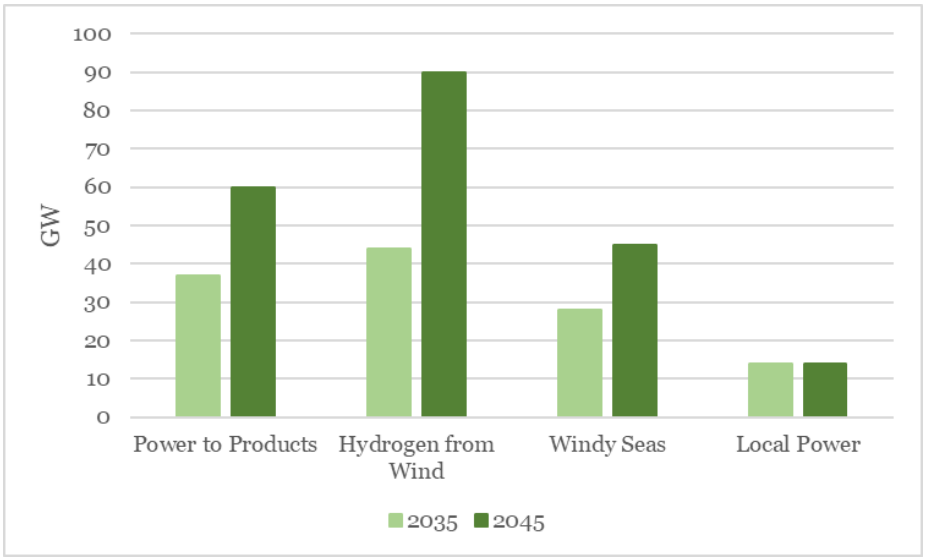

Figure 4: Projected wind power capacity in different scenarios. Modified from Fingrid (2023a, p. 14).

From Figure 4 it can be seen that the most significant increase in wind power capacity is in the Hydrogen from Wind -scenario, where the combined offshore and onshore wind power capacity is 44 GW and 90 GW in 2035 and 2045 respectively. The onshore wind power capacity is expected to reach 39 GW and 79 GW in 2035 and 2045 respectively. In this scenario Finland becomes a significant exporter of green hydrogen which enables a very high share of VRE sources in the electricity system. This scenario also assumes a great increase in electricity consumption and in addition to the cross-border hydrogen pipelines, a significant hydrogen pipeline network is developed within Finland (Fingrid 2023a, p. 18).

The Power to Products -scenario predicts a similar onshore wind power capacity for 2035 of 30 GW, but the overall capacity in this scenario in 2045 reaches 50 GW (Fingrid 2023a, p. 16). This is because the Hydrogen from Wind -scenario expects a greater increase in wind power production in eastern Finland and in southern and central Lapland. The Windy Seas -scenario assumes that the onshore wind power capacity reaches a maximum of 13 GW by 2035 and does not increase after that (Fingrid 2023a, p. 20-21). The scenario also assumes a hydrogen economy in Finland, but in a much smaller scale than in the previous two scenarios. In this scenario offshore wind power production increases rapidly to 32 GW by 2045. The Local Power -scenario assumes the lowest increase in electricity consumption and the highest share of nuclear power in electricity production in Finland (Fingrid 2023a, p. 22-

23). Also, this scenario sees no significant build-up of hydrogen network. This leads to only 13 GW and 1 GW of onshore and offshore wind power production by 2035 and 2045 respectively.

3.3 The effect of wind power on the power grid

The most significant difference between wind power production and the conventional power plants using fossil fuels is the inherent variability of wind power production (Benzohra et al. 2020). The unpredictability of wind conditions and the ensuing power fluctuations can be even more difficult to manage than the typical load variations caused by load forecasting errors. The production can be decreased but it cannot be increased more than the current weather conditions allow. The variability of production affects the power quality of the system through for example voltage, frequency and power fluctuations, all which decrease the system's stability. These challenges are not significant if the wind power penetration levels in overall market are smaller than 10 % of the total load (IEA 2017, p. 14-17). With higher penetration levels, additional regulation and spinning reserve resources are required to ensure control of grid stability.

A high amount of wind turbines can significantly impact voltage magnitudes which occur due to incapability of a power system to meet a growing demand of reactive power (Londero et al. 2014). A single wind turbine can also affect the system's voltage stability through the variability of active power output, which leads to changes in reactive power output and consequently affects the voltage at the Point of Connection (POC) (Sarkar et al. 2017). These voltage instabilities can occur both in the long- and short-term and can lead to loss of load or to voltage collapses (Londero et al. 2014). Short-term voltage stability means maintaining an acceptable level of voltage in a time frame of few seconds after a disturbance. Short-term voltage stability involves fast acting load components such as induction motors, electronically controlled loads and inverter-based generators, like wind turbines (Glavic & Greene 2022). Alzubaidi et al. (2022) simulated the effect of three wind farms in a 39-bus network with varying wind penetration and system load uncertainties. The study showed that the ability of a system to recover from small disturbances weakened considerably with higher wind penetration levels. The study also found that the amount of voltage violations and the range of the uncertainty level of the short-term voltage increased greatly with more wind power. Wind turbines also have a lower tolerance to voltage deviations than the traditional generators (Shair et al. 2021).

Long-term voltage stability is defined as disturbances in voltage levels over a time frame of minutes or hours and they occur due to the actions of load variations and discrete type devices (Londero et al. 2014). The increased

penetration of wind power is seen to enhance the long-term voltage stability. Krismanto et al. (2021) concluded that higher voltage profiles were monitored with increasing amount of wind power and the system's flexibility to maintain static voltage stability increased under higher maximum loading. Under small disturbances and longer voltage changes the presence of wind power improves the voltage stability of the system, but under shorter and larger voltage instabilities it may decrease the overall voltage stability of the system (Elkington 2012).

The increased amount of RES also affects the frequency stability of the power system (Aziz et al. 2018). The energy balance between load and generation is reflected in the system frequency, which decreases with load increment and increases with overgeneration. The frequency of the system is regulated by active power production in power plants. The nominal frequency of the Finnish power system is 50 Hz and the normal operation range is between 49.9 - 50.1 Hz (Fingrid 2024a). If power generation exceeds the demand, the frequency rises above 50 Hz and vice-versa. The imbalance between load and generation is controlled through the inertia generated by the rotation of large power plant turbines, where synchronized generators operate with the same frequency as the system (Aziz et al. 2018).

Frequency control becomes significantly more challenging if the share of wind power increases in the power system (Aziz et al. 2018). In steady-state operation the wind turbines produce only negligible amount of inertia, as they are normally operated by the Maximum Power Point Tracking (MPPT) -method (Lim et al. 2022). MPPT is used to control the rotation speed of the turbine to guarantee a maximum output during wind speed changes (Li & Chengxin 2018). However, when a disturbance in the system occurs, wind turbines operated by MPPT cannot provide any additional power (Lim et al. 2022). A large share of wind power production therefore requires a method for quickly adjusting the amount of generated power. This reserve power is acquired in Finland by Fingrid (Fingrid 2024a). Elovaara & Haarla (2011, p. 41) have estimated that an addition of 2000 MW of new wind power capacity in the power system may require around 500 MW of new reserve capacity. The frequency response of a power system after a large generator trip with high and low system inertia is depicted in Figure 5.

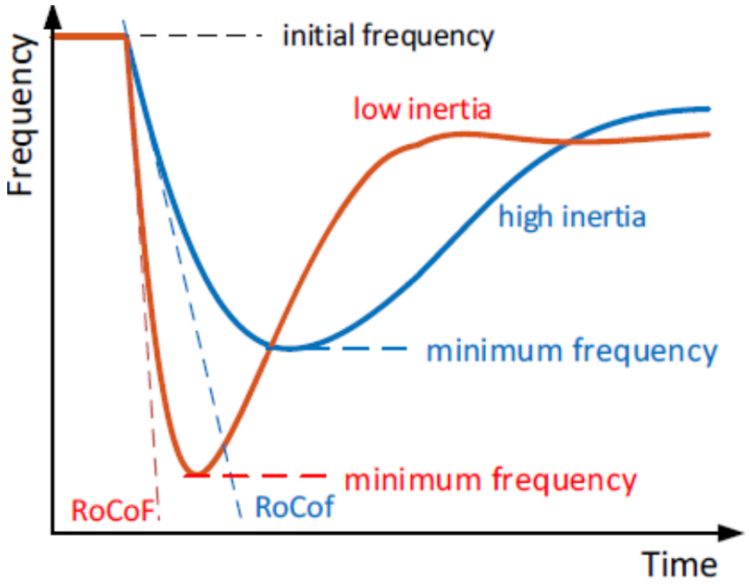

Figure 5: The frequency response after a large generator trip in high and low inertia systems (ENTSO-E 2019, p. 6).

As shown in Figure 5, with higher inertia, the system can resist the frequency decrease more effectively and recover the frequency much smoother compared to lower inertia (ENTSO-E 2019, p. 6). The variability of wind speed, both in terms of time and space, leads to the instability of wind production (Ren et al. 2017). The constant and unpredictable changes in wind speed intensity and direction make it impossible to control (Johnson et al. 2012).

Wind speed fluctuates over short, medium and long time intervals. The variations of wind speeds on a global scale can be attributed to different climate regions, which are influenced by factors such as solar insulation and altitude (Albadi & El-Saadany 2010). Wind speed variations on a regional scale are more influenced by the presence of mountains, plains and water systems. On a local scale the vegetation and local topography are the main driving factors for wind speeds. Long-term, defined as seasonal and annual, variations in wind speeds are challenging to predict. However, these variations do not significantly impact the output of the wind turbine over its overall lifetime, with the maximum standard deviation of mean wind power output over a 20-year period being 10 % (Albadi & El-Saadany 2010). Medium-term variability involves changes in wind speeds over a timeframe of hours to a few days, which are more predictable. These combined with the long-term variations of wind speeds affect the reliability and sufficiency of production when preparing for long-term peak load periods and overall resource planning. The short-term turbulences, over seconds and minutes, are very hard to predict and influence significantly the quality of output power (Albadi & El-Saadany 2010). The relationship between realized wind power generation and generation

forecast during the period between 01.01.2024 and 05.01.2024 is depicted in Figure 6.

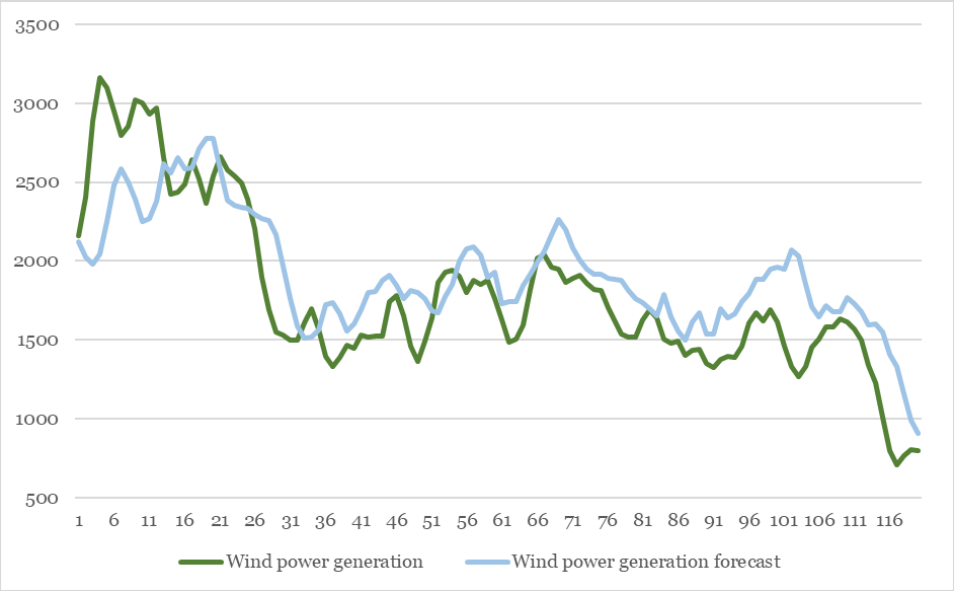

Figure 6: The relationship between the realized wind power generation and the generation forecast between 01.01.2024 and 05.01.2024 (Fingrid 2024b).

For day-ahead timeframe, wind speed forecasts are often produced using numerical weather prediction models, which are often improved with machine learning methods (Hodge et al. 2018). In addition to these prediction models on-site measurement data from Supervisory Control and Data Acquisition (SCADA) systems, neural network and statistical analysis-based approaches are used to predict the wind power production (Tsai et al. 2023). As previously concluded, the medium-term day-ahead variations of wind speeds can be predicted with some accuracy. However, the mean absolute error in wind power production can still increase to nearly 20 % for a single wind turbine, while forecasts with a mean absolute error of 5-7 % can be reached one to two hours ahead (Milligan et al. 2009). Wind power production can also be affected in Finland and in other Northern countries through ice buildup on wind turbine blades. The accumulation of ice over wind turbine blade will alter the blades' aerodynamic properties, which causes a decrease in power production (Davis et al. 2016). A thin ice cover can cause power losses between 15 % and 20 %, whereas a moderate ice cover can result in losses up to 29 % (Turkia et al. 2013).

3.4 Wind power balance error

The operation of a power system is based on the balance between consumption and production at any given moment. Imbalances between these two components arise from uncertainties of future consumption and production and the possible failures of the power grid (eSett 2024, s. 8). To smooth out these imbalances the TSO's use balancing power which is procured through the balancing power market. After the balancing power has been used to smooth out the imbalances, a mechanism called the imbalance settlement is used in the electricity market to restore financial balance after the operating hour (eSett 2024, s. 14). In the Nordic electricity markets the imbalances are calculated based on The Nordic Imbalance Settlement Model, which is operated by eSett Oy, a company which is owned by the four TSO's in the Nordic electricity market. After the imbalances have been calculated, each Balance Responsible Party (BRP) is financially responsible of the imbalances from its' operation (eSett 2024, s. 14). A BRP is a company that has an imbalance settlement agreement with eSett and a balance agreement with a TSO. There are also Balancing Service Providers (BSPs), which have reserve-providing units to provide balancing services to TSOs in return for payment (eSett 2024, s. 11).

The balance service model was revised in 2021, in which the one balance model was introduced (Fingrid 2024c). This unified the previously separated production and consumption balances under one model. Other revisions included the exclusion of production plans from the imbalance settlement and changes in the cost structure relating to balance service. The current balance service model is depicted in Figure 7.

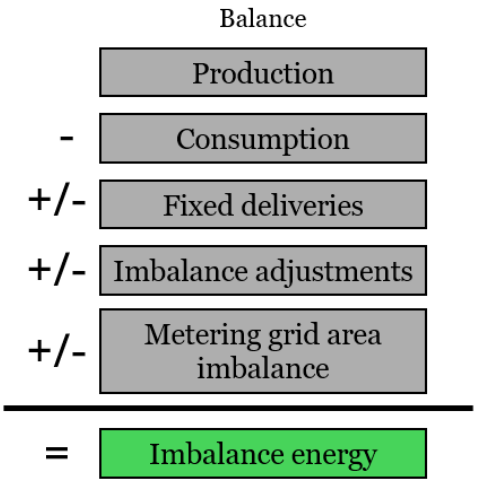

Figure 7: The balance service model used in the Nordic electricity markets. Modified from (Fingrid 2024c).

Figure 7 depicts how the balance service model can have both positive and negative implications for electricity producers. The outcome depends on whether there is positive or negative imbalance, indicating a surplus or deficit of energy in the market (eSett 2024, s. 66). During a negative imbalance period the producers must pay compensation for the energy not delivered, while in a positive imbalance period they are compensated for the overproduction. The positive and negative imbalances carry the same price, but the pricing depends on if the imbalance period was an upregulation or a downregulation period (eSett 2024, s. 66). Upregulation means that the resource owner either increases production or decreases consumption, whereas downregulation entails the resource owner either decreasing production or increasing consumption (Fingrid 2024d). Figure 8 depicts the prices of up- and downregulation bids in the Finnish electricity price area for the period between 01.01.2024 and 05.01.2024.

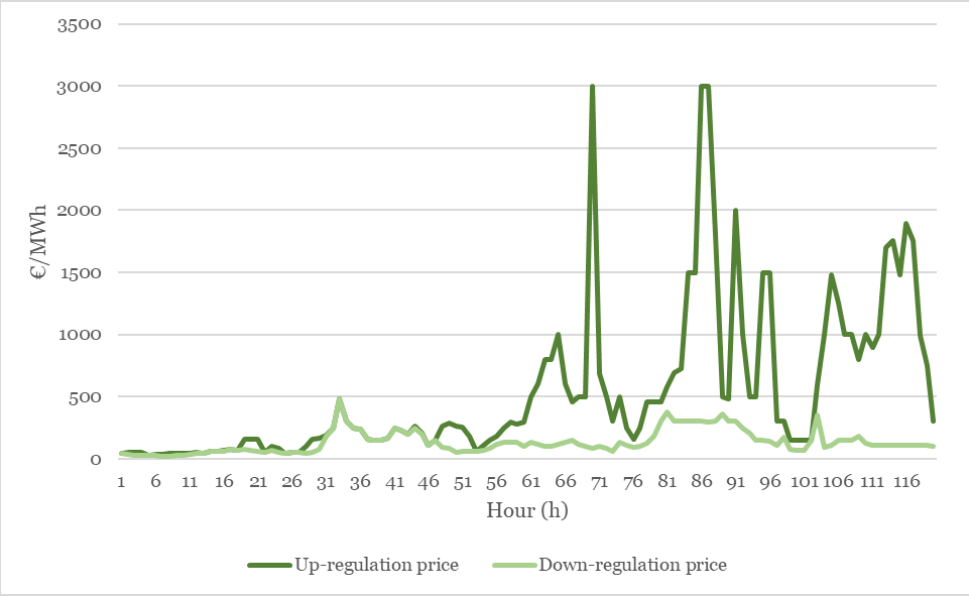

Figure 8: The prices of up- and downregulation bids during the period between 01.01.2024 and 05.01.2024 in the Finnish price area (Fingrid 2024b).

For a wind power producer, the imbalance settlement can cause significant additional costs. As mentioned earlier, the wind power production is highly variable due to the uncontrollable and unpredictable nature of wind speeds and the production plans for the next day are always based on forecasts. The imbalance production is therefore a noticeable risk for the wind power producers. For example, on Thursday 4.1.2024 at 13:00 the upregulation price was 3000 €/MWh whereas the DA market price for the same hour was 296.18 €/MWh (Nord Pool 2024a). In this case, an underproduction of

approximately 10 % would have led to negative profit for the hour. Frade et al. (2019) calculated that the balancing costs for intermittent renewable power producers in Portugal are around 2 €/MWh. This is in line with similar calculations in Finland, where balancing costs of 3 €/MWh for a wind power site were reported (Holttinen et al. 2013, p. 3). However, balancing costs could be lowered up to 60 % by aggregating the sites to a larger area.

4 Electricity markets in Finland

This chapter provides a comprehensive overview of the electricity markets in Finland. It begins with a brief introduction to the structure and evolution of the Nordic electricity markets. Following this, the chapter examines the various physical electricity markets. The chapter focuses on the Day-ahead (DA) and Intraday (ID) markets, in which their operation and the mechanics behind their price formation are analyzed. After that, the five different reserve marketplaces in Finland are researched more closely, including a deeper investigation into the technical requirements they impose on reserve providers, as well as the bidding process involved.

4.1 Market structure

Functioning electricity markets are the most effective way to ensure a secure supply of electricity between the producers and the consumers (Fingrid 2024e). The price of electricity in the market guides the market participants' decisions on electricity production and consumption and signals the long-term investment possibilities. The Finnish electricity market is part of the larger Nordic electricity market with Sweden, Norway and Denmark. The Nordic electricity market is also integrated into the wider European power market through interconnectors to, for example, Baltic states, Germany and the Netherlands (Fingrid 2024e). The electricity markets in the Nordics were dominated by monopolies until 1991, when Norway started the deregulation of its electricity market (Lundgren 2012, p. 6-7). Finland liberalised its own electricity market in 1995 (Electricity Market Act 386/1995). The first international power exchange Nord Pool was created in 1996 when Sweden joined the Norwegian power exchange market. Finland and Denmark joined the market in 1998 and 2000 respectively (Lundgren 2012, p. 6-7). The current Nordic electricity system is depicted in Figure 9.

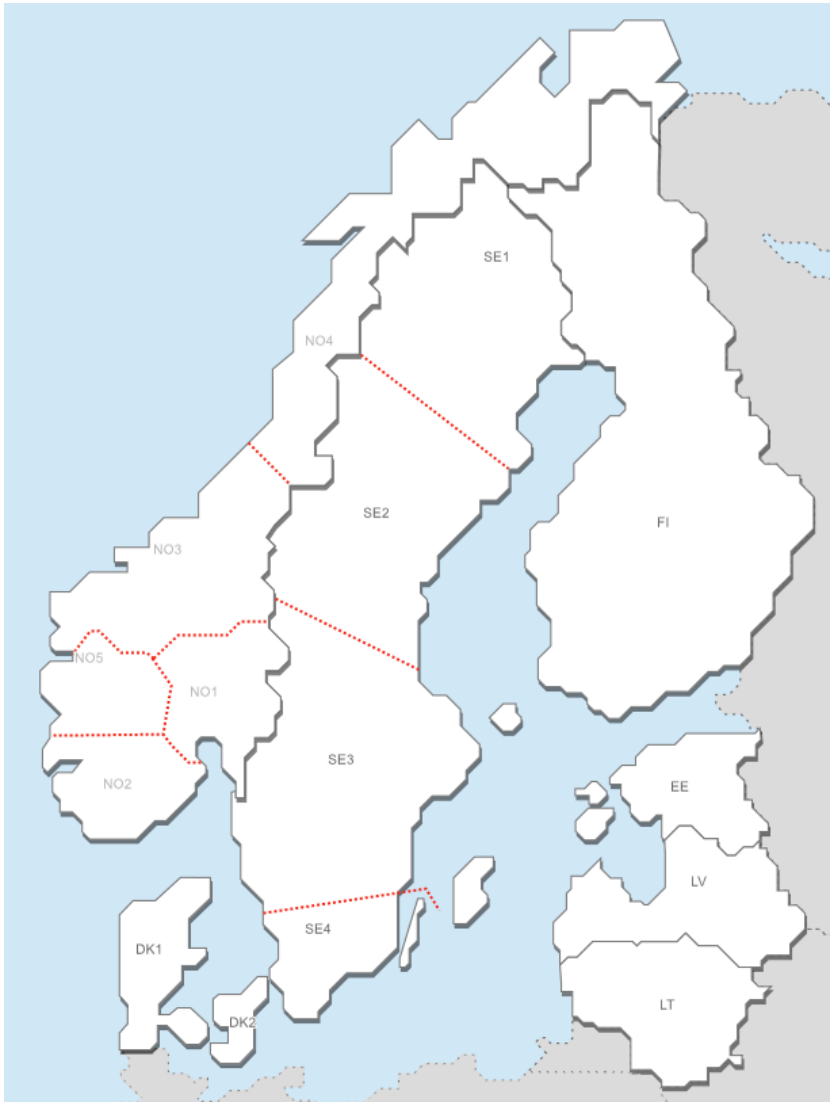

Figure 9: The Nordic and Baltic bidding regions (Statnett 2024).

Currently there are 12 bidding zones in the Nordic electricity market. Finland has only one bidding zone, whereas Sweden, Norway and Denmark all have several (Nord Pool 2023a). The different bidding zones are connected with interconnectors and the different bidding areas have an individual energy balance. Electricity is distributed from areas where the offered price is lower to areas with a higher demand and therefore resulting in a higher price. The wholesale electricity price remains uniform across the Nordic electricity market for only some hours of the year due to constraints in transmission capacities of the interconnectors. These limitations restrict the amount of electricity that can be transmitted between the different bidding areas (Kauniskangas 2009, p. 11-12). Figure 10 depicts the market structure of Nordic electricity markets.

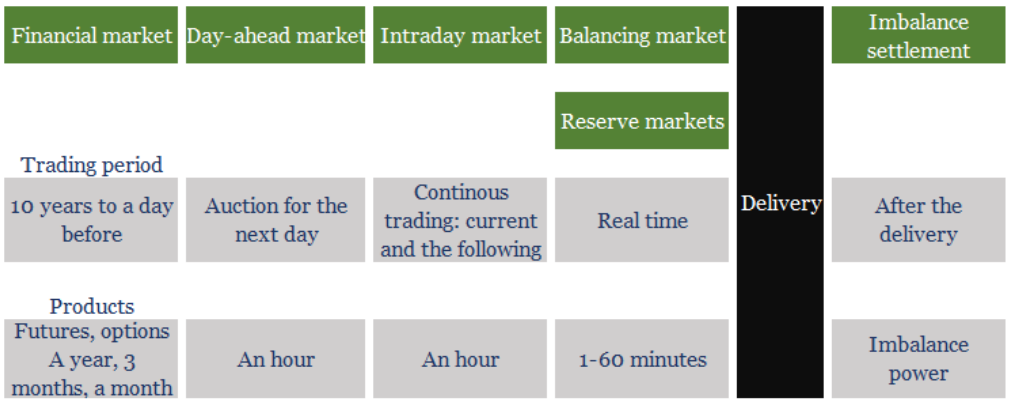

Figure 10: The market structure of the Nordic electricity market. Modified from (Fingrid 2024e).

The Nordic electricity market can be divided into financial and physical markets (Spodniak et al. 2019, p. 3). Financial markets do not involve any physical delivery of electricity and are for hedging purposes. In the financial markets, market participants can settle and clear their exchange-traded or Over-The-Counter (OTC) contracts. The physical markets can be comprised into Day-ahead (DA), Intraday (ID), balancing and reserve markets and they always involve the physical delivery of electricity. Most of the today's electricity in the Nordic countries, around 70 %, is traded through Nord Pool in DA and ID markets (Lundgren 2022, p. 7).

4.2 Day-ahead market

The most important wholesale electricity market in the Nordics is the DA market which is operated by Nord Pool. In the DA market customers can sell or buy energy for the next 24 hours in a closed auction (Nord Pool 2024b). The market prices are determined based on supply and demand bids, while also considering the binding transmission capacities between the bidding areas (Spodniak et a. 2019, p. 5). The market participants receive information on the transmission capacities for the DA auction at 10:00 Central European Time (CET) from Nord Pool and submit their bids including price (€/MWh) and volume (MWh/h) by 12:00 CET. After the auction has closed, the next day's hourly prices are revealed. The DA market price for each hour of the next day is calculated based on the equilibrium between supply and demand (Spodniak et a. 2019, p. 5).

The suppliers bid in how much they are willing to sell electricity and at what price (Lundgren 2012, p. 8). If the market functions as intended, the bid prices are based on the suppliers' marginal costs of production. After the bids have been received, they are arranged in merit order, which is a ranking

system to determine the order at which the different electricity sources are used to meet the demand at any given hour. Demand is calculated as a function of how much electricity is needed at a given time (Lundgren 2012, p. 8). Household demand is predicted in advance based on the historical consumption on similar days, while considering the forecasted outside temperature, wind and solar conditions and precipitation (Elovaara & Haarla 2011, p. 79). Industrial demand can be determined based on the economic situation (Lundgren 2012, p. 8). Figure 11 depicts the price formation in the DA market based on the demand bids and the merit order of supplier bids.

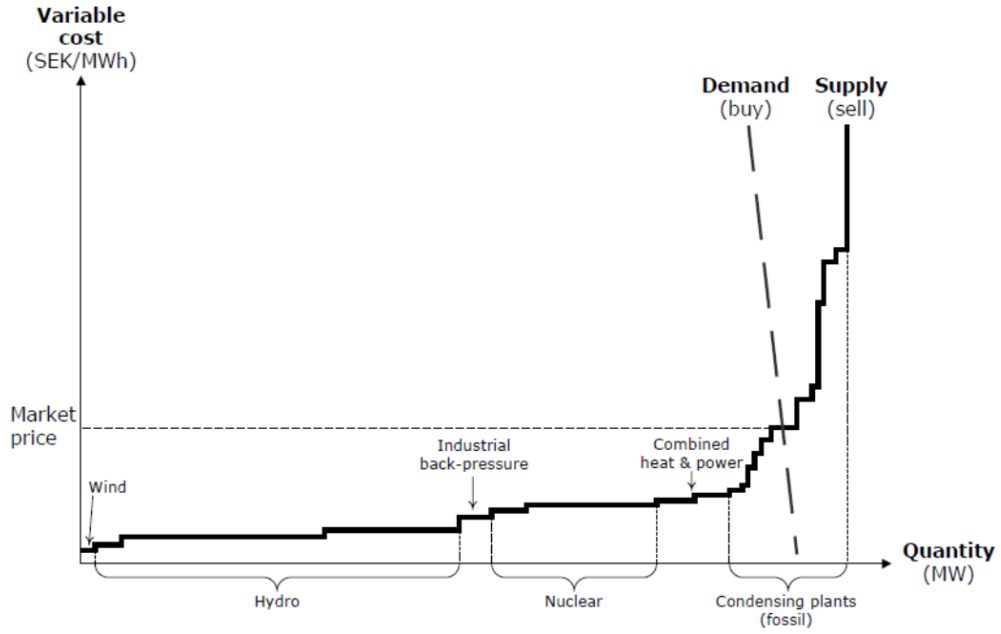

Figure 11: Price formation in the DA market (Lundgren 2012, p.8).

Figure 11 illustrates how the market clearing price for each hour is determined by the intersection of the demand and supply curves. All consumers have to subsequently pay that price, while suppliers who bid at the market clearing price or lower, will receive payment at the market clearing price (Lundgren 2012, p. 9). The operation of the Nordic electric market is affected by the transmission capacities of the interconnectors between the bidding areas. Figure 12 depicts the price formation in Nord Pool and the behaviour of market prices between surplus and deficit bidding areas.

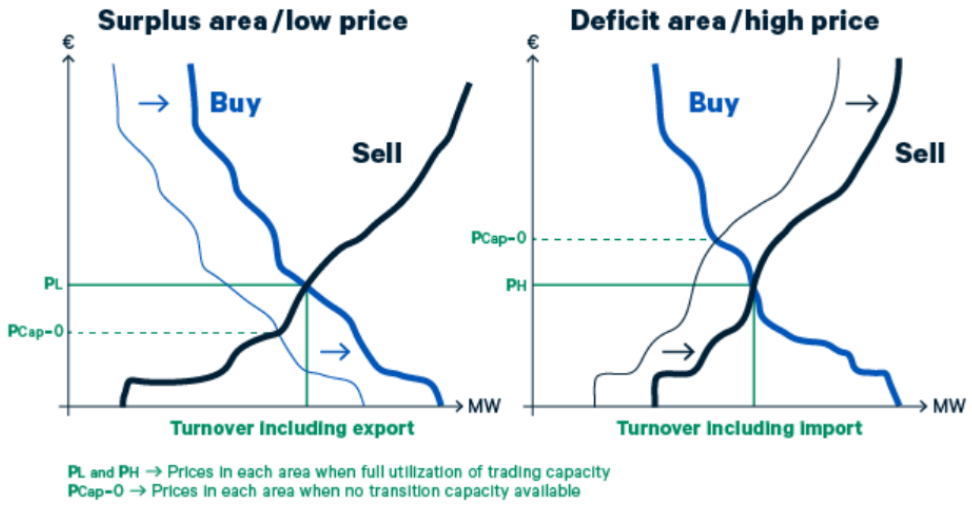

Figure 12: Nord Pool DA clearing price in surplus and deficit bidding areas (Nord Pool 2023a).

In Figure 12 the price P_{cap} is the market clearing price in a situation where each bidding area is using only its own production to meet the demand. P_H and P_L are the market prices in the deficit and surplus bidding areas when the full transmission capacity between them is available. For the surplus area P_H is actually higher than P_{cap} since there is higher demand which moves the demand curve to the right (Nord Pool 2023a). In addition to the regional prices for each bidding area, the system price is also calculated for the whole Nordic region. The calculation assumes no network congestion within the Nordic market and it is used as a reference price in the financial markets (Jääskeläinen et al. 2022).

4.3 Intraday market

Once the DA market has closed, trading is continued in the ID market until one hour before the physical delivery of electricity. However, in Finland trading is allowed until zero minutes before the delivery (Spodniak et a. 2019, p. 5; Fingrid 2024e). This way market participants can correct the errors in their demand and supply bids, with more timely information and minimize the energy imbalance. ID market is open 24/7 and the market allows market participants to trade 15- and 30-minute , hourly and block products from 14:00 CET the day before delivery onwards (Nord Pool 2024c; Spodniak et a. 2019, p. 5-6). The ID market is a joint marketplace between the Nordic, Baltic and Continental markets (Spodniak et a. 2019, p. 5). It follows a continuous pay-as-bid double auction, where the bids are arranged in order based on their time of offer and price. The important transmission capacities are given by TSOs after the DA market settlement. However, these capacities can change before the delivery.

The increasing share of RES in the power system is considered to increase the role of the ID market, as it provides an opportunity for the renewable energy producers to trade their generation imbalances for a lower cost than in the balancing markets (Hu et al. 2021). The ID market prices are also higher than the DA market prices, which would provide incentives for VRE producers to decrease their activity in the DA market in favour of the ID market (Soysal et al. 2017). The trading volumes on the ID market have increased significantly over the last few years. In 2022 Nord Pool's ID market saw an annual trading growth of more than 50 % compared to the previous year (Nord Pool 2023b). The transition into sub-hourly contracts has been a key factor contributing to the increase in trading volumes in the ID market (Lundberg 2012, p. 6). The ID market allows the market participants to reduce the need for additional reserve capacity which could decrease the volume of balancing market trading and consequently decrease the profitability of storage systems. However, the transition into shorter contracts both in ID and, in the future, in DA market will allow these systems to be used beyond the balancing market.

4.4 Balancing and reserve markets

Electricity generation and production are initially planned and forecasted as accurately as possible in advance for the DA market. Once the DA market closes, trading continues in the ID market, where market participants can correct their production and consumption errors with more timely information. However, it is natural that sudden consumption and production changes happen during the operating hour. To smooth out the final imbalances of energy during the operating hour in the Nordic electricity market, balancing and reserve markets are operated by the Nordic TSOs (Fingrid 2024a). Since the Nordic electricity system is very connected, Nordic TSOs share the reserves across the bidding zones with each TSO procuring its' share of reserves as it considers best. In a normal situation, each TSO can only procure 1/3 of its reserve obligations from other Nordic countries (Fingrid 2024a).

The reserves available in the reserve markets are power plants, consumption resources and energy storages which can flexibly adjust their electric power according to the need of the power system (Fingrid 2024a). The reserve markets are divided into five separate marketplaces which are (Fingrid 2023b, p. 5):

- Frequency Restoration Reserve for Normal Operation (FCR-N)
- Frequency Containment Reserve for Disturbances (FCR-D)
- Fast Frequency Reserve (FFR)

- Automatic Frequency Restoration Reserve (aFRR)
- Manual Frequency Restoration Reserve (mFRR)

The different reserve marketplaces have their individual operation periods and frequency deviation limits. The reserve marketplaces in Finland have been depicted in Figure 13.

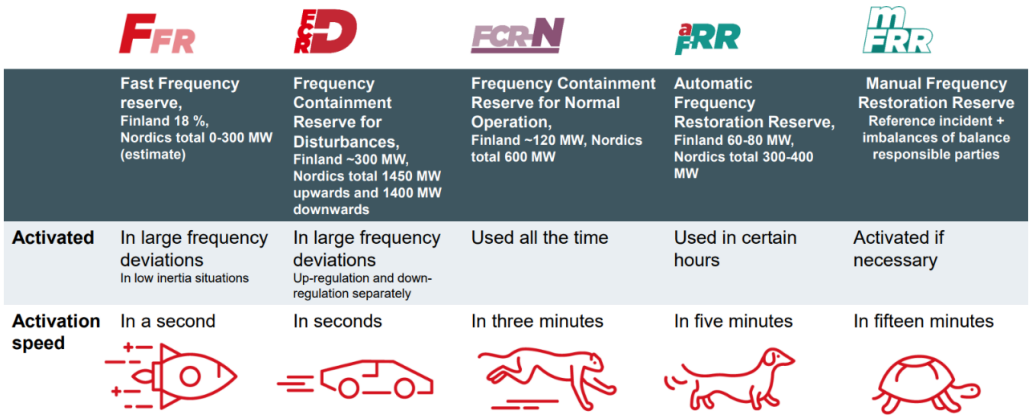

Figure 13: The reserve marketplaces in Finland operated by Fingrid (Fingrid 2023b, p. 5).

As seen in Figure 13, different reserve products are needed in different frequency deviation situations and have different activation speeds. Consequently, different reserve products call for different technologies. For example, battery energy storage systems are considered to be particularly suitable for FCR-N, FCR-D and FFR operations and wind power is a suitable technology for FFR, FCR-D, aFRR and mFRR operations (Fingrid 2023b, p. 6). Traditional fossil fuel-based power plants are used mainly for FCR-N, aFRR and mFRR operations.

4.4.1 Frequency Containment Reserves FCR-N and FCR-D

FCR-N and FCR-D are active power reserves which are automatically controlled based on frequency deviation in the power system (Fingrid 2024f). FCR-N is used to keep the frequency within the normal operating range of 49.9 Hz to 50.1 Hz. FCR-D aims to limit the larger frequency deviations to 49.5 Hz or 50.5 Hz during major demand or generation changes. FCR-N is a symmetrical marketplace where the reserves must be able to provide both up- and downregulation. FCR-D in turn is divided into separate up- and downregulation products (Fingrid 2024f). Fingrid's reserve obligations and procurement sources for FCR-N and FCR-D in 2023 have been depicted in Table 1.

Table 1: Fingrid's reserve obligations and procurement sources for FCR-N and FCR-D in 2023. Modified from (Fingrid 2024a).

Reserve product	Obligation	Procurement channel	Maximum contracted capacity
FCR-N	121 MW	Yearly market Hourly market Other Nordic countries Estonia	68 MW 253 MW - 35 MW
FCR-D up	290 MW	Yearly market Hourly market Other Nordic countries Estonia	345 MW 733 MW - 80 MW
FCR-D down	230 MW	Yearly market Hourly market Other Nordic countries Estonia	186 MW 248 MW - 50 MW

The total amount of FCR-N in the Nordic power system is 600 MW and FCR-D up and FCR-D down are dimensioned separately for under- and overfrequency events (Fingrid 2024a). The overall FCR-D up- and downregulation capacities in the Nordics are 1450 MW and 1400 MW respectively, which are divided annually between the countries based on the annual production and consumption.

There are a number of technical requirements for FCR provision in the Nordics. When the frequency deviates from 50 Hz, FCR-N capacity is activated and at frequencies equal or below 49.9 Hz, 100 % of the FCR-N upregulation capacity is activated. This also applies to FCR-N downregulation capacity at 50.1 Hz (Fingrid 2024f). The activation of reserves must be proportional to the frequency deviation within the normal operation range and the capacity is used for as long as the frequency deviation persists (ENTSO-E 2023, p. 15). The reserve products in FCR-N also have to meet certain activation performance requirements (Fingrid 2024f). When a frequency deviation of 0.1 Hz in either direction happens, the resource has to provide around 63 % of its reserve capacity in 1 minute and around 95 % in 3 minutes (Fingrid 2024f). The performance of a potential FCR-N resource is tested with a step sequence test (ENTSOE 2023, p. 13).

At frequency levels of 49.9 Hz or 50.1 Hz, 0 % of FCR-D capacity is activated. At frequencies below or equal to 49.5 Hz, 100 % of the upregulation capacity is to be activated. Respectively, at frequencies above or equal to 50.5 Hz, 100 % of the downregulation capacity is to be activated (Fingrid 2024f). The response has to stay active as long as the frequency deviation persists (ENTSO-E 2023, p.18). Both the FCR-D up- and downregulation reserves must be able

to activate 86 % of their reserve capacity in 7.5 seconds after the disturbance (Fingrid 2024f). The steady-state response, endurance and time domain dynamic performance of potential FCR-D resources are tested using a ramp sequence test (ENTSOE 2023, p. 15).

For both FCR-N and FCR-D resources, the activation should happen as linearly as possible, with some deviations allowed (ENTSO-E 2023, p. 47-48). The activation of FCR-N and FCR-D products is done by changing the frequency input of the controller from zero activation to the currently measured system frequency. The smoothness of the activation is ensured using a stepwise change in input frequency. The deactivation process follows the same principle, involving a stepwise adjustment of the system frequency to ensure a gradual ramp down of the resource. FCR-D response is allowed to ramp down if the frequency deviation has persisted 15 minutes after the scheduled end. The ramp is required to be over a period of 5 minutes (ENTSO-E 2023, p. 47-48).

The maximum capacity for a single bid for FCR-N and FCR-D are 5 MW and 10 MW respectively and the minimum capacity bids are 0.1 MW and 1.0 MW (Fingrid 2023c, p. 8). The bidding accuracy is 0.1 MW. A single BSP can submit multiple bids. However, the bids must not be linked together, as they are processed separately. The maximum lost capacity in FCR-N or FCR-D due to an individual fault in a reserve unit is 70 MW for both up- and downregulation. If the reserve resource is providing both FCR-N and FCR-D, in steady-state the resource must activate the sum of FCR-N and FCR-D at any frequency deviation (ENTSO-E 2023, p.45). This arrangement requires that all of the different products are controlled separately and the resource must be able to switch from FCR-N controls to FCR-D controls if the frequency rises above 50.1 Hz or decreases below 49.9 Hz. The activation protocol for resources participating in both FCR-N and FCR-D has been depicted in Figure 14.

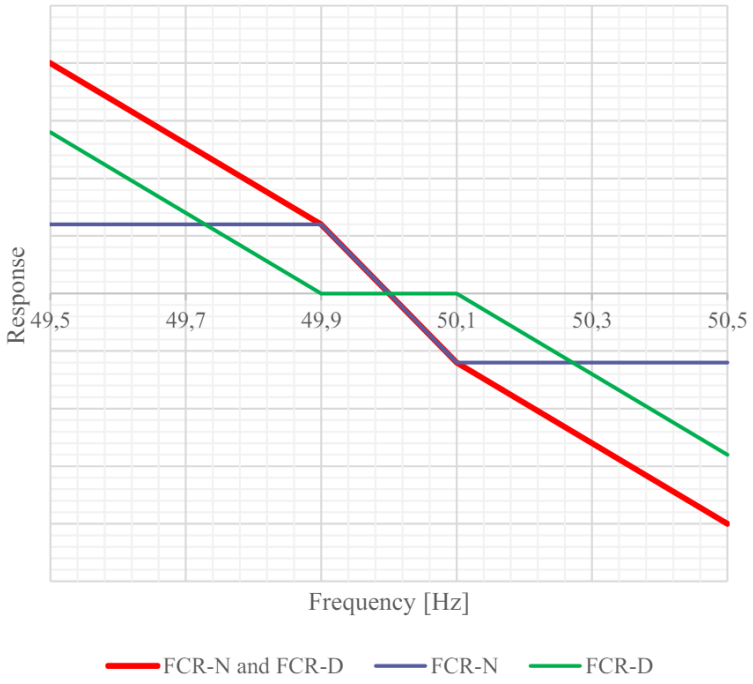

Figure 14: Steady-state power activation for a resource participating in both FCR-N and FCR-D. Modified from (ENTSO-E 2023, p. 46).

The switching between controls has to happen without any intentional delay, with the maximum delay, when switching back from FCR-D to FCR-N, being 30 seconds (ENTSO-E 2023, p. 46).

FCR resources, which have an energy reserve smaller than the equivalent of a continuous full activation of the prequalified FCR, which is 2 hours, are called Limited Energy Reservoir (LER) (ENTSO-E 2023, p. 38). For example, a BESS can be categorized as a LER. These entities must reserve power in both activation and deactivation directions. The usage of energy storages in FCR provision calls for State of Charge (SOC) management, which means managing the amount of energy available in the reservoir (Abdi et al. 2017). SOC management is done by defining two battery management states which are Normal State Energy Management (NEM) and Alert State Energy Management (AEM) (ENTSO-E 2023, p. 39-41). NEM ensures that the LER has enough energy available to activate FCR and to reduce imbalances by SOC management (ENTSO-E 2023, p. 39-41).

In full FCR-N activation, the endurance requirement of LERs is 60 minutes in both charging and discharging, which are handled mainly by the frequency deviations within the normal operation range. This means that in symmetrical provision the SOC level of the resource must be close to 50 % at the start of the period (ENTSO-E 2023, p. 38). For FCR-D provision, as of triggering

the alert stare or during the alert state, each LER must be ready to provide FCR for a minimum of 15 minutes (ENTSO-E 2023, p. 38). Because FCR-D can be provided both in alert and in steady-state, the endurance requirement is thus a minimum of 20 minutes. For asymmetrical provision the LER's SOC must be close to 0 % or 100 % depending on the direction of the power flow.

A BSP can participate in FCR provision both in the yearly and hourly market. Participation in the yearly FCR market in Finland is possible through a yearly tender competition held by Fingrid (Fingrid 2023c, p. 8). The tender competition is held every autumn for the following calendar year. For example, the tender competition for the calendar year 2024 closed on 29.9.2023 (Fingrid 2023d). The amount of FCR capacity that Fingrid acquires from the yearly FCR market depends on the forecasted price level, availability of other reserve products and on the price level of realized bids (Fingrid 2023c, p. 9). The bids are then approved separately for each product in price order. The bid must contain information about the reserve product, capacity (MW) and price of capacity for the whole year (€/MWh) (Fingrid 2023c, p. 8).

Fingrid acquires FCR resources also from the FCR hourly market, which is operated by having a day-ahead competitive tendering for each FCR product and each hour of the next day (Fingrid 2023c, p. 10-11). The bids have to contain similar information to FCR yearly market. However, for the hourly FCR market also the hour of delivery needs to be specified. Bids can be submitted until 18.30 Eastern European Time (EET). After the bids have been received, they are arranged from the cheapest to the most expensive for each hour. Every service provider for each hour is paid the price of the most expensive approved bid (Fingrid 2023c, p. 10-11). Figure 15 depicts the price duration curves for FCR-N and FCR-D markets in 2023.

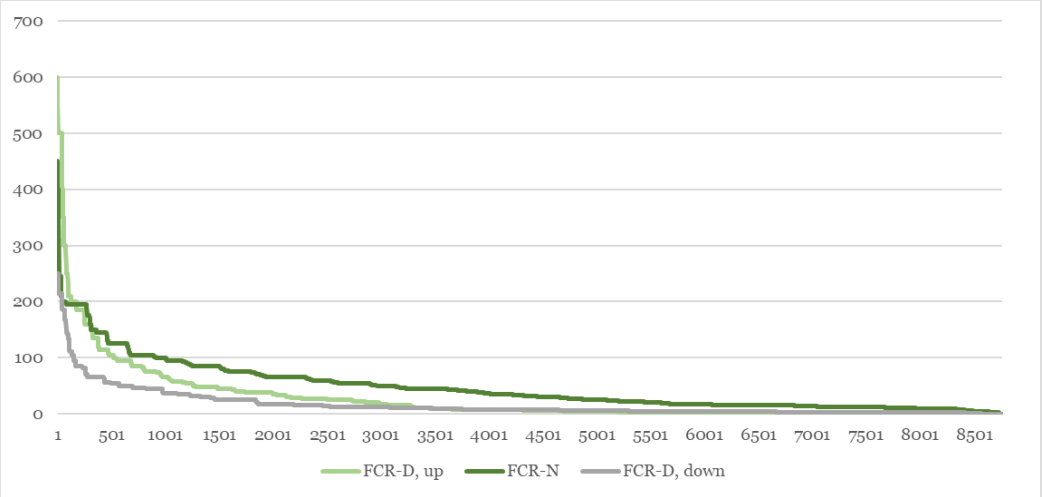

Figure 15: FCR-N and FCR-D price duration curves for the year 2023. Modified from (Fingrid 2024b).

The yearly FCR markets have the same price for each FCR product for the whole year. The yearly price of FCR-N in 2024 has been the highest since 2011, with 25.39 €/MWh (Fingrid 2024f). This is a major increase compared to the years 2023 and 2022, which saw prices of 19.10 €/MWh and 12.24 €/MWh respectively. The prices of FCR-D up- and downregulation on the yearly FCR market in 2024 are 4.00 €/MWh and 9.50 €/MWh. These prices have stayed rather stable through the years (Fingrid 2024f). The average hourly prices in the FCR hourly market for FCR-N, FCR-D up- and downregulation are 47.10 €/MWh, 27.45 €/MWh and 16.38 €/MWh. This indicates that the prices are higher in the hourly markets compared to the yearly markets (Fingrid 2024b).

4.4.2 Fast Frequency Reserve (FFR)

Fingrid acquires FFR to handle low-inertia situations which typically occur during spring, summer and autumn with lower consumption and increased production from RES (Statnett 2022, p. 2). Inertia in the Nordic power system is mostly delivered by hydropower and thermal power plants, so the overall need of FFR is strongly dependent on the hydrological situation in the Nordics (Fingrid 2023b, p.7). FFR is also needed to ensure that the loss of an electricity production facility or a High Voltage Direct Current (HVDC) link from other bidding areas will not cause a frequency deviation beyond 49 Hz (Fingrid 2023d, p.2). The total amount of FFR capacity in the Nordics is approximately 300 MW (Fingrid 2024a). The reserve obligation of Fingrid in 2023 was 0-60 MW. In 2023 Fingrid procured FFR from its own hourly FFR market and from Estonia, with maximum contracted capacities being 123 MW and 50 MW respectively.

The operation of FFR is based on automatic control signals with each reserve unit locally controlling the power output based on the frequency measurements of the power system (Fingrid 2024g). The power system frequency for the control system can be measured from anywhere in the system (Fingrid 2023d, p. 8). The required accuracy of the measurement must be at least 10 mHz, with the maximum sampling interval being 0.1 seconds. When participating in the FFR, the BSP can select one of three reserve activation options. The three activation options have been depicted in Table 2.

Table 2: The different activation options for FFR. Modified from (Fingrid 2024g).

Activation frequency (Hz)	Maximum activation time (s)
≤ 49.7	≤ 1.3
≤ 49.6	≤ 1
≤ 49.5	≤ 0.7

For example, in the option ≤ 49.7 Hz and ≤ 1.3 seconds the reserve must be fully activated within the 1.3 second time limit if the overall system frequency falls to 49.7 Hz or below (Fingrid 2023d, p. 5). The activation of the reserve can be either a step or a ramp activation method and during the activation period the activated power must be at least the power value at the start of the activation period. There are two options for the minimum activation duration in full activation mode which are 30 and 5 seconds (Fingrid 2023d, p. 5-6). There are no technical requirements regarding the SOC management of reserve units like BESSs for FFR provision.

Fingrid acquires FFR capacity in the FFR market through a DA tendering process (Fingrid 2023e, p.6). The auction is organized for the hours of the next day. The maximum capacity of a single bid for FFR provision is 10 MW and the minimum is 1 MW. The accuracy of the bids must be 0.1 MW. The bids must contain information about the type of reserve, the capacity (MW), capacity price (€/MW, h) and the activation hour. The type of reserve must be specified, as the reserve could be a production, a consumption or an aggregated reserve unit. If a BSP is participating in FCR provision in addition to FFR provision, the provider must submit a combination bid which must include a combined reserve capacity plan and the capacity prices for both markets. If the capacity in the combination bid is not used in the FFR market, it will be transferred to the FCR market and vice-versa. The auction for the next day's hours closes at 18:00 EET and the transactions are confirmed by 22:00 the previous day (Fingrid 2023e, p. 6). Figure 16 depicts the price duration curve for FFR in Finland in 2023.

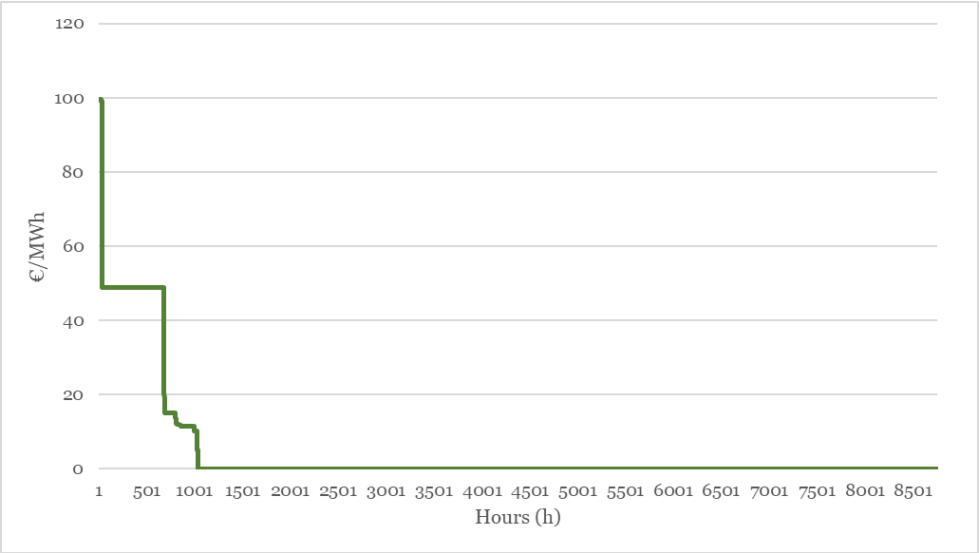

Figure 16: The price duration curve for FFR in Finland in 2023. Modified from (Fingrid 2024b).

In 2023 the average price of FFR provision was 38.2 €/MWh and the highest price was 99.5 €/MWh (Fingrid 2024b). However, the procured volume of FFR is rather low. In 2023, FFR was only procured for 1034 hours and no capacity has been procured in 2024 as of January (Fingrid 2024b). Figure 17 depicts the procurement volume in FFR and FCR-D -up markets in 2023.

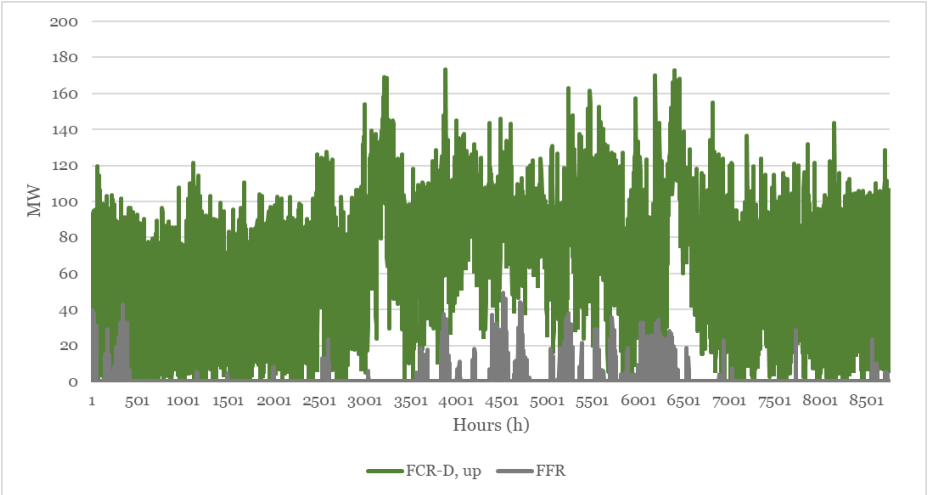

Figure 17: The procurement volume in FFR and FCR-D -up markets in 2023. Modified from (Fingrid 2024b).

Analysis of Figure 17 reveals a significant difference between the volumes of the FCR-D upregulation market and the FFR market. This signals that for an

individual BESS, only participating in the FFR market would not be as profitable as bidding in both the FFR and FCR markets. Figure 17 also depicts clearly that FFR is mostly needed during the spring and summer times.

4.4.3 Manual Frequency Restoration Reserve (mFRR)

Fingrid together with the other Nordic TSOs maintain the balancing market. The reserve providers offer their balancing capacity to the market in exchange for a financial compensation (Fingrid 2024d). The procurement of mFRR happens in the balancing energy market and in the balancing capacity market, as well as in competitive tendering by means of balancing capacity agreements. In Finland the balancing energy market is operated by Fingrid in co-operation with eSett Oy, which has from 20.11.2023 onwards handled all the invoicing of the balancing energy market. All balancing service providers must sign a balancing agreement with eSett as well as a separate balancing market contract with Fingrid (Fingrid 2024d). There are no prequalification tests or other verification of reserve units before they can participate in the balancing energy market, unlike in the FFR and FCR markets.

The minimum capacity for a balancing energy bid is 5 MW. However, for resources using electronic activation, the minimum capacity is 1 MW (Fingrid 2023f, p. 9). The maximum capacity for a single balancing bid is 200 MW. The accuracy of the balancing bid must be 1 MW. In order to participate in the balancing energy market, the resource unit must be located in the same transmission area (Fingrid 2023f, p. 8-9). During the delivery hour, the balancing must be delivered to its full power within 15 minutes of activation. For a BESS, the minimum activation durations at a full reserve capacity for balancing energy and capacity markets are one and three hours respectively (Fingrid 2023b, p.21). The bids can be submitted, at the earliest, 30 days before the operating hour and the service provider can cancel or modify the bid up to 45 minutes before the start of the delivery, after which the bid becomes binding. A bid to the balancing market must include information about the power (MW), price (€/MWh), name of the reserve unit, hour of the delivery and other information about the reserve unit. As the offered balancing service can be both up- and downregulation, the power and price information have to be given separately for both bids (Fingrid 2023f, p. 8-9).

The price of balancing energy for each hour is based on the amount of balancing carried out during that period (Fingrid 2024d). The upregulation price is the price of the most expensive upregulation energy bid used during that hour. Every balance provider from whom Fingrid has ordered balancing during that hour will receive the agreed upregulation price. The downregulation price is the price of the cheapest downregulation bid used for that hour

and every service provider which has been ordered to provide downregulation during that hour, receives the agreed price (Fingrid 2024d).

In addition to the balancing energy market, Fingrid can also procure additional up- and downregulation capacity from the balancing capacity market through a DA competitive tendering (Fingrid 2023f, p. 10). The auction is set-up for each hour of the next day. Through the balancing capacity market, the reserve service provider offers reserve volume which was accepted in the tendering process to the balancing energy market.

The minimum and maximum capacities for a single capacity market bid are 1 MW and 50 MW respectively (Fingrid 2023f, p. 10). The capacity provider can submit several bids, however, the bids must not be linked together. The bids must include information about the capacity product, hour of delivery, price (€/MWh), capacity (MW), the minimum order volume if the bid cannot be divided, transmission area and the name of the reserve unit (Fingrid 2023f, p. 10-11). The bids are processed based on the capacity price and arrival time, but also based on if the bids can be divided into smaller bids to match the balance need. The price duration curves of mFRR up- and downregulation in the capacity market in Finland in 2023 have been depicted in Figure 18.

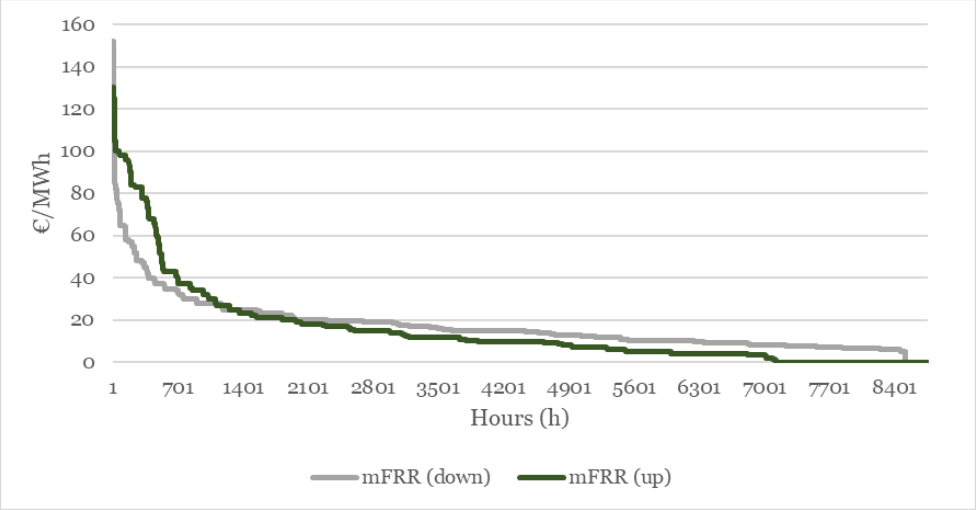

Figure 18: The price duration curves for mFRR up- and down-regulation in the capacity market in 2023. Modified from (Fingrid 2024b).

The highest prices of mFRR up- and downregulation in the balancing capacity market in 2023 were 130 €/MWh and 152 €/MWh respectively and the average prices were 18.65 €/MWh and 17.46 €/MWh (Fingrid 2024b). Compared to the prices in FCR-N and FCR-D hourly markets, the peak and

average hourly prices were lower in the mFRR hourly market. However, mFRR was used during more hours in 2023 than the other markets.

Fingrid can also procure balancing capacity with a balancing capacity agreement through a separate competitive tendering which is announced separately by Fingrid, containing information about the capacity product and the agreement period (Fingrid 2023f, p. 11-12). The bids can then be submitted for one month after the tendering procedure. A reserve unit which has offered for the competitive offering of the balancing capacity agreement must be able to maintain their continuous activation for three hours (Fingrid 2023f, p. 12). After the activation period, the unit is allowed to rest the time equal to the last activation period but at least three hours and at most six hours. The bids for the balance capacity agreement for all hours of the next day must be submitted by 8:00 EET on the morning of the previous day. The minimum capacity of a single bid is 5 MW and the accuracy must be 1 MW. A bidder can submit several bids and the bid has to include the same information that was required in bids for the balancing energy and balancing capacity markets (Fingrid 2023f, p. 12).

4.4.4 Automatic Frequency Restoration Reserve (aFRR)

aFRR was introduced in 2013 by the Nordic TSOs to return the power system frequency back to the nominal value of 50 Hz by sending an activation request signal (Fingrid 2024h). The centralised reserve is activated automatically through the activation signal which is sent every 10 seconds. The activation request is calculated based on the frequency deviation in the Nordic power system. In Finland, Fingrid procures aFRR both from the hourly market and from the other Nordic countries and the procurement is done only for certain hours with the most variation in frequency (Fingrid 2024h). In 2023, the reserve obligation of Fingrid was 46-62 MW (Fingrid 2024a). The procurement hours and the procure volume are informed by Fingrid at least two hours before the closing of the aFRR hourly market. Up- and downregulation capacities are submitted separately (Fingrid 2024h).

Reserve units contributing to aFRR have to first pass a prequalification test supervised by Fingrid (Fingrid 2019, p. 2). The prequalification test is used to measure the activation speed and accuracy of the reserve unit. The unit must be able to activate its entire capacity within 5 minutes from receiving the activation signal from Fingrid and the activation must start 30 seconds after the signal (Fingrid 2019, p. 4).

The minimum capacity of a single bid in the aFRR hourly market is 1 MW, with the accuracy of the bid being the same (Fingrid 2023g, p. 6). The maximum capacity for a single bid is 50 MW. As in mFRR provision, the bids can

be divided into smaller bids to potentially speed up the bid approval process. The bids must contain information about the capacity (MW), capacity price (€/MWh), hour of delivery and the bidding area of the reserve capacity (Fingrid 2023g, p. 7). Bids for up- and downregulation must be submitted separately. The reserve service providers can submit bids for the hours of the next day by 8:30 (EET) on the previous day and no earlier than seven days before the delivery hour. The bids are then accepted in price order separately for up- and downregulation capacity, while considering the possible aFRR trading between the bidding zones (Fingrid 2023g, p. 7). Figure 19 depicts the price duration curves for aFRR up- and downregulation.

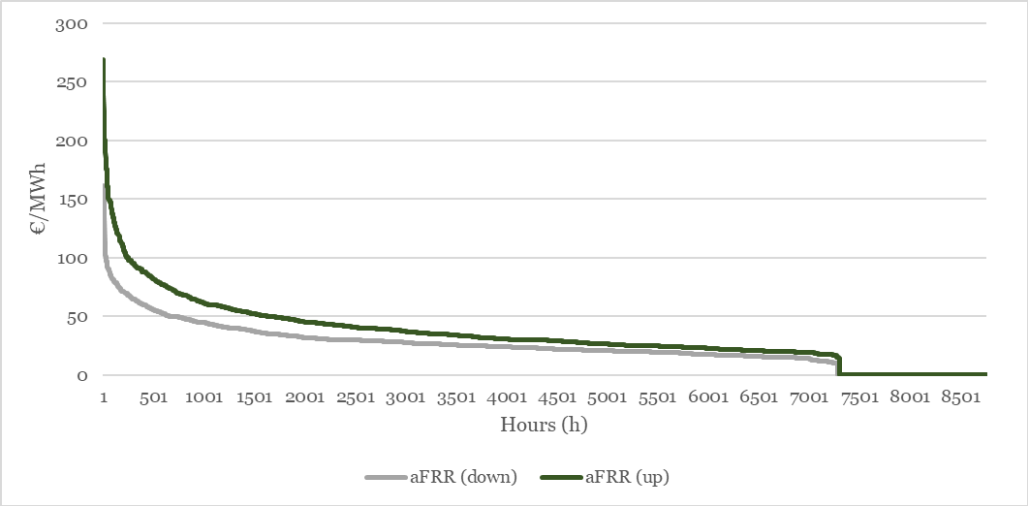

Figure 19: The price duration curves for aFRR up- and down-regulation in 2023. Modified from (Fingrid 2024b).

As seen in Figure 19, the price duration curves for aFRR behave very similar to FCR-N and FCR-D curves, with high peak prices and high usage rates. The highest prices for aFRR up- and downregulation in Finland in 2023 were 269 €/MWh and 161.8 €/MWh respectively, while the average market prices were 40.93 €/MWh and 29.93 €/MWh (Fingrid 2024b). The peak prices in 2023 were higher in FCR-N and FCR-D hourly markets, but the average prices in the hourly markets were higher with aFRR. Both the peak and average prices were higher than in the mFRR hourly market.

4.5 15-minute imbalance settlement

The increased share of RES in the power system has made it imperative to transition into a more timely and accurate energy market (Empower 2018, p. 11). The old 60-minute imbalance settlement period also raised some questions about the fairness of the imbalance settlement system, which would not share the costs of imbalances accurately to those market participants who

caused the imbalances. To transition into a fairer treatment of market participants, to incentivise better management of imbalance risk in terms of price and volume and most importantly to increase the control the imbalances between supply and demand, the Nordic TSOs have decided to switch to a shorter imbalance settlement period (Empower 2018, p. 11).

The transition from 60-minute imbalance settlement to 15-minute imbalance settlement was started in Finland in May 2023 and the transition will happen in phases (Fingrid 2023h, p. 7-9). During the first phase, the imbalance settlement system transitioned from the 60-minute resolution to 15-minute resolution, consisting of the centralised information exchange unit, datahub and energy measurement. Also, energy exchanges such as Nord Pool can offer 15-minute products in the ID market. The imbalance settlement price is based on the 60-minute mFRR market, which means that the price stays the same for each quarter of the hour (Fingrid 2023h, p. 7-9). This means that the imbalances are measured every 15-minutes but priced using the same price for each quarter of the hour (eSett 2023, p. 20). After the operation hour, the hourly netted imbalance cost is calculated by summarizing the quarterly imbalance fees.

During the next phase, the ID auctions will transition into 60-minute resolution in Q1 2024 and in Q2 2024 the imbalance prices, ID continuous and auctions will transition into 15-minute resolution. It is estimated that the final phase, in which the DA auctions and prices will transition into 15-minute resolution, will happen in 2025 (eSett 2023, p. 10).

5 Battery Energy Storage System (BESS)

In this chapter lithium-ion batteries and BESSs are discussed in more detail. First the operation and the different cell types of lithium-ion batteries are reviewed. The different cell technologies are then compared to determine the most suitable option for the simulations, followed by analysis of Lithium-ion Battery (LIB) degradation. This includes the examination of different degradation root causes and how to model the degradation process through different empirical and semi-empirical methods. Then the overall battery storage system and its components are researched. This chapter concludes with an analysis of the life-cycle costs of BESSs, including a more detailed review of the Investment Costs (CAPEX) and Operation and Maintenance Costs (OPEX).

Electrical energy can be converted and stored in many ways. In principle, energy storage technologies can be divided into electrochemical, mechanical, electrical, chemical and thermal energy storages, with each of them having various subsidiary storing technologies (Kebede et al. 2022). Figure 20 depicts a classification of energy storage technologies.

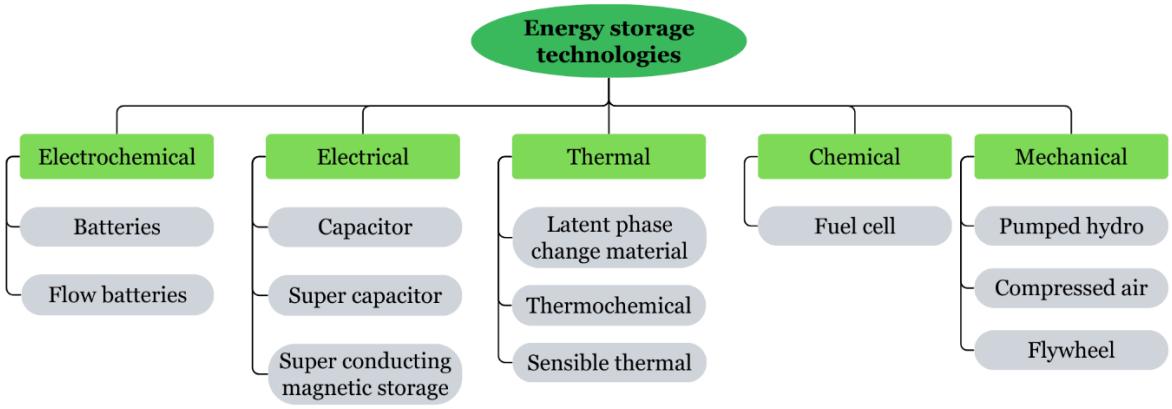

Figure 20: A classification of energy storage technologies. Modified from (Kebede et al. 2022).

Traditional pumped hydro energy storages are currently the most important energy storage technology, as they account for over 96 % of the overall energy storage capacity in the world (Choi et al. 2021). Various electrochemical energy storage technologies, such as lithium-ion, lead-acid, flow and sodium- and zinc-based batteries have however been developed very intensively during the last few decades and they are considered to be very important in integrating more RES into the power system and advance the energy transition further (Hannan et al. 2021). Figure 21 depicts the cumulative increase in rated power capacity for five different BESS technologies.

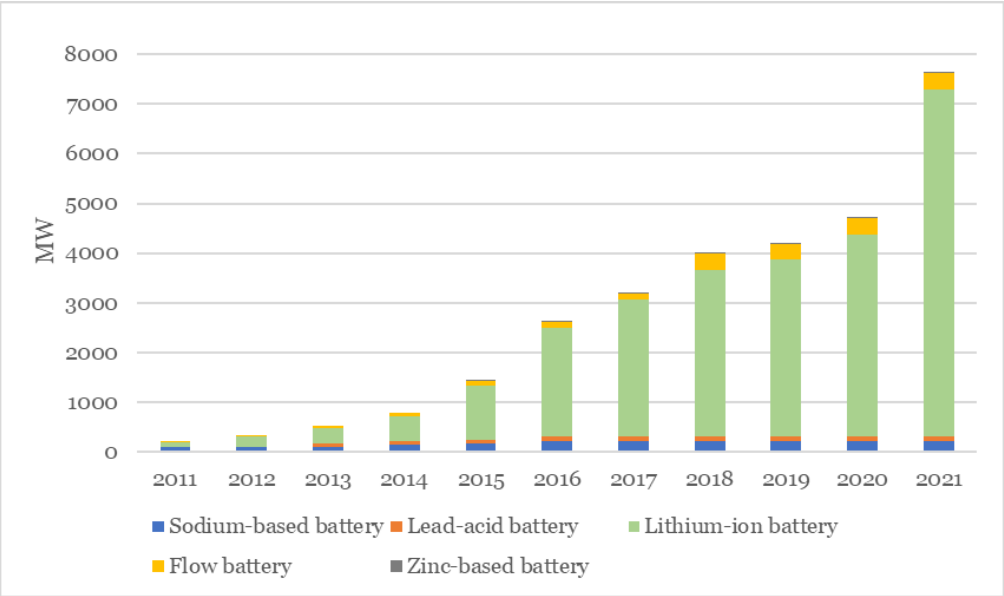

Figure 21: The cumulative increase in rated power capacity for different battery energy storage technologies. Modified from Sandia National Laboratories (2023).

As can be seen from Figure 21, lithium-ion batteries are the most widely deployed BESS for grid-scale energy storage services. The wide deployment of lithium-ion batteries is due to their power and energy performance compared to the other battery technologies (IRENA 2017, p. 63-70). The high efficiency coupled with high power output and relatively low self-discharge rates make them a very competitive choice of technology for grid-scale energy storage (IRENA 2017, p. 63-70). Additionally, the long lifespan of these batteries and their ability to handle high-discharge cycles give them superior performance compared to other technologies (Lavoie et al. 2017).

In this thesis the focus will be on lithium-ion batteries. The obtained results can also be utilized when analyzing the profitability of other battery technologies.

5.1 Lithium-ion batteries

Lithium-ion batteries have rapidly become one of the most crucial technologies in electronics. They are widely used in various electronic devices such as phones, computers and electric vehicles and they are currently the most used battery technology for grid-scale energy storages (Choi et al. 2021). The breakthrough of the LIB started in 1991 after Sony commercialized its first LIB, which largely enabled the wider development of lightweight portable

electronic devices (Bresser et al. 2015, p. 125). The first LIBs entered to the market in the 70s. However, these batteries relied on pure lithium metal, which had many drawbacks such as low lithium plating, stripping efficiency and high instability (Bresser et al. 2015, p. 125).

The operation of LIBs is mainly based on the movement of lithium-ions between the positive and negative electrodes (Díaz-González et al. 2012). The main components of LIBs are the positive and negative electrodes called the cathode and the anode, the electrolyte which serves as a conductor and the separator between the electrodes. Although, literature often talks about LIBs in a more general sense, the term encompasses various technologies and different material options, which causes their performance and characteristics to differ significantly. Different applications and performance requirements guide the choice of materials used in electrodes and electrolytes (Díaz-González et al. 2012).

Figure 22 depicts the typical operation of a LIB cell in charge and discharge cycles. When the LIB is charged the positive lithium-ions migrate from the cathode through the electrolyte to the anode (Choi et al. 2021). At the same time electrons released from the cathode migrate to the anode through an external circuit. During discharging, the process is reversed and lithium-ions now migrate from the anode to the cathode.

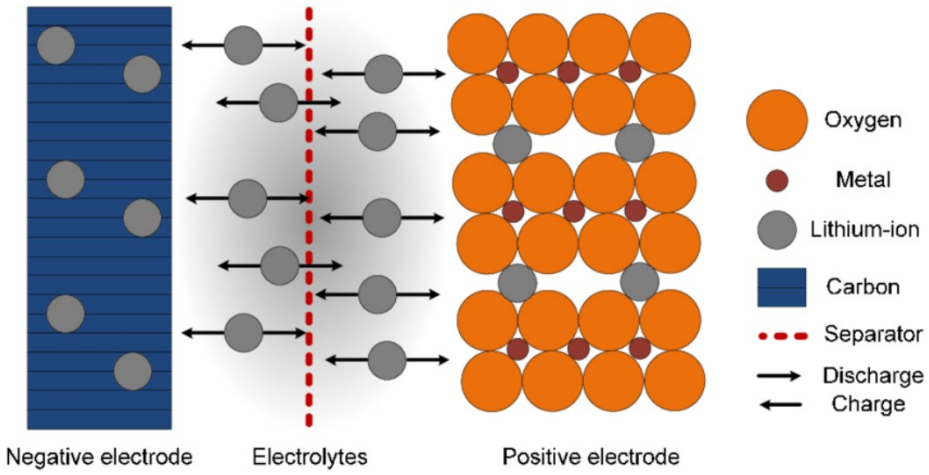

Figure 22: The typical operation of a LIB in a charge and discharge cycle (Sauer et al. 2012).

The electrolyte guarantees the ionic conductivity between the electrodes and it must remain stable under various temperatures (Kurzweil 2015, p. 282). They are generally optimized for a specific battery chemistry and they can be liquids, gels, solid polymers or inorganic solids (Choi et al. 2021). The majority of LIB cells use liquid electrolyte containing lithium salt dissolved in a

mixture of carbonate solvents. This is due to the relatively high oxidation and reduction potentials, low activation energy and low viscosity, which increase the performance of the cells. Separators are used in battery cells with a liquid electrolyte, in which they facilitate free ionic transport and at the same time prevent the physical contact between the electrodes (Choi et al. 2021). Separators are usually a microporous layer made from polyethylene or polypropylene to hold sufficient liquid electrolyte and to prevent the movement of particles from electrodes (Kurzweil 2015, p. 287-288). Most commercial lithium-ion battery cells use lithium metal oxide as the activate material in the positive electrode (Kurzweil 2015, p. 270). The materials are usually either in an olivine lattice, in a layered or in a spinal lattice structure. The cell potential, capacity and energy density characteristics are very dependent on the properties and materials of the positive electrode (Kurzweil 2015, p. 271-272). Carbon lithium intercalation compounds are mostly used as the active material in the negative electrode (Kurzweil 2015, p. 270). The choice of negative electrode significantly affects the stability and the specific charge of the lithium-ion cell.

There are various battery cell types for LIBs. Hesse et al. (2017) introduced three formats, which are cylindrical, pouch and prismatic. All these cell structures include different variations of electrode and electrolyte materials, which can be employed to meet certain performance requirements. The chosen battery cell type is important, as it can affect aspects such as storage system installation and thermal management of the battery. One advantage of LIB cells is that they are almost always sealed. This allows them to be used in any orientation possible (Kurzweil et al. 2015, p. 289). The most common form of lithium-ion cell package is a cylindrical cell package with a stainless steel exterior (Yang et al. 2011). This design is easy to manufacture and it can withstand very high pressures due to the resealable vent which can be used to release excess pressure.

Various LIB technologies have already been commercialized. One way to categorize and name these different technologies is based on the active material used in the positive electrode. The most commonly used LIB technologies used in stationary applications, according to IRENA (2017, p. 65) are Lithium Manganese Oxide (LMO), Lithium Nickel Manganese Cobalt Oxide (NMC), Lithium Nickel Cobalt Aluminium (NCA), Lithium Iron Phosphate (LFP) and Lithium Titanate (LTO). The projected cycle life of the different LIB technologies in 2030 is depicted in Figure 23.

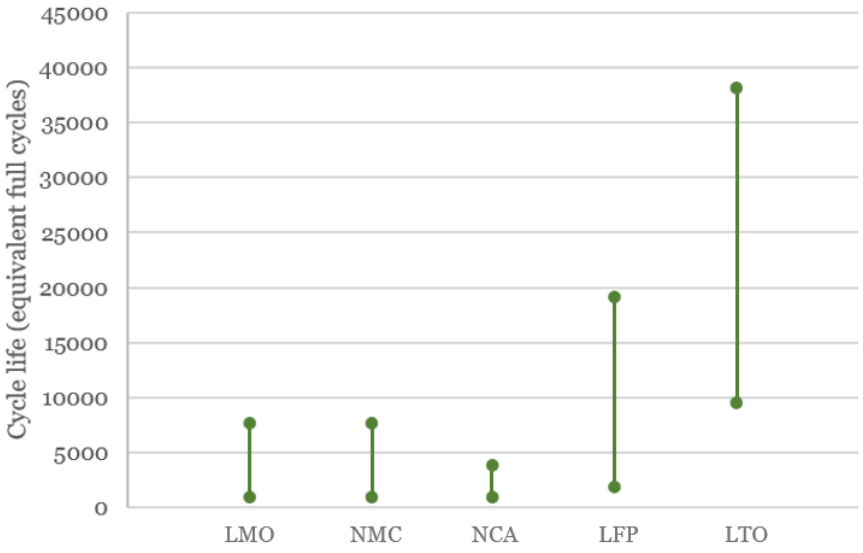

Figure 23: The projected cycle life of different LIB technologies in 2030. Modified from IRENA (2017, p. 124).

In Figure 23 LFP and LTO are projected to have the longest cycle life. These technologies have already the longest lifespan measured both in calendar years and in cycles (Kebede et al. 2022; IRENA 2017, p. 124). NCA has the shortest lifespan.

LMO is one of the cheapest lithium-ion technologies due to its reliance on cheap manganese (IRENA 2017, p. 66). It also has high power capabilities and the tree-dimensional spinel structure favours the lithium-ion flow in the cell, enabling high-current discharging capabilities. Despite these advantages, the low energy performance and moderate life cycle properties restrict the use of LMOs in stationary storage applications (IRENA 2017, p. 66).

LFP has an olivine lattice structure and it is considered to be one of the safest lithium-ion technologies (Kurzweil 2015, p. 276). The safeness of the technology comes from the great chemical and thermal stability, which is due to the low electrical conductivity. It also has a wide operation temperature range between – 30 °C and + 60 °C and offers a very long cycle life (Miao et al. 2019). LFP is considered to be a very suitable option for grid-scale energy storages, as it has good power characteristics and a high discharge rate (Stroe et al. 2017). LFP's drawbacks include lower energy properties than other technologies and the need for a sophisticated Battery Management System (BMS) to control the higher self-discharge rate, which will increase costs (IRENA 2017, p. 66). The low battery cell performance could however be increased by doping the structure with other metals such as titanium (Su et al. 2017).

NMC is one of the most used lithium-ion technologies today due to its excellent trade-off between safety, energy density, lifetime expectation and material costs. These properties have made it the most used technology for portable applications and automotive industry (Hesse et al. 2017). NMC was developed from LMO by adding nickel to it and its crystal structured material composes of equal parts of nickel, cobalt and manganese (IRENA 2017, p. 66). In addition to providing better energy, power and cycle life characteristics than LMO, the lower cobalt content in the structure enables the technology to have better thermal stability. One of the focuses of NMC development is on improving the energy and degradation properties of the technology (Hesse et al. 2017).

Another technology that is widely used in the EV market is NCA, which has better energy properties and higher discharge performance than NMC, while also being more cost effective due to the use of aluminium (IRENA 2017, p. 66). NCA also has greater cycling stability due to the reduced manganese dissolution (Wang et al. 2021). The drawbacks of NCA include, for example, the high degradation of electrolytes which has been researched extensively (Krause et al. 2017). Research has also been conducted to enhance the electrochemical performance and cyclability of NCA cathodes through layered coating techniques (Bin Abu Sofian et al. 2024). Through these advancements NCA batteries could become a popular technology also in grid-scale applications.

LTO differs from other lithium-ion technologies in that it uses titanium instead of graphite as the anode material. LTO offers the best life cycle performance out of the technologies mentioned and it is also safe due to titanium having better safety properties than graphite as an anode active material (da Silva Lima et al. 2023). LTO also has very good fast charging properties, however the costs are higher than with graphite-based batteries (Nemeth et al. 2020). This is partly due to the still low worldwide production volume (IRENA 2017, p. 67). Research has also been conducted to improve the low energy properties of LTO batteries, for example, through doping the structure with niobium (da Silva Lima 2023).

In Table 3 an overview of different LIBs is presented considering life cycle, round-trip efficiency, specific energy, energy density, discharging and charging current, advantages, limitations and applications. Life cycle at 80 % Depth of Discharge (DOD) indicates how long the battery can survive given that the battery is always discharged to 20 % of its full capacity (Koniak & Czerepicki 2017). Specific energy relates to how much energy can be stored in the battery relative to its' mass. Energy density indicates how much space the storage needs to store a specific amount of energy. For discharging and

charging currents, the C-rate indicates how quickly or slowly the battery can be charged or discharged. 1 C current is one-hour current, which would allow to charge the battery from 0 % to 100 % or discharge the battery from 100 % to 0% in one hour (Koniak & Czerepicki 2017). For example, for 5 C the same operation would only take a fifth of an hour, which is 12 minutes.

Table 3: An overview of the different LIB technologies based on certain metrics. Modified from Hannan et al. (2021); IRENA (2017, p. 124-125) and Koniak & Czerepicki (2017).

	Life cycle (80 % depth of discharge, DOD)	Efficiency (%)	Specific energy (Wh/L)	Energy density (W/L)	Discharging current	Charging current	Advantages	Drawbacks	Applications
LMO	300-700	80	100-150	2310	-	-	- High power capacity - Relatively safe	- Low capacity - Low efficiency	- Power tools -Medical devices - Electric powertrains
LFP	> 2000	92	90-120	1932	3 C	1 C	- Safe technology - Stable voltage discharge	- Low capacity	- Stationary energy storages, where high load current needed
NMC	1000-2000	95	150-220	735	2 to 3 C	1 C	- High capacity - High power capacity	- Complex monitoring -Expensive	- Electric vehicles - Industry
NCA	500	95	200-260	620	2 C	0.5 C	- High specific energy - Good stability	- Expensive -Limited power capacity	- Industry - Medical applications
LTO	3000-7000	96	50-80	620	5 to 10 C	5 to 10 C	- High life cycle - Fast charging - Safe technology -Wide thermal range	- Low specific energy - Expensive	- Uninterruptible power supply - Solar powered street lighting

In this thesis a LIB using LFP cell technology is used, as it has a high life cycle, high round-trip efficiency, relatively high specific energy and energy density and high C-rates. LFP is also one of the safest LIB technologies and the most used lithium-ion technology in grid-scale energy storage, representing over 50 % of overall global capacity. NMC is the second largest with a share of around 26 % (Sandia National Laboratories 2023). NMC was not selected due to the lower life cycle properties, even though they might be an attractive alternative to LFP. Also, NCA and LMO had too low life cycle estimates and LMO was deemed to be too inefficient. Even though LTO provides long life-times and high charge and discharge rates, the low specific energy and the associated high costs are the primary reasons for not selecting this technology.

5.2 Lithium-ion battery degradation

The life cycle performance is one of the most important aspects when comparing different battery chemistries. The life cycle properties of lithium-ion batteries are better than other battery types (Stecca et al. 2020). For example, the cycling life of a typical lead-acid battery is only around 300 full cycles.

The cycling life of a battery is decreased through degradation which is caused by a series of electrochemical processes occurring in the electrolyte and on the electrodes (García-Miguel et al. 2022). One electrochemical process causing battery degradation is the formation of a layer called the Solid Electrolyte Interphase (SEI) on the negative electrode (Wang et al. 2018). The formation of SEI consumes active lithium and electrolyte materials which in turn leads to capacity fading and decreases the power density of the battery.

The capacity degradation of a lithium-ion battery can be classified into calendar and cyclic aging. Cyclic aging is the degradation of the battery from the charge and discharge cycles and calendar aging decreases the battery capacity while it is idling (Mahesh et al. 2022). The main factors causing calendar aging are the battery SOC and temperature, while cyclic aging is mainly caused by the discharging and charging current, temperature and the DOD of charging and discharging cycles (Lam et al. 2023). Figure 24 depicts calendar ageing of a lithium-ion battery at different SOC and temperature levels.

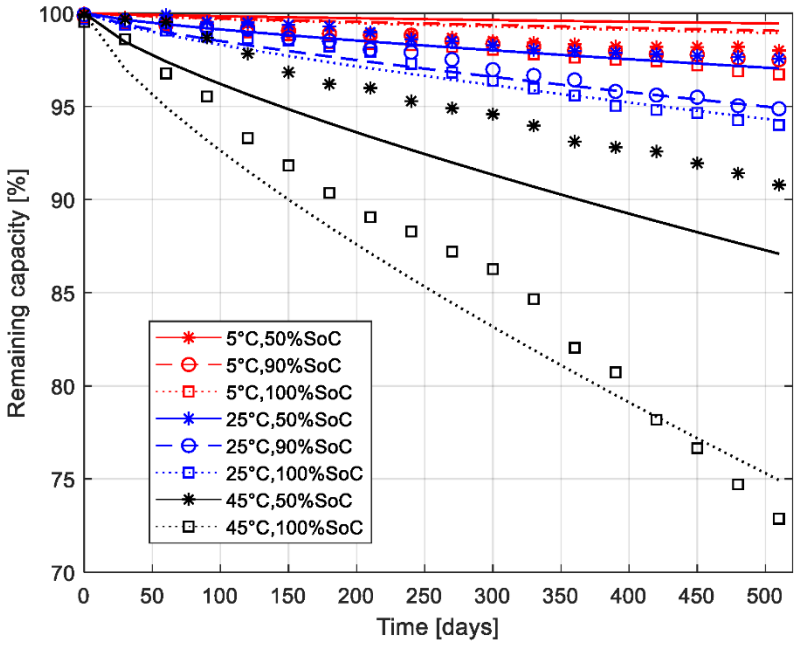

Figure 24: Lithium-ion battery calendar ageing at various SOC and temperature levels (Gailani et al. 2020).

As seen in Figure 24, higher temperature and SOC levels increase the degradation of the battery. Figure 25 depicts cycling ageing of lithium-ion batteries at various DOD and C-rates. It indicates that batteries with larger DOD ranges and higher C-rates experience much higher cycling degradation than batteries with smaller DOD ranges and C-rates (Gailani et al. 2020).

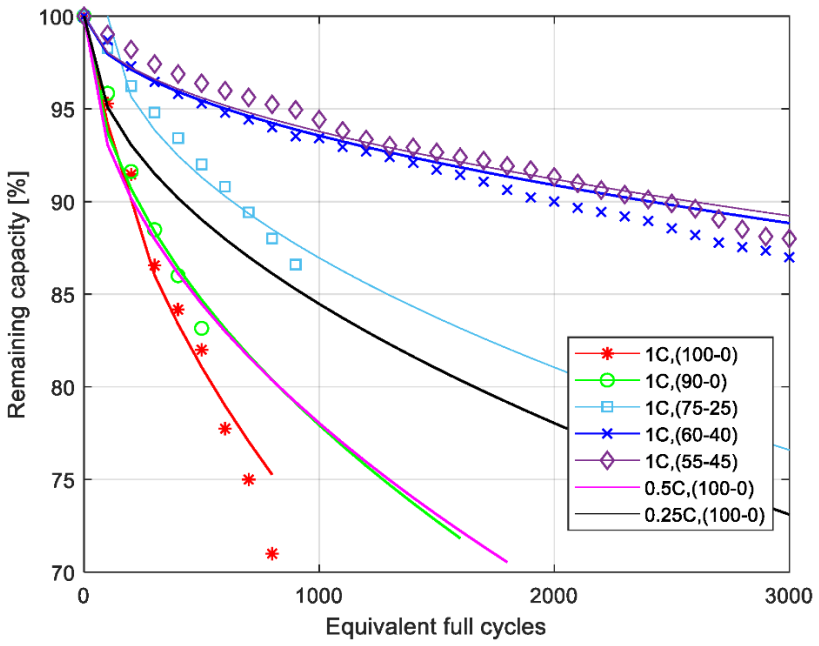

Figure 25: Cycling ageing of lithium-ion batteries at different DOD levels and C-rates (Gailani et al. 2020).

Lithium-ion battery degradation can be modelled in different ways. Sayfutdinov et al. (2020) created an empirical model to determine the cycling and idling capacity degradation rates using battery SOC and DOD, where idling corresponds to the calendar ageing. The idling and cycling degradation models have been given in (3) and (4).

$$\gamma^{idling}\left(SOC_{j_3,k_3}\right) = {A_{j_3}}^{idle} \cdot {SOC_{j_3,k_3}}^2 + {B_{j_3}}^{idle} \cdot SOC_{j_3,k_3} + {C_{j_3}}^{idle}, \quad (3)$$

$$\gamma^{cycling}\left(DOD_{j_3,k_3,n_3}\right) = {A_{j_3}}^{cycle} \cdot {DOD_{j_3,k_3,n_3}}^2 + {B_{j_3}}^{cycle} \cdot DOD_{j_3,k_3,n_3}, \quad (4)$$

where $\gamma^{idling}\left(SOC_{j_3,k_3}\right)$ and $\gamma^{cycling}\left(DOD_{j_3,k_3,n_3}\right)$ are fade rate characteristics from idling and cycling, SOC_{j_3,k_3} is the average daily SOC, DOD_{j_3,k_3,n_3} is the cycle depth of a discharge cycle and ${A_{j_3}}^{idle}$, ${B_{j_3}}^{idle}$, ${C_{j_3}}^{idle}$, ${A_{j_3}}^{cycle}$ and ${B_{j_3}}^{cycle}$ are fitting parameters.

Based on the model, the battery reached the End of Life (EoL) criterion after eight to ten years of operation (Sayfutdinov et al. 2020). The EoL is reached when the battery capacity decreases to a specific percentage of the initial capacity, after which it needs to be replaced (Ma & Qin 2022; Fallah & Fitzpatrick 2024). A typical EoL limit is 70-80 % of the initial capacity. Stroe et al. (2017) created a similar empirical model to estimate capacity fade of lithium-

ion batteries through cycling and calendar ageing but also considered the number of cycles for a certain cycle depth. The cycling and calendar aging models have been provided in (5) and (6).

$$C_{f\_cyc} = 0.021 \cdot e^{-0.01943 \cdot SOC_{av}} \cdot cd^{0.7162} \cdot nc^{0.5}, \quad (5)$$

$$C_{f\_cal} = 0.1723 \cdot e^{0.007388 \cdot SOC_l} \cdot t_s^{0.8} \quad (6)$$

where SOC_{av} is the average SOC during one cycle, SOC_l is the storage SOC level, nc is the number of cycles for a certain cycle depth cd and t_s is the storage time. C_{f_cyc} and C_{f_cal} represent the capacity fade from cycling and calendar degradation. Based on the model, Stroe et al. (2017) concluded that the lifetime of a LFP battery is between 8.5 and 13.5 years depending on the SOC management strategy. Mahesh et al. (2022) also used an empirical model to determine the lifetime of a LFP battery. They concluded that depending on the battery application the total number of charge and discharge cycles would be between 5800 and 6500.

Semi-empirical models have also been proposed to model battery degradation. Sarasketa-Zabala et al. (2015) proposed a model to predict battery cycle ageing for DODs between 10 % and 50 %. This has been depicted in (7).

$$Q_{loss,cyc}\ (10\% \leq DOD \leq 50\%) = Ah^{0.87} \cdot (\gamma_1 \cdot DOD^2 + \gamma_2 \cdot DOD + \gamma_3), \quad (7)$$

where $Q_{loss,cyc}$ is the percentage of capacity loss, Ah is the current throughput of the battery and γ_1, γ_2 and γ_3 are constant fitting parameters, which have been determined based on accelerated cell ageing tests.

In this thesis battery degradation is considered using a degradation cost coefficient similar to Bera et al. (2020). In this method the battery degradation coefficient is derived from battery lifetime energy throughput, total number of cycles and the cost of battery packs. The battery cost coefficient has been defined in (8).

$$c^{deg} = \frac{c^{battery}}{E^{let}}, \quad (8)$$

where c^{deg} is the degradation coefficient (€/MWh), $c_{battery}$ is the cost of battery packs and E^{let} is the lifetime energy throughput of the battery, which in turn is defined in (9) (Bera et al. 2020).

$$E^{let} = N^c \cdot E^s \cdot DOD^{avg}, \quad (9)$$

where N^c is the total number of cycles, E^s is the energy capacity of the battery and DOD^{avg} is the average DOD.

In this thesis, the total number of cycles for the BESS is determined from existing literature. Sophisticated battery degradation models rely on cycle counting when estimating the lifetime of a battery (Gundogdu & Gladwin 2018). Since batteries experience varying charge and discharge cycle depths throughout their lifetime, counting the total number of full cycles and comparing them can be challenging. One method to estimate the number of full cycles a battery undergoes within a given timeframe is by using Full Equivalent Cycle (FEC) counting (Gundogdu & Gladwin 2018). There are several methods to calculate the FEC count for a battery. Akpinar et al. (2023) employed an algorithm based on SOC cycle area calculation to calculate the FEC count for a battery used in frequency regulation. Similarly, Gundogdu & Gladwin (2018) proposed an algorithm to calculate the number of FECs for a grid-tied BESS used in frequency regulation. This algorithm analyzed smaller cycles with cycle depths less than 5 %, using grid frequency data.

In this thesis the number of FECs is calculated using a method proposed by Urquizo & Singh (2024). This method involves counting FECs by measuring the total charge and discharge energy throughput of the battery over a specific time period which is then compared to the battery's nominal capacity. This has been defined in (10):

$$EFC = \frac{\sum_{t=1}^{J}(P_t^{charge} + P_t^{discharge})}{2 \cdot E^s}, \tag{10}$$

where P_t^{charge} and $P_t^{discharge}$ are the charging and discharging power at time t and E^s is the battery capacity. The charge and discharge powers are then summed over the time period J. In this thesis FEC counting is used to analyze the usage rate of the BESS and the results are compared with existing literature.

5.3 BESS and its components

A single grid-scale BESS consists of various components which can be roughly divided into three groups based on their intended function. These groups are the battery components, grid connection components and the components needed for reliable system operation (Hesse et al. 2017). The system is usually built in a container. An overview of a typical BESS system setup has been depicted in Figure 26.

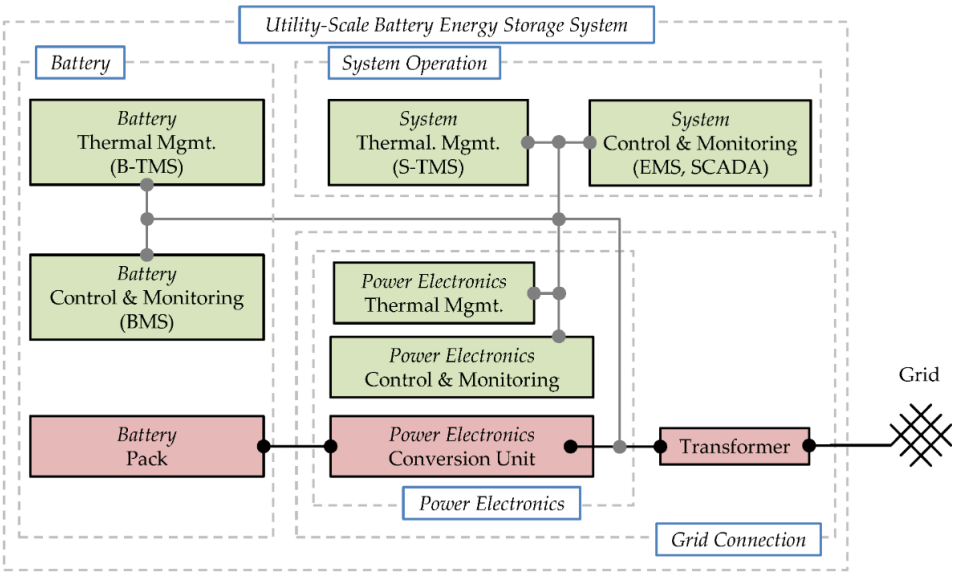

Figure 26: A schematic system setup for a typical grid-scale BESS (Hesse et al. 2017).

The battery components include the battery pack, the Battery Control and Monitoring System (BMS) and the Battery Thermal Management System (B-TMS). The battery pack consists of battery cells which usually have a nominal voltage of 1-4 V (Ma et al. 2023). For lithium-ion batteries the nominal cell voltage is between 3.7 V and 4.2 V (Rouhi et al. 2021). The battery cells are first connected in series or parallel to form a battery module, which are in turn connected in series to form a battery rack or cluster. Finally, the multiple battery racks are connected in parallel to form a grid-scale battery pack, which usually has a nominal voltage between 0.5 MWh to 2.5 MWh (Ma et al. 2023). The BMS system is responsible for overseeing the voltage, temperature and current levels to guarantee safe and reliable operation (Hesse et al. 2017). BMS also controls the SOC of the cells within the serial connection. The B-TMS controls the temperature of the cells based on given specifications and temperature gradients, to limit battery cell aging which strongly depends on operation temperature (Hesse et al. 2017).

The system operation components ensure the reliable operation of the overall system. It consists of the System Thermal Management System (S-TMS), the Energy Management System (EMS) and the System Control and Data Acquisition (SCADA) (Hesse et al. 2017). The EMS is responsible for the overall management and control of the power flow. EMS gathers information from the BMS about the cell specific State of Health (SOH) and SOC and controls the power flow based on the received information. SCADA is used for general monitoring of the system and may also include the fire protection and alarm units.

The grid connection can be divided into power electronics and the transformer (Hesse et al. 2017). Power electronics are used to convert Direct Current (DC) from the battery to Alternating Current (AC). The transformer in turn connects the overall system to the grid voltage level. The grid connection typically consists of multiple battery packs and inverter units. The power electronics can be either installed to individual battery packs or the battery packs can be connected parallel to a common DC-bus, which is then connected through the power electronics. Figure 27 depicts on the left a dedicated and on the right a parallel connection of battery packs and power electronics (Hesse et al. 2017).

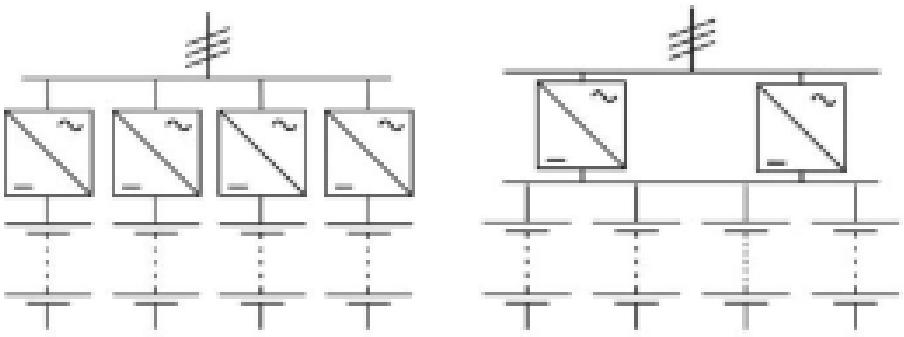

Figure 27: The depicted and parallel connection of battery packs and power electronics (Hesse et al. 2017).

The advantage of the dedicated connection of battery pack and inverter is that each battery pack can be individually controlled (Hesse et al. 2017). This configuration increases the reliability of the system, as a malfunction of a single battery pack or inverter does not affect the operation of other units. This configuration is also more efficient and decreases the burden of BMS (Ma et al. 2023). A complete single-line diagram for a BESS is depicted in Figure 28.

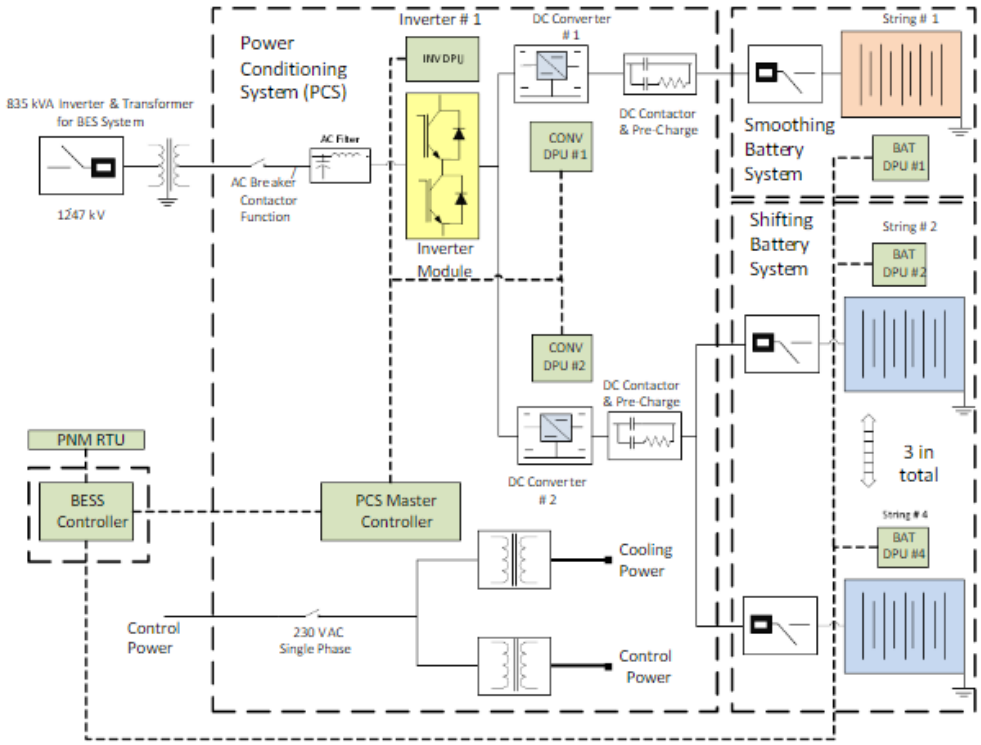

Figure 28: A single-line diagram of a BESS (Roberson et al. 2014).

In the system depicted in Figure 28, there is a 0.25 MW/1 MWh energy-shifting battery system and a 0.5 MW/0.35 MWh power-smoothing battery system (Roberson et al. 2014). The system is connected to the grid with a bi-directional inverter which is also connected to each battery system through bi-directional DC converters.

The optimal sizing of the BESS in terms of rated power and energy depend heavily on the application of the system and the specific requirements given (Das et al. 2018; Chreim et al. 2024). In Whitelee, Scotland a 50 MW /50 MWh BESS was installed to balance energy demand and the electricity production of the Whitelee Windfarm, which has 215 turbines and a rated power of 539 MW (Power Technology 2021). Similar projects have also been initiated in Finland. For example, Taaleri Energy Oy has invested in a 30 MW/36 MWh standalone BESS in Lempäälä, which operates in the Finnish FCR market (Taaleri Oyj 2023). Also, the French renewable energy producer Neoen has built a 30 MW/30 MWh standalone BESS in Ylikkälä to be used in frequency regulation (Neoen 2020). The Finnish energy company Ilmatar has in turn invested in a 30 MW/41 MWh BESS to be built adjacent to the 211 MW Piiparinmäki onshore wind farm (Ilmatar 2023).

5.4 BESS Life Cycle Costs (LCC)

LCC for any product refers to the sum of all the cost factors relating to the asset during its operational life (Kambanou & Lindahl 2016). The aim of LCC analysis is used to ensure that the asset provides best quality and function with the lowest overall cost to the ownership (Kambanou & Lindahl 2016). When evaluating the costs over the entire lifetime of the asset, there are many different aspects that need to be considered. Typically, the components that are to be included when evaluating the LCC for an asset include the Investment Costs (CAPEX), annual Operation and Maintenance Costs (OPEX) and the Residual Value (RV) of the asset at the end of its operational life (Ikäheimo et al. 2019, p. 180-183).

The CAPEX can consist of various items depending on the asset and its function (Ikäheimo et al. 2019, p. 180-183). For example, acquiring the product, building the surrounding infrastructure, market research, equipment installation and staff training are items that should be considered when assessing the investment costs for an asset. OPEX in turn refers to the annual cash outflows which occur when the asset is in the operation phase. These could involve personnel salary costs, equipment repairs and maintenance and insurance payments. Evaluating the RV of an asset is often difficult and it is usually assumed to be zero to simplify the investment calculations. However, in some cases the RV could be even negative due to recycling fees or storage costs (Ikäheimo et al. 2019, p. 180-183).

On top of the CAPEX, OPEX and RV, an investor also has to consider the investment holding period, which is the period during which an investment is in operation and from which annual cash in- and outflows are estimated to be generated (Ikäheimo et al. 2019, p. 180-183). The technical holding period refers to how long the asset is modern enough to operate. Physical holding period in turn refers to how long the asset can operate due to wearing. For example, for a BESS the degradation of the battery cell due to high operation temperatures, SOC, charge-discharge rate and cycle count significantly limit the physical holding period (Collath et al. 2022).

5.4.1 Investment Costs (CAPEX)

The CAPEX for a BESS includes many different items varying from land acquisition and legal fees to electrical infrastructure and labour costs. The components of CAPEX for a grid-scale BESS have been depicted in Table 4.

Table 4: The components of CAPEX for a grid-scale BESS. Modified from (NREL 2023).

Balance of the System	Balance of System
Electrical Infrastructure & Interconnection	Internal and control connections On-site electrical equipment Power electronics Transmission substation upgrades Wiring and conduits DC cabling Inverter Switch gear Transformers EMS Monitors, controls and communications
Generation Equipment & Infrastructure	Plant construction Power plant equipment Battery pack BMS TMS Fire suppression system Battery racking Foundation for battery and inverters Inverter housing
Installation & Indirect	Distributable labour and materials Engineering Start up and commissioning
Owner's Costs	Development costs Environmental studies and permitting Insurance costs Legal fees Preliminary feasibility and engineering studies Property taxes during construction
Site	Access roads Buildings for operations and maintenance Fencing Land acquisition Site preparation Transformers Underground utilities

One major cost component of the overall CAPEX for a BESS is the battery pack. In 2023, the battery pack prices hit record low of 127.95 €/kWh, decreasing 14 % compared to the previous year. The decrease in prices was mainly driven by decreasing component and material prices, increased production capacity across the whole battery value chain and increased demand (BloombergNEF 2023a). The prices are also expected to fall again to new record lows in 2024 (Sekine 2024). Different estimations of CAPEX for various grid-scale BESSs from selected sources have been given in Table 5.

Table 5: Different estimations of CAPEX for various BESSs from selected sources.

Rated power	C-rating	CAPEX (€/kWh)	Source
-	0.17 C	276	BloombergNEF 2023b
-	-	184	IEA 2023a, P. 100
-	-	368	Setiawan et al. 2022
-	-	552	Setiawan et al. 2022
2 MW	1 C	552	Rystad Energy 2023, p. 4
2 MW	0.5 C	423	Rystad Energy 2023, p. 4
10 MW	1 C	469	Rystad Energy 2023, p. 4
10 MW	0.5 C	391	Rystad Energy 2023, p. 4
10 MW	0.5	352	WSP 2020, p. 5
10 MW	0.5 C	433	Viswanathan et al. 2022, p. 12-17
10 MW	0.25 C	377	Viswanathan et al. 2022, p. 12-17
25 MW	0.25 C	322	AES Indiana 2022, P. 79
25 MW	0.25 C	253	AES Indiana 2022, P. 79
25 MW	0.25 C	368	AES Indiana 2022, P. 79
25 MW	0.17 C	307	AES Indiana 2022, P. 79
25 MW	0.17 C	269	AES Indiana 2022, P. 79
25 MW	0,17 C	368	AES Indiana 2022, P. 79
50 MW	1 C	460	Rystad Energy 2023, p. 4
50 MW	0.5 C	352	WSP 2020, p. 5
50 MW	0.5 C	377	Rystad Energy 2023, p. 4
100 MW	0.5 C	308	Asealen 2023, p. 12
100 MW	0.5 C	290	WSP 2020, p. 5
100 MW	0.5 C	357	Rystad Energy 2023, p. 4
100 MW	0.25 C	262	Asealen 2023, p.12
100 MW	0.1 C	328	Viswanathan et al. 2022, p. 12-17
200 MW	0.25 C	387	Newell et al. 2022, p. 72; Marzewski 2023, p. 11

As seen in Table 5, the CAPEX for a BESS depends significantly on the rated power and the C-rating of the system. The overall range of CAPEX for a BESS can be estimated to be between 300 €/kWh and 550 €/kWh, depending on the size and C-rate of the battery. The various CAPEX estimates have been converted from U.S. dollars and British pounds to Euros, using the following exchange rates 1 $ = 0.92 € and 1 £ = 1.17 €. Figure 29 depicts changes in required CAPEX for a BESS with different rated powers and C-rates.

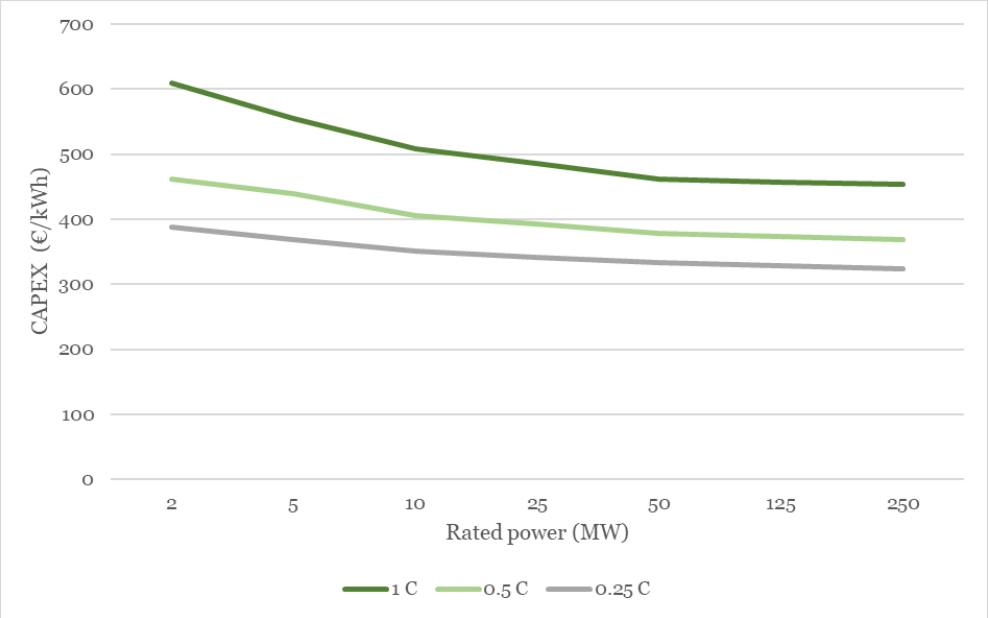

Figure 29: The CAPEX for a BESS with different capacities and storage durations. Modified from Rystad Energy (2023, p. 4).

Based on the graph in Figure 29, for a 50 MW/50 MWh BESS, the CAPEX would be around 450 €/kWh, which is generally in line with the other findings earlier. In Finland, the recently announced 30 MW/36 MWh standalone BESS for Taaleri Oyj in Lempäälä had a CAPEX of around 20 000 000 € which would correspond to 555 €/kWh (Cision 2023), which is in line with other observations. The CAPEX estimations are for a standalone BESS.

5.4.2 Operation and Maintenance Costs (OPEX)

Also, the OPEX for a BESS include different components. These cost components can be divided into fixed costs and maintenance and replacement costs. Components of OPEX for a BESS are depicted in Table 6.

Table 6: The components of OPEX for a typical BESS (NREL 2023).

Fixed costs	Administrative fees Administrative labour Insurance Land lease payments Legal fees Operating labour Site security Property taxes Taxes Other
Maintenance	General maintenance Scheduled maintenance over technical life Unscheduled maintenance over technical life
Replacement costs	Annualized present value of large component replacemenr over technical life

The OPEX, much like the CAPEX for a BESS, depend significantly on the size of the system. Different warranty arrangements can also affect the overall OPEX significantly (WSP 2020, p. 5). OPEX can be measured in different terms. In this thesis €/kWh/year and the percentage of total CAPEX to measure the annual OPEX is used. Table 7 depicts different estimations of OPEX for a typical grid-scale BESS from various sources.

Table 7: Different estimations of OPEX for a grid-scale BESS.

Rated power	C-rating	OPEX (€/kWh/year)	OPEX (% of CAPEX)	Source
-	-	-	4 %	Setiawan et al. 2022
200 MW	0.25 C	8.5	-	Newell et al. 2022, p. 71; Marzewski 2023, p.11
100 MW	1 C	1.6 - 8.9	-	Lazard 2023, p. 41
100 MW	0.5 C	1.2 - 7.1		Lazard 2023, p. 41
100 MW	0.5 C	-	3 %	Asealen 2023, p. 12
100 MW	0.25 C	1.1 - 6.2		Lazard 2023, p. 41
100 MW	0.25 C	-	3.3 %	Asealen 2023, p. 12
60 MW	0.25 C	8	-	Ramasamy et al. 2023, p. 28-30
40 MW	1 C	-	1 - 2 %	ENTEC 2023
25 MW	0.25 C	6.25	-	AES Indiana 2022, p. 80

The OPEX estimations vary from source to source, however, it can be observed from Table 7 that the annual OPEX for a grid-scale BESS vary between 1 % and 4 % of the overall CAPEX of the system. Figure 30 depicts the behaviour of OPEX for a grid-scale BESS with varying energy capacities.

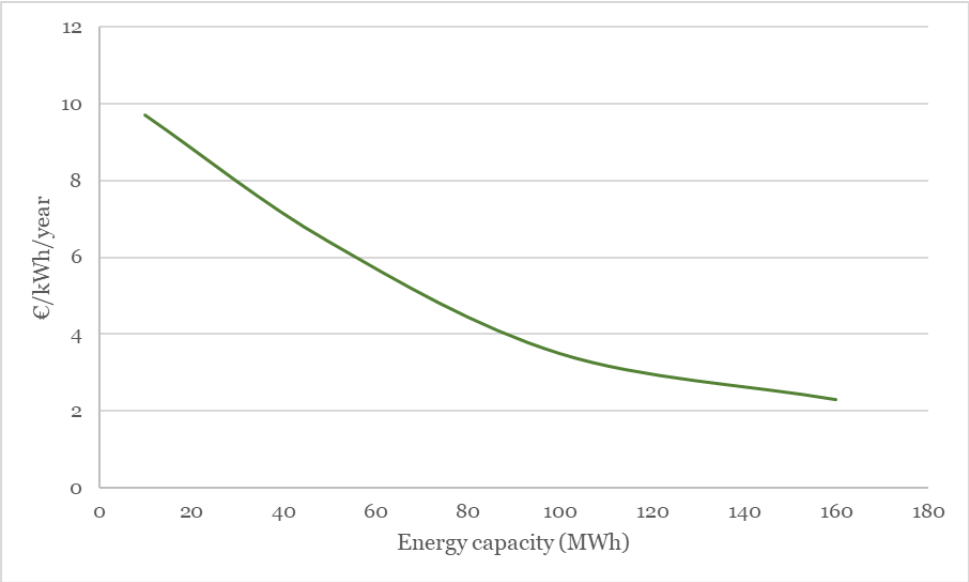

Figure 30: The yearly OPEX in relation to the energy capacity of a BESS (WSP 2020, P. 5).

In Figure 30, the unit cost OPEX decreases more steeply than CAPEX, when the size of the BESS is increased. For a 10 MWh system the unit cost of OPEX is nearly 10 €/kWh/year but for a nearly 200 MWh system they are only around 2 €/kWh/year. These estimations are in line with the values presented in Table 7. These values for OPEX have been estimated for a standalone BESS.

6 Different investment calculation methods

In this chapter different investment calculation methods are introduced, including the Net Present Value (NPV) method, Internal Rate of Return (IRR) method and the payback period method. For each method, the general formulations are presented and method specific advantages and disadvantages are reviewed.

6.1 Net Present Value (NPV) method

One of the most preferred metrics to quantify the valuation of a project is the NPV method, in which all of the cash in- and outflows which happen during the lifetime of the investment are discounted to the same point in time (Arnold 2014, p. 186). This time is usually the beginning of the investment (Ikäheimo et al. p. 186). If the sum of all cash flows is positive, the investment can be considered a profitable one which means that it adds value to the company. A negative NPV in turn means that the investment will likely decrease the value of the company which is to be avoided (Arnold 2014, p. 186). (11) depicts the formula for calculating the NPV (Ikäheimo et al. 2019, p. 186).

$$NPV = CAPEX + \sum_{t_1=1}^{n} \left(\frac{Net\ cash\ flow_t}{(1+r)^{t_1}}\right) \tag{11}$$

CAPEX is the initial investment cost, net cash flow is the difference between cash inflows and outflows for the year t_1 and r is the discount rate (Ikäheimo et al. 2019, p. 186).

If the company drives to maximize the value of its shareholders, it should only invest in projects with a positive NPV (Ikäheimo et al. 2019, p. 186). The drawback of the NPV method as an investment calculation method is that is does not consider the capital tied up to the investment. This means that both small and large investments are treated equally, which is not accurate if the company has only a certain amount of capital and cannot finance every investment. There are also major uncertainties with the future cash flows which are usually very hard to predict accurately (Huang et al. 2022). The strength of the method is that it indicates clearly whether the investment adds value to the company or not. It also indicates how much the value increases or decreases (Ikäheimo et al. 2019, p. 186).

6.2 Internal Rate of Return (IRR) method

The IRR method is used to measure the percentage yield on an investment, which is then compared to the investor's minimum rate of return (Ruegg &

Marshall 1990). If the calculated IRR is greater than the investor's minimum rate of return, the investment can be considered profitable. Usually, IRR is obtained by calculating the rate of return when NPV is zero. The formula for calculating the IRR has been given in (12) (Ikäheimo et al. 2019, p. 185).

$$NPV = \sum_{t_1=1}^{n} \left(\frac{FCF}{(1+IRR)^{t_1}} + \frac{RV}{(1+IRR)^{t_1}}\right) + CAPEX = 0 \qquad (12)$$

FCF is the free cash flow for the year t_1 and RV is the residual value of the investment at year t_1. The RV for a BESS is hard to determine as it involves different cost components, such as recycling of the battery modules, disconnection and removal of electrical equipment and transportation of the materials from the site (Viswanathan et al. 2022, p. 17-18).

One advantage of IRR is it being a strictly defined term which clearly illustrates the profitability of the project. This method allows the management to choose the highest IRR, which exceeds the minimum rate of return, allowing profit maximation (Huang et al. 2022). A clear advantage of the IRR over NPV is that it allows the management to compare the profitability of different projects due to the form of ratio, while avoiding the use of uncertain interest rates (Huang et al. 2022). One clear disadvantage of IRR is that it assumes strict preconditions on the payment streams which must be flat and annual (Huang et al. 2022). IRR also assumes that the capital raised for another investment can be released and invested straightaway to an alternate investment which would yield the IRR (Ikäheimo et al. 2019, p. 185). Also, the results given by IRR calculations can be hard to analyze, as it can give multiple correct answers.

6.3 The payback period method

The payback period is one of the simplest investment calculation methods. This method indicates the time period within which the investment pays back its' initial costs at the beginning, in other words the time it takes for the cash flows generated by the investment to equal the initial investment (Ikäheimo et al. 2019, p. 183). The quicker the investment can earn its money back the better, as it decreases the risk of uncertain cash flows further into the future. The formula for calculating the payback period for an investment has been given in (13) (Ikäheimo et al. 2019, p. 183).

$$Payback\ period = \sum_{t_1=1}^{n} (Net\ cash\ flow_{t_1}) - CAPEX = 0 \qquad (13)$$

N is the number of years. As can be seen from (13), the obvious deficiency of the payback period method is that it does not consider the cash flows which happen after the payback time (Al-Ani 2015). This can lead to the rejection of investments which require longer capital recovery times, even though they would otherwise be very profitable. (13) also indicates that the payback period method does not consider the time value of money when calculating the cash flows. The discounted payback period can be simply obtained by discounting the future net cash flows, which is done by multiplying the future net cash flows with the discount rate (Al-Ani 2015).

One of the strengths of the payback period method is that it is relatively easy to calculate, as the investor usually defines a minimum period within which the investment must pay itself back (Ikäheimo et al. 2019, p. 184). Payback period is also used because it emphasizes the cash flows generated in the near future. This potentially decreases the need to predict the very uncertain cash flows generated far in the future. However, due to the before mentioned disadvantages of the method, it is often used as a complementary method to other investment calculation methods (Ikäheimo et al. 2019, p. 184).

7 Optimization problem solving

In this chapter an overview of optimization problem solving is presented. First the basics of optimization problem modelling are given, including the formulation of a Nonlinear Programming (NLP) problem and the graphical description of an arbitrary optimization problem. This is followed by an examination of Mixed-Integer Programming Problems (MILPs) in a more detail, including the general mathematical formulation and some linearization methods, which can be used to handle nonlinearities and discontinuities which can be present in MILPs.

Optimization is the process of maximizing or minimizing a desired objective function, while simultaneously satisfying the pre-defined constraints (Belegundu & Chandrupatla 2011, p. 1). Rao (2020, p. 1) defines optimization as the act of obtaining the best possible result under given circumstances. Optimization problem modelling is used to translate a physical real-life problem into a mathematical problem (Belegundu & Chandrupatla 2011, p. 1). Optimization techniques are used widely in different applications, ranging from manufacturing and production control in different industries to minimizing transportation costs and scheduling airline operations.

Today optimization problems are solved mainly using optimization software packages. There is a wide range of these packages used to solve even the most complex and time-consuming optimization problems. Popular packages include MATLAB optimization toolbox, General Algebraic Modeling System (GAMS) tool, CPLEX and Excel Solver (Belegundu & Chandrupatla 2011, p. 3-4). There are also simulation-based software packages such as Altair and Genesis.

7.1 Optimization problem modelling

Many optimization problems in engineering can be expressed in terms of minimizing or maximizing an objective function subject to equality and inequality constraints (Belegundu & Chandrupatla 2011, p. 4). The inequality constraints could be either less-than-or-equal-to or greater-than-or-equal-to type (Sioshansi & Conejo 2017, p. 2). The optimization problem also includes decision variables, which represent the decisions being optimized. Figure 31 depicts the minimization and maximization of an arbitrary function f (Rao 2020, p. 1).

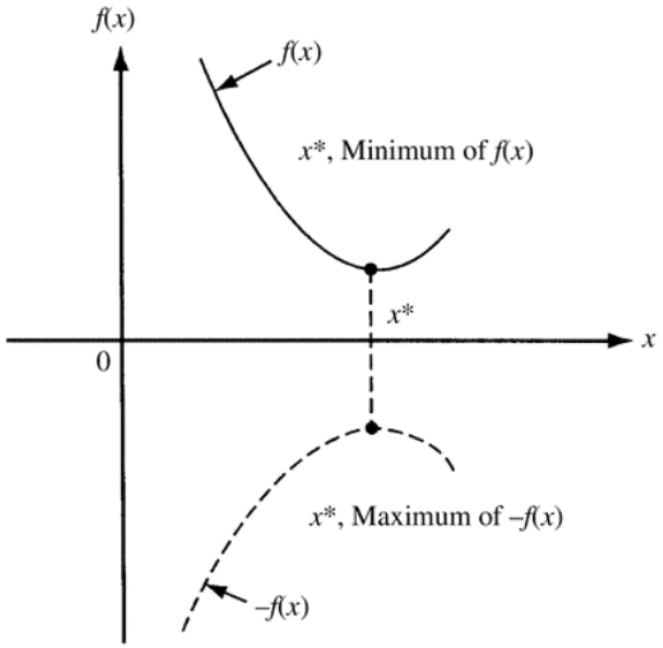

Figure 31: The minimization and maximization of an arbitrary function f(x) (Rao 2020, p. 1).

As can be seen from Figure 31, maximizing f is equivalent to minimizing $-f$. There is no single optimization method, which can be used to solve all different problems. The most general programming problem is Nonlinear Programming (NLP) problem (Rao 2020, p. 18). A problem is an NLP problem if any constraint or the objective function is nonlinear. All optimization problems can be considered as special cases of NLP (Rao 2020, p. 18). The most used optimization technique is Linear Programming (LP), which is relatively easy to formulate, understand and use (Belegundu & Chandrupatla 2011, p. 6-7). In LPs all terms are required to be linear. Also, several other advanced modelling categories exist such as Integer Linear Programming (ILP), Mixed-Integer Linear Programming (MILP), Mixed Integer Nonlinear Programming (MINLP), Quadratic Programming (QP) and convex programming.

In ILP all variables are required to be integers and in MILP some variables are required to be integers and others are continuous. MINLP is similar to MILP, but the problem is nonlinear and in QP the objective function is a quadratic function and all the constraints are linear. In convex programming the objective function is either convex for minimization or concave for maximization (Belegundu & Chandrupatla 2011, p. 6-7). An arbitrary function f is said to be convex if a line segment between any two points lies entirely above or on the graph of f (Rao 2020, p. 761). An arbitrary function f is said to be concave if a line segment between any two points does not yield a higher

value than the function f. When a function f is convex, any local minimum or maximum is also the global minimum or maximum (Rao 2019, p. 761). The general form of an NLP has been given in (14) (Belegundu & Chandrupatla 2011, p. 4):

$$\begin{aligned} &minimize\ \ f(x) \\ &subject\ to\ g_i(x) \leq 0 \quad i = 1,..,m \\ &and \qquad h_j(x) = 0 \quad j = 1,..,L \\ &and \qquad r^L \leq r \leq r^U, \end{aligned} \tag{14}$$

where $r = (r_1, r_2, .., r_{n_1})^T$ is a column vector of n_1 real-valued decision variables, $g_i(x)$ represents all of the inequality constraints, $h_j(x)$ represents all of the equality constraint and vectors r^L and r^U are explicit lower and upper bounds for the decision variables (Belegundu & Chandrupatla 2011, p. 4). In a two-dimensional case, where there are only two decision variables, the optimization problem can be depicted and solved graphically, where the constraints define the feasible region in the plane (Rao 2020, p. 8). This has been illustrated in Figure 32.

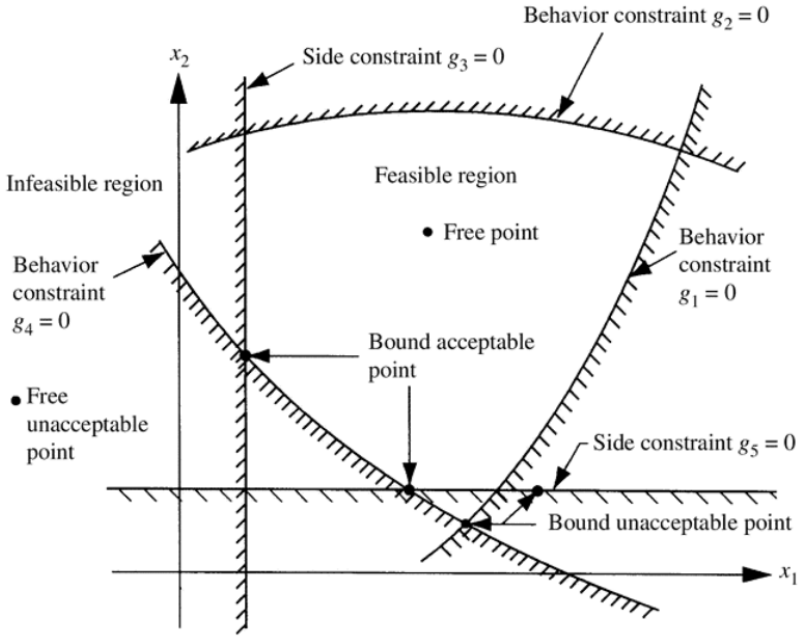

Figure 32: The feasible region of an arbitrary optimization problem (Rao 2020, p. 8).

After the constraints have been drawn to define the feasible region of the problem, level curves of the objective function can be drawn to form an objective function surface, from which an optimal point can be determined. This has been depicted in Figure 33.

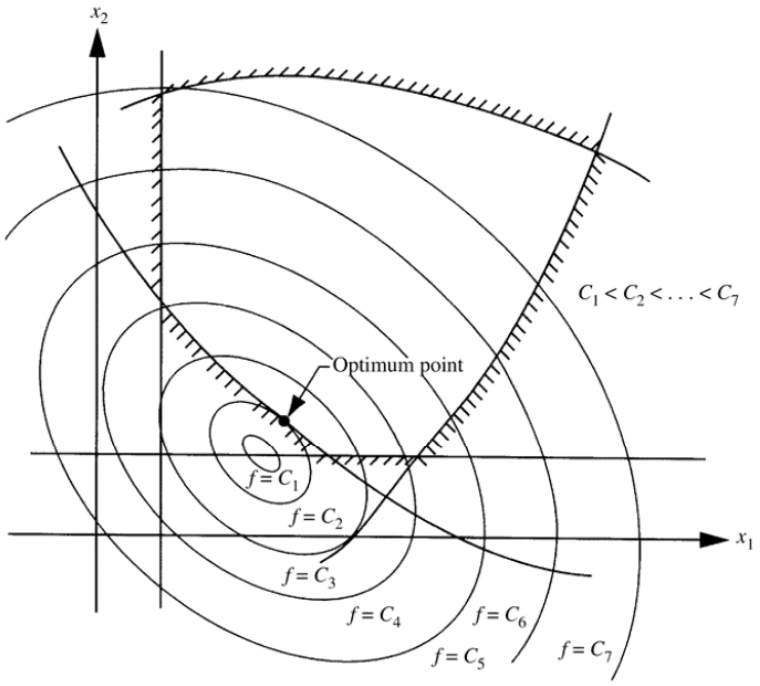

Figure 33: Level curves of an arbitrary objective function *f* (Rao 2020, p. 10).

As can be seen from Figure 33, the optimal point can be determined rather easily once the level curves of the objective function have been drawn across the feasible region illustrated by the constraints (Rao 2020, p. 9). However, as the amount of decision variables increases to three or more, the illustration of the feasible region and the level curves of the objective function become so complex that the problem cannot be solved graphically and has to be solved mathematically.

7.2 Mixed-Integer Linear Programming (MILP)

MILP problems are optimization problems with a linear objective function and linear constraints. MILP problems differ from standard LP problems in that they also include variables, which are constrained to take integer values (Sioshansi & Conejo 2017, p. 125). Integer variables can also be referred to as binary variables and they are restricted to take only two values, which are almost always either 0 or 1. These variables are typically used to model logical decisions or conditions. Sioshansi & Conejo (2017, p.138) have given a general form of a MILP in (15) :

$$
\begin{aligned}
&\max_{r_1,\ldots,r_{n_1}} \; c_0 + \sum_{k=1}^{n_1} c_k \cdot r_k \\
&s.t. \quad \sum_{k=1}^{n_1} A^e_{j,k} \cdot r_k = b^e_j, \quad \forall\, j = 1,\ldots,\, m_e \\
&\qquad \sum_{k=1}^{n_1} A^g_{j_1,k} \cdot r_k \geq b^g_{j_1}, \quad \forall\, j_1 = 1,\ldots,\, m_g \\
&\qquad \sum_{k=1}^{n_1} A^l_{j_2,k} \cdot r_k \leq b^l_{j_2}, \quad \forall\, j_2 = 1,\ldots,\, m_l \\
&\qquad r_k \in \mathbb{Z} \qquad\qquad for\ some\ k\ = 1,..,n_1 \\
&\qquad r_k \in \mathbb{R} \qquad\qquad for\ the\ remaining\ k = 1,\ldots,n_1,
\end{aligned}
\tag{15}
$$

where m_e, m_g and m_l are the amount of equal-to, greater-than-or-equal-to and less-than-or-equal-to constraints (Sioshansi & Conejo 2017, p. 138). The coefficients, $A^e_{j,k}, \forall\, k = 1,\ldots,\ n_1, j = 1,\ldots,\ m_e, A^g_{j_1,k},\ \forall\, k = 1,\ldots,\ n_1, j_1 = 1,\ldots,\ m_g$ and $A^l_{j_2,k}, \forall\, k = 1,\ldots,\ n_1,\ j_2 = 1,\ldots,\ m_l$ are all constants. Also, terms b^e_j, $\forall j = 1,\ldots,\ m_e, b^g_{j_1},\ \forall j_1 = 1,\ldots,\ m_g$ and $b^l_{j_2},\ \forall j_2 = 1,\ldots,\ m_l$ and $c_0, \ldots, c_{n_1}$ are all constants. Some of the decision variables are constrained to take integer values, as given in (16) and (17) (Sioshansi & Conejo 2017, p. 138):

$$
r_k \in \mathbb{Z}, for\ some\ k = 1, \ldots, n_1, \tag{16}
$$

where:

$$
\mathbb{Z} = \{\ldots., -2, -1, 0, 1, 2, \ldots.\}, \tag{17}
$$

is the standard notation for integer values. Other variables, which are not constrained to be binary variables can take any non-integer values (Sioshansi & Conejo 2017, p. 138).

Using binary and real variables together in a MILP can sometimes lead to nonlinearities and discontinuities in the model, which need to be linearized for easier solving (Sioshansi & Conejo 2017, p. 149). One example of a case like this is the product of a real and binary variable. Assuming an arbitrary real variable $d \in \mathbb{R}$ and a binary variable $y \in \{0, 1\}$. The product q can be defined as $q = d \cdot y$, where q can only take a value of 0 or d depending on if the value of y is 0 or 1. This expression can be linearized using a method by Sioshansi & Conejo (2017, p.149-150) given in (18), (19), (20) and (21).

$$-l \leq d \leq u \tag{18}$$

$$q = d - z \tag{19}$$

$$-l \cdot y \leq d \leq u \cdot y \tag{20}$$

$$-l \cdot (1 - y) \leq s \leq u \cdot (1 - y), \tag{21}$$

where u and $-l$ are explicit boundaries imposed on d and s is a new variable which acts as a slack variable in the definition. The upper and lower bounds in (18) can be imposed in the optimization problem by making the lower bound $-l$ sufficiently small and the higher bound u sufficiently large. After d has been bounded, the variable q can be defined using the constraints (19), (20) and (21).

The product of one binary and one continuous variable can also be linearized using equations (22)-(26). Here B is a continuous and bounded variable and $C \in \{0,1\}$ is a binary variable. The nonlinear product $C \cdot B$ can be linearized by defining a new variable D (Kordkheili et al. 2021).

$$D = C \cdot B \tag{22}$$
$$C \cdot \underline{B} \leq D \leq C \cdot \overline{B} \tag{23}$$
$$D \leq B - \underline{B} \cdot (1 - C) \tag{24}$$
$$D \geq B - \overline{B} \cdot (1 - C) \tag{25}$$
$$\underline{B} \leq B \leq \overline{B} \tag{26}$$

Linearization is also needed when dealing with the multiplication of two binary variables. Assuming two binary variables $y_1 \in \{0, 1\}$ and $y_2 \in \{0, 1\}$. The nonlinear product $y_1 \cdot y_2$ can be linearized using an additional binary variable $w \in \{0,1\}$ (Kordkheili et al. 2021).

$$w = y_1 \cdot y_2 \tag{27}$$
$$w \leq y_1 \tag{28}$$
$$w \leq y_2 \tag{29}$$
$$w \geq y_1 + y_2 - 1 \tag{30}$$

MILP problems might also include situations, where the enforcement of an either-or constraint is necessary (Sioshansi & Conejo 2017, p. 148). Assuming a situation, where either the constraint (31) or (32) must be enforced (Sioshansi & Conejo 2017, p. 148):

$$\sum_{k=1}^{n_1} a_{1,k} r_k \leq b_1, \tag{31}$$

$$\sum_{k=1}^{n_1} a_{2,k} r_k \leq b_2, \tag{32}$$

but not both. Here $a_{1,k}$, $a_{2,k}$, b_1 and b_2 are parameters. In an optimization problem, (31) and (32) would be represented with a single constraint, including a logical "or" statement, which is not valid. The logical "or" statement can be linearized using an arbitrary binary variable y, which has been defined in (33) (Sioshansi & Conejo 2017, p. 148).

$$y = \begin{cases} 1, if\ the\ constraint \sum_{k=1}^{n_1} a_{1,k} r_k \leq b_1\ is\ enforced, \\ 0, otherwise \end{cases} \tag{33}$$

We can then restate the constraints (31) and (32) using the Big M method which is described in (34) and (35) (Sioshansi & Conejo 2017, p. 148):

$$\sum_{k=1}^{n_1} a_{1,k} r_k \leq b_1 + M3 \cdot (1 - y) \tag{34}$$

$$\sum_{k=1}^{n_1} a_{2,k} r_k \leq b_2 + M4 \cdot y, \tag{35}$$

where the variables $M3$ and $M4$ are sufficiently large constants. To see how the formulation works, it is assumed that binary variable y has the value of 1. This means that (34) would be the same as (31), and if the variable $M4$ is large enough, (35) is relaxed so that any values for x would satisfy this constraint. Hence (35) is then not imposed on the problem. Since (35) is not imposed on the problem, (34) becomes the binding constraint (Sioshansi & Conejo 2017, p. 148).

Most MILPs, especially if they take the form of the generic MILP which was introduced in (15), are solved by the branch-and-bound algorithm (Sioshansi & Conejo 2017, p. 155-156). The problem solving starts by solving a relaxed version of the original problem. Relaxation in optimization problem solving is a method where one or more of the original constraints of the problem are loosened, which eases the problem solving (Sioshansi & Conejo 2017, p. 152). This is due to the available feasible region being larger. After the relaxed

problem has been solved, the algorithm adds constraints to the relaxed linear problem, thus generating new optimization problems and solving them (Sioshansi & Conejo 2017, p. 155-156). By solving sufficient amounts of new optimization problems, the algorithm is able to provide upper and lower bounds to the original MILP, which decrease and increase after every new problem. This process is then continued until all of the additional problems are solved and the optimal solution of the original problem is found (Sioshansi & Conejo 2017, p. 155-156).

8 Utilization of a BESS in wind power balance error management

In this chapter, the utilization of a BESS in wind power balance error management is researched. The research methods and the battery characteristics are presented, after which the used data and data sources are introduced. Then the mathematical formulation of the model is presented, followed by the analysis of the obtained simulation results. This chapter concludes with a sensitivity analysis, where the robustness of the results is assessed.

8.1 Research methods and battery characteristics

The research method used to assess the utilization of a BESS to decrease wind power imbalance costs is to mathematically formulate an optimization problem based on the knowledge acquired from the literature review and collected data. The optimal operation of the battery is achieved by maximizing the profit of the WFO in the DA market. This is achieved by selling the produced power from the wind power plant in the DA market and decreasing the imbalance costs using the BESS. The model also considers the cost of battery degradation and the overall OPEX of the storage system. The model is deterministic, meaning that it considers perfect information about the hourly market prices and imbalances in the simulation. The owner of the wind farm and the BESS is assumed to be a price taker, thus is unable to influence the market price.

The response time of a battery is assumed to be immediate, as the intrinsic non-linear dynamic response times of a BESS, such as ramp rates and delays, are neglected (Alcaide-Godinez et al. 2022). The imbalance costs are also assumed to pass through to the wind farm and BESS owner directly without any intermediaries. The wind farm and BESS are assumed to be connected directly to the main grid operated by Fingrid. The model is optimized on an hourly basis.

The formulated model is a Mixed-Integer Linear Programming (MILP) model. Following the model formulation, the simulation is carried out in the General Algebraic Modelling System (GAMS), which is a high-level modelling system for mathematical programming and optimization (GAMS 2023). The solving process is handled using LINDO, which is a global solver for mathematical optimization (LINDO Systems 2024). In the simulation, 2023 electricity prices and wind power data are used. The battery's performance is analyzed across four distinct scenarios. For each scenario, first the baseline case is tested, where the wind farm only participates in the electricity market without using the battery. The generated cash flows of the baseline case are

then compared with the cash flows of the full model, where the BESS tries to balance the wind farm forecast error. Furthermore the operation of the BESS in each scenario is analyzed. Finally, both the baseline case and the full model are simulated for the year 2023 and the difference in generated revenue and the operation of the battery are examined.

The analysis of the annual operation of the battery in 2023 also includes a profitability analysis using some of the investment calculation methods presented in Section 6. This analysis examines the value of the investment over the entire investment holding period of 10 years. In the profitability analysis it is assumed that the 2023 conditions remain the same throughout the entire investment holding period. A more detailed profitability analysis would have required precise market analysis and accurate forecasting of electricity prices and wind power production far into the future, which is beyond the scope of this thesis.

In the simulation, a 30 MW/30 MWh lithium-ion battery using LFP battery cell technology is used, as it is the most used battery technology in grid-scale battery storage systems. It is also the safest lithium-ion technology, has good power characteristics and a long cyclic life. The round-trip efficiency of the battery is also high at 92 %. The size of the battery was chosen based on similar BESS projects in Finland, which were examined in Section 5.3. The OPEX for the BESS is estimated using Figure 30. The annual OPEX for a 30 MW / 30 MWh BESS is estimated to be 8 €/kWh. Since the model is optimized on an hourly basis, the OPEX needs to be modified to a per hour value, which is done by dividing 8 €/kWh by 8760 hours. This gives an hourly OPEX of 0.000913 €/kWh or 0.913 €/MWh. Taxation is not considered for the generated cash flows.

In the simulation, the degradation of the battery is considered using a degradation coefficient c^{deg}, which can be calculated using equations (8) and (9). In (9) the lifetime energy throughput of the battery is calculated using the battery lifetime in cycles N^c, the average DOD of the battery DOD^{avg} and the energy capacity of the battery E^s. Mahesh et al. (2022) estimated that an LFP battery performing energy time shift or peak shaving services could perform around 6600 cycles before reaching its EoL criteria, which is also used in this simulation as the value for N^c. The DOD^{avg} was assumed to be 70 %, which is in line with Kim & Shin (2023) and Bera et al. (2020). Similar to Bera et al. (2020) this assumption is used to accommodate the worst case scenario, as the SOC of the battery has been restricted to be between 20 % and 90 % of the overall battery capacity. The cost of battery packs $c^{battery}$ was obtained from Camuñas García-Miguel et al. (2024), who calculated the replacement costs of the battery cells to be 37.33 €/kWh. Using these values and equations (8) and (9) c^{deg} can be calculated to be 8.08 €/MWh.

8.2 Data and sources

This model uses DA and balancing market prices and forecasted and realized wind power production to simulate the battery operation. The hourly DA market price was obtained through Nord Pool AS. In this thesis the 2023 market prices are used, as these represent the most recent electricity price data for a full year. The hourly DA market prices in 2023 have been depicted in Figure 34.

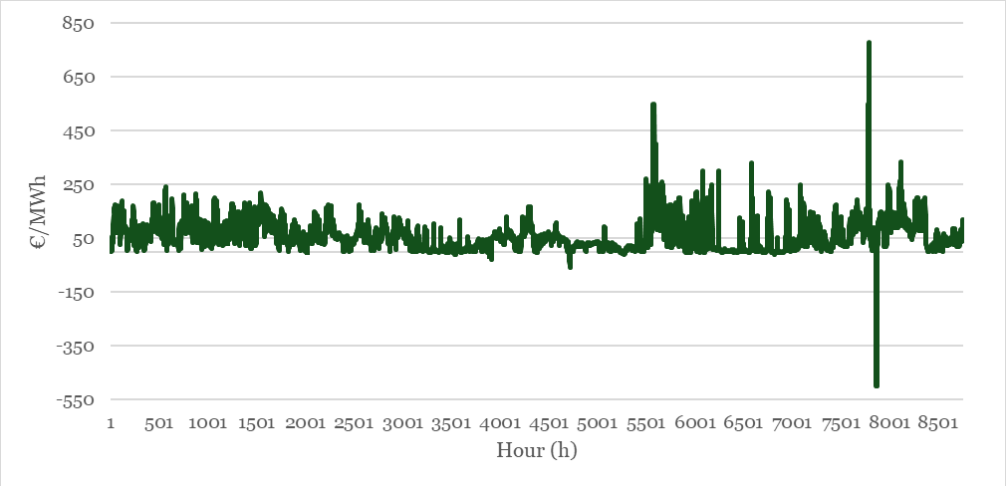

Figure 34: The hourly DA market price in 2023.

The price data provided by Nord Pool AS for the DA market is not openly accessible. For this thesis, Nord Pool provided access to the price data. Fingrid's open data platform was used to obtain the hourly up- and downregulation prices in the balancing market (Fingrid 2024b).

The hourly forecasted and realized wind power production data has been gathered from a real wind farm in the Nordic-region and was provided by the company Modity. The hourly forecasted wind power production represents the production that has been bid to the DA market the previous day. The wind power production data has been modified afterwards for anonymization purposes by scaling the wind farm to a nominal capacity of 100 MW. The battery parameters and other constant values used in this simulation are depicted in Table 8.

Table 8: Data for simulation.

Symbol	Value	Symbol	Value
λ^{BA} (€/MWh)	1.15	η^{c}	0.92
λ^{output} (€/MWh)	0.92	η^{d}	0.92
λ^{input} (€/MWh)	0.61	SOC_0 (MWh)	15
OM^{s} (€/MWh)	0.913	SOC^{min} (MWh)	6
c^{deg} (€/MWh)	8.08	SOC^{max} (MWh)	27
P^{BESS} (MW)	30		

In the investment calculations a discount rate of 5 % and the investment holding period of 10 years are used. The CAPEX for a 30 MW/30 MWh battery are estimated to be 470 €/kWh. The CAPEX was estimated using Figure 29.

8.3 Problem formulation

The primary goal of the model is to maximize the overall profit (36) by adding up all the revenues and costs from the hourly operation across the entire simulation period. This simulation period T is either 96 or 8760 hours depending on if the model is run for four days or for the entire year. In (36), revenue is obtained by selling the forecasted wind power production to the DA market and by selling the wind farm's overproduction to the balancing market. The hourly costs include the fees for the transferred energy from the wind farm to the grid and the imbalance costs from underproduction, which the BESS is trying to minimize. Other costs in the model include the battery degradation costs and OPEX and the battery grid connection fees. In the model, it is assumed that all underproduction hours correspond to upregulation hours in the Finnish balancing market, and conversely, all overproduction hours are considered downregulation hours in the balancing market.

In practice it is also possible that a positive balance error might occur during an upregulation hour, resulting in the supplier being compensated for overproduction based on the upregulation price. Similarly, a negative balance error could occur during a downregulation hour. Then the supplier would have to pay imbalance fees according to the downregulation prices. In this model, the hourly up- and downregulation prices in the balancing market are represented using the parameters λ_t^- and λ_t^+. Regardless of whether the wind power producer provides energy surplus or deficit, an imbalance fee λ^{BA} is to be paid for causing the imbalance in the first place (Klyve et al. 2023). This fee has been 1.15 €/MWh in 2023 and 2024 (Fingrid 2024i). The variable OM^s represents the hourly OPEX for the BESS. The final two terms represent

the fees for the energy transferred through the connection point by the BESS. λ^{output} is 0.92 €/MWh and λ^{input} 0.61 €/MWh (Fingrid 2024j).

$$\max \left\{ \sum_{t=1}^{T} \left[\lambda_t^{DA} \cdot P_t^F - P_t^W \cdot \lambda^{input} - \lambda_t^- \cdot P_t^{up,r} + \lambda_t^+ \cdot P_t^{op,r} - \lambda_t^{BA} \cdot \left(P_t^{up,r} + P_t^{op,r}\right) - c^{deg} \cdot \left(P_t^{ch} \cdot \eta^c - \frac{P_t^{dch}}{\eta^d}\right) - OM^s \cdot \left(P_t^{ch} \cdot \eta^c - \frac{P_t^{dch}}{\eta^d}\right) - \lambda^{output} \cdot P_t^{ch} - \lambda^{input} \cdot P_t^{dch} \right] \right\} \quad (36)$$

$$-\left(P_t^{dch} + P_t^{up,r}\right);\ \forall t, (P_t^W - P_t^F) < 0 \quad (37)$$

$$\left(P_t^{ch} + P_t^{op,r}\right); \forall t, (P_t^W - P_t^F) \geq 0 \quad (38)$$

$$\begin{cases} SOC_t = SOC_0 + \left(P_t^{ch} \cdot \eta^c - \frac{P_t^{dch}}{\eta^d}\right);\ \forall t = 1 \\ SOC_t = SOC_{t-1} + \left(P_t^{ch} \cdot \eta^c - \frac{P_t^{dch}}{\eta^d}\right);\ \forall t \backslash t = 1 \end{cases} \quad (39)$$

$$SOC^{min} \leq SOC_t \leq SOC^{max}; \forall t \quad (40)$$

$$0 \leq P_t^{ch} \leq \delta 1_t \cdot P^{BESS};\ \forall t \quad (41)$$

$$0 \leq P_t^{dch} \leq \delta 2_t \cdot P^{BESS};\ \forall t \quad (42)$$

$$\delta 1_t + \delta 2_t \leq 1;\ \forall t \quad (43)$$

Equations (37) and (38) check if the wind farm produced less or more than the previous day's forecast. A negative forecast error indicates that the wind farm produced less energy than forecasted, while a positive forecast means that the wind farm produced more than anticipated. In (37) the model attempts to decrease the wind farm's total underproduction by discharging the battery and the rest is considered to be remaining underproduction, for which the Wind Farm Owner (WFO) incurs imbalance costs. In (38) the wind farm's total overproduction is used to charge the battery and the rest is considered as remaining overproduction, which is sold to the balancing market.

Equations (39) and (40) model the SOC level of the battery. In (39) the hourly SOC level SOC_t is calculated in two different ways based on which operation hour it is in. During the first operation hour, SOC_t is calculated based on the initial SOC level which has been set to 50 % of the overall capacity. After that SOC_t is calculated based on the SOC level of the previous hour. Charging the battery increases the SOC level, whereas discharging decreases it. Energy is lost during the charge and discharge cycles, which is represented by the efficiencies η^c and η^d. (40) ensures that the battery SOC level stays within the minimum and maximum limits to avoid overcharging and -discharging. Equations (41) and (42) bound the charging and discharging power to

minimum and maximum nominal values, with the maximum value being the rated power capacity of the BESS. Binary variables $\delta 1_t$ and $\delta 2_t$ are used to ensure that charging and discharging does not happen simultaneously.

The problem formulation for the baseline case, in which the wind farm operates in the electricity market without the battery, consists only of equations (37) and (38). In the baseline case there is no battery to decrease the deviation between the forecasted and realized wind power production, so the variables $P^{up,r}$ and $P^{op,r}$ represent the negative and positive differences between the two. Since there is no battery, the costs from battery degradation and operation and also the fees related to the energy transfer between the battery and the grid are set as zero.

8.4 Simulation scenarios

To investigate the performance of the battery under different market prices and varying wind forecast accuracies, four different scenarios are created. The scenarios represent four different four-day time periods, in which the electricity market prices and wind power forecast errors have been either lower or higher than the yearly averages. For 2023, the average DA market price was 56.47 €/MWh. The scenarios were also chosen to represent periods in which the average wind power production of the wind farm was at least 30 % of its nominal capacity. Also, the periods chosen contained several hours of both over- and underproduction. The higher transfer of energy between the wind farm, battery and the electricity grid provide better information on the operation of the battery under different charging and discharging conditions. In the scenarios with more accurate wind power forecasting, time periods in which the maximum forecast error was as small as possible, were favoured. This made it possible to avoid large battery charge and discharge cycles. The scenarios do not necessarily represent the largest forecast errors or deviations from the average yearly DA market price, but provide sufficient information on the operation of the battery and the generated cash flows under similar conditions.

8.4.1 Scenario 1

The first scenario represents a four-day period where both the DA market prices and the forecast accuracy have been high. Figure 35 represents the relationship between the forecasted and realized wind power production during this period.

Figure 35: The relationship between forecasted and realized wind power production in Scenario 1.

The average hourly forecast error is 42.4 %. In this scenario the most notable imbalances occur during hours 30-60 and 68-71. During hours 30-60, the wind farm overproduces for several consecutive hours and during hour 68-71, the wind farm does not produce at all even though the forecasted hourly production is around 40 MW. Figure 36 depicts the behaviour of electricity prices in the DA and balancing markets in this scenario.

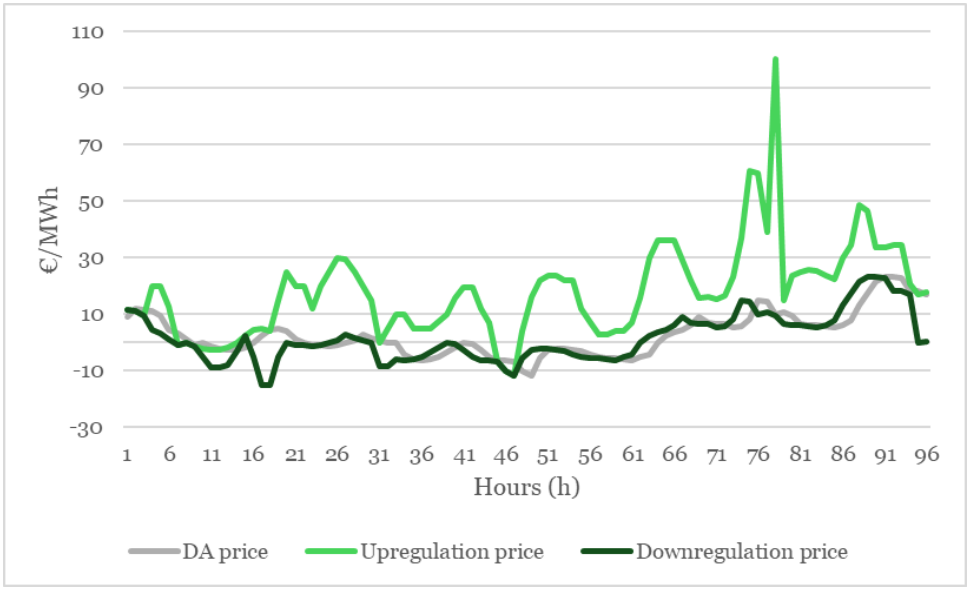

Figure 36: The behaviour of electricity prices in the DA and balancing markets in Scenario 1.

As seen in Figure 36, the upregulation price has been significantly higher than the DA and downregulation prices, which have been largely negative.

8.4.2 Scenario 2

In the second scenario, both the electricity prices and the wind power forecast error are high. The average hourly electricity price in this scenario is 117.03 €/MWh, while the average hourly forecast error is 59.67 %. Figure 37 represents the relationship between the forecasted and realized wind power production during the period.

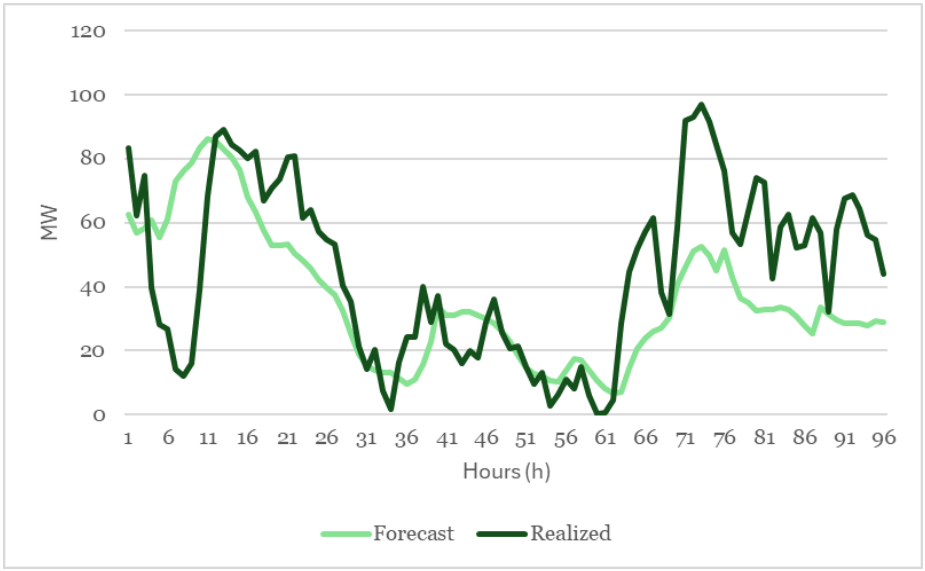

Figure 37: The relationship between forecasted and realized wind power production in Scenario 2.

In this scenario, the largest wind power forecast error occurs at the beginning of the simulation where the wind farm produces over 60 MW less than what was forecasted for the DA market the previous day. Also, at the end of the simulation period the wind farm overproduces for several consecutive hours compared to the forecast. Compared to Scenario 1, the over- and underproduction hours in this scenario are more evenly distributed along the entire simulation period. Figure 38 depicts the change in DA and up- and downregulation prices during the simulation period.

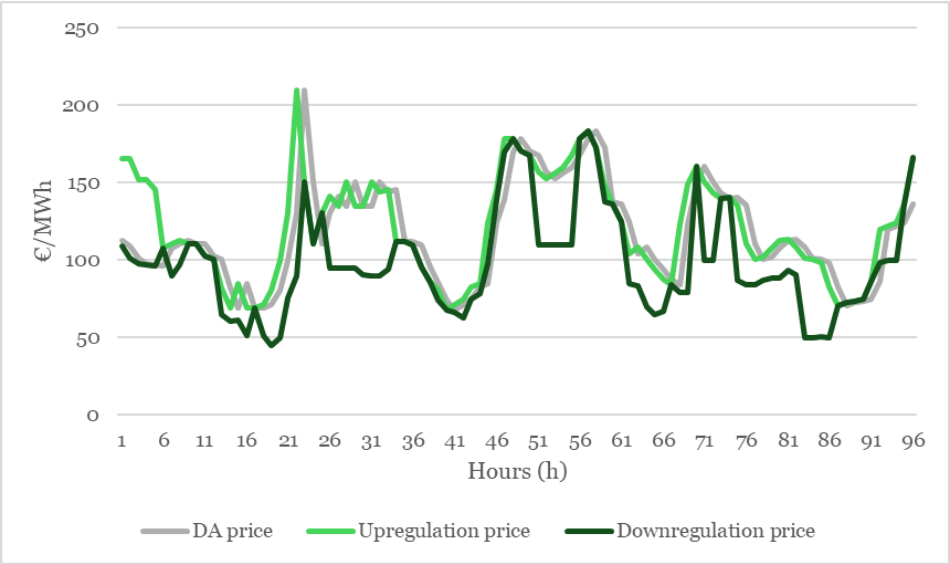

Figure 38: The change in DA and up- and downregulation prices during the simulation period in Scenario 2.

In this scenario the electricity prices are also correlating more than in Scenario 1. The DA and upregulation prices are similar during the entire simulation period and there are also hours, in which the downregulation price is close to same as the other two. DA and upregulation electricity prices reach their peak of 200 €/MWh during hours 22 and 23, while downregulation price reaches its peak price of 183 €/MWh at hour 57. The electricity prices in this scenario are also more volatile than in Scenario 1.

8.4.3 Scenario 3

In the third scenario, both the average hourly electricity price and the wind power forecast error are lower than the yearly averages, with 3.04 €/MWh and 16 %. Figure 39 represents the relationship between the forecasted and realized wind power production during the period.

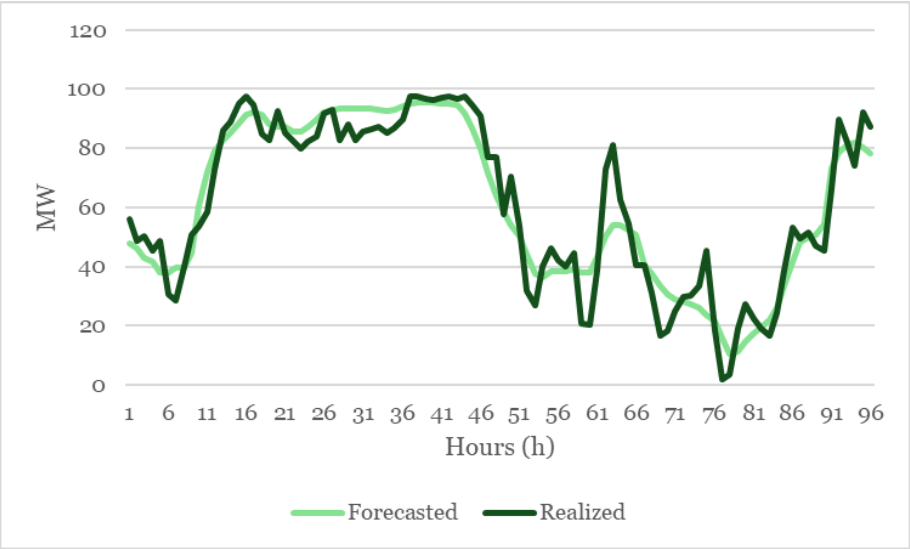

Figure 39: The relationship between forecasted and realized wind power production in Scenario 3.

In this scenario, the forecasts of the previous day predict the next day's production accurately, with only some exceptions. The most notable forecast errors in this scenario occur during the hours 62 and 63, where the realized wind production is around 20 MW higher than the forecasted production. Figure 40 depicts the behaviour of DA and up- and downregulation electricity prices in this scenario.

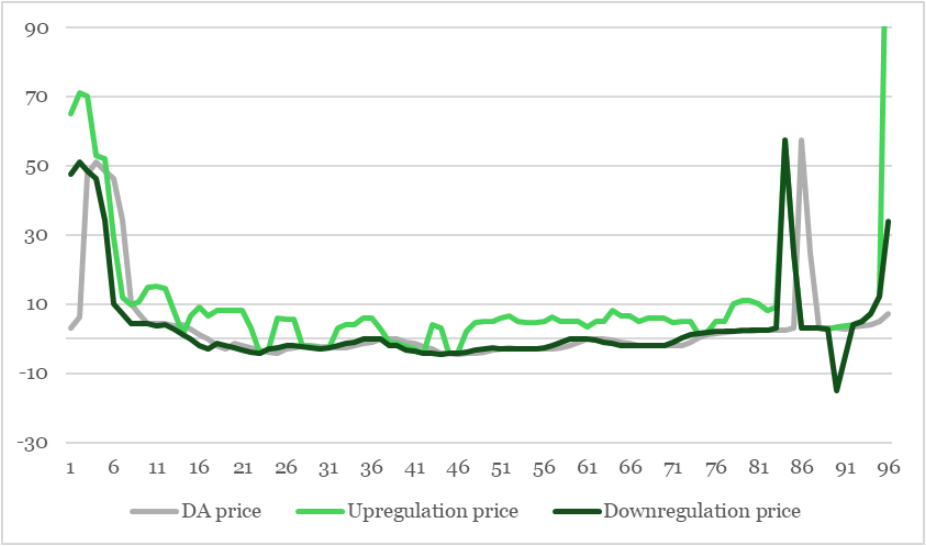

Figure 40: The behaviour of DA, up- and downregulation prices in Scenario 3.

The DA, upregulation and downregulation prices are the highest both at the beginning and towards the end of the simulation period. The DA market price reaches its peak of 57.23 €/MWh during hour 86. Conversely, the lowest price -4.43 €/MWh is observed at hour 46. The maximum downregulation price is 57.23 €/MWh, while the minimum price reaches -15 €/MWh. The highest upregulation price occurs during the final hour of the simulation, reaching 156.26 €/MWh. The lowest upregulation price is reached at hour 42 with -4.37 €/MWh. Figure 40 depicts the DA and downregulation prices remaining negative for several consecutive hours in the middle of the simulation period, while the upregulation price remains predominantly positive.

8.4.4 Scenario 4

In the fourth scenario the electricity price is high and the wind power forecast error is low. The average DA market price during this time period is 81.93 €/MWh, while the average hourly wind forecast error is 21.51 %. Figure 41 represents the relationship between the forecasted and realized wind power production during the period.

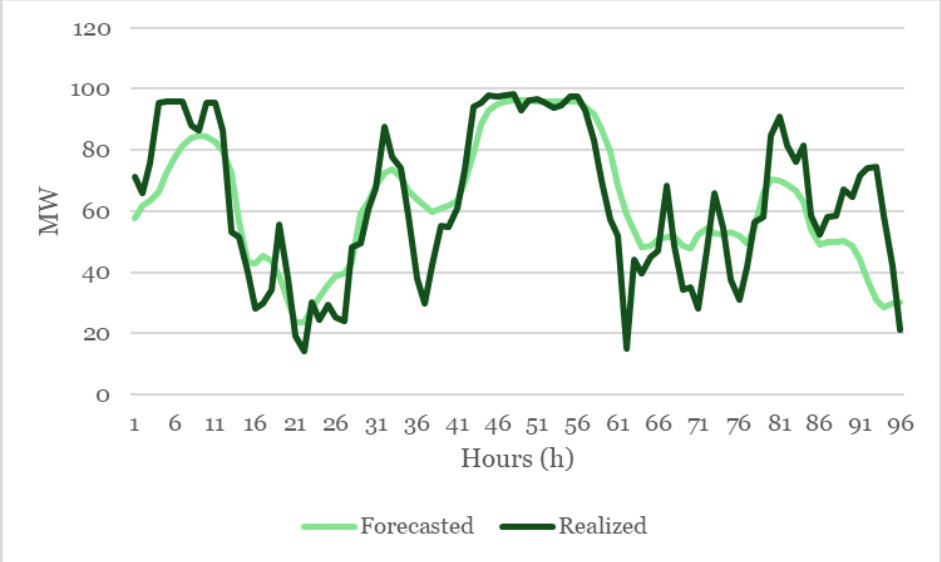

Figure 41: The relationship between forecasted and realized wind power production in Scenario 4.

In this scenario, the most notable forecast errors occur at the end of the simulation period between the hours 90-96, where the wind farm produces around 20-40 MW more than the previous day's forecast. The forecast predicted with good accuracy the high production peaks in the beginning and middle of the simulation period. Figure 42 depicts the DA, upregulation and downregulation electricity prices in this scenario.

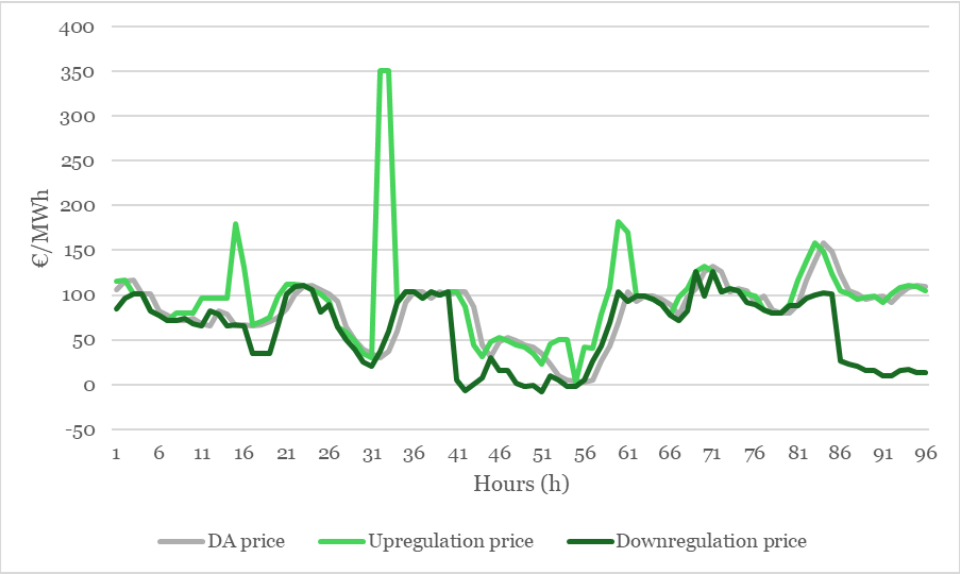

Figure 42: DA, upregulation and downregulation electricity prices during the simulation period in Scenario 4.

The electricity prices in this scenario are volatile. Over the simulation period, the DA price fluctuates, with a maximum value of 158.7 €/MWh occurring at hour 84 and a minimum of 2.48 €/MWh occurring at hour 56. The upregulation price reaches its lowest point of 2.48 €/MWh one hour earlier at hour 55, while its peak is 350 €/MWh. Also, the downregulation price varies considerably throughout the simulation, reaching the maximum price of 126.21 €/MWh at hour 71 and the minimum price of – 8 €/MWh at hour 51. Both the DA and upregulation prices remain positive throughout the entire period, but the downregulation price turns negative for some hours in the middle of the simulation.

8.5 Simulation results

8.5.1 Scenario 1

In the first scenario, the DA market price is low, while the wind power forecast error is high. In the baseline case, where the wind farm operates independently in the electricity market, the revenue over the four-day period amounts to -4628.4 €. Consequently, the wind farm operates at a loss during this time period. The primary causes of this loss are the large underproduction periods between hours 28-32 and 68-71. Figure 36 indicates that throughout the entire four-day period, the upregulation prices consistently surpass the downregulation prices, which remain largely negative. During

the negative downregulation price hours, the WFO incurs imbalance fees, even during the overproduction of the wind farm.

In this scenario the battery usage is able to decrease the imbalance errors but not significantly. The battery usage is able to decrease the average forecast error by 2.3 percentage points from 42.43 % without the battery to 40.08 % with the battery. Using the battery, the WFO is able to decrease the imbalance costs by 1105.86 €, resulting in an operating loss during this period of -3522.58 €. Had these comparable conditions endured for an entire year, the battery would have been able to increase the revenue by approximately 100 000 €. Figure 43 depicts the battery SOC level during the simulation period.

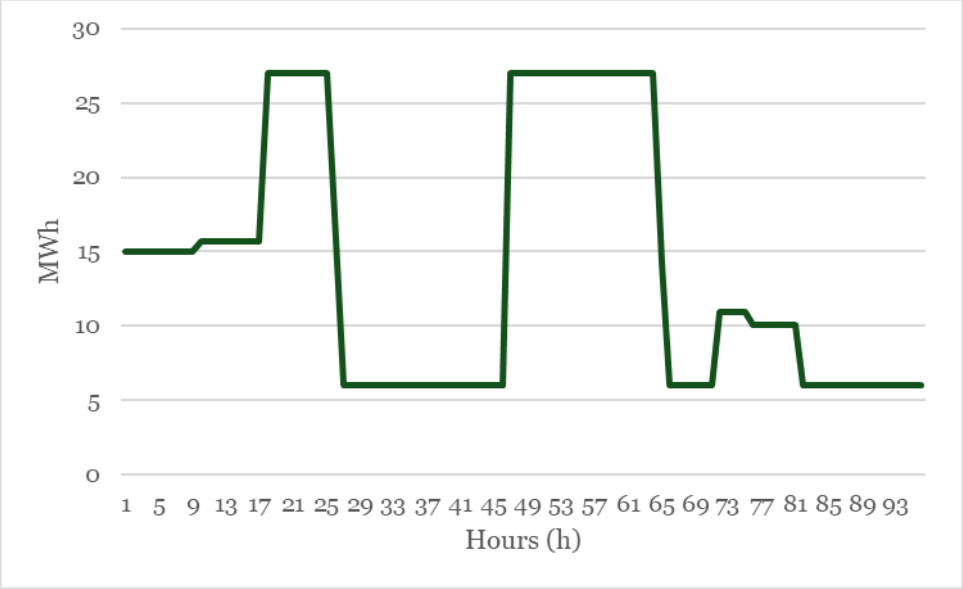

Figure 43: Battery SOC level during the simulation period in Scenario 1.

The battery SOC level data in Figure 43 indicates that the battery has a very low usage rate, which can also be determined from the FEC count of 1.4. This is due to most of the consecutive over- and underproduction periods lasting for several hours at a time. First the battery is charged for many hours, followed by several hours of discharging. The battery capacity would have to be larger to effectively compensate for the longer individual imbalance periods.

The charging and discharging periods are not divided across multiple hours of over- or underproduction. Instead, the battery focuses on charging at specific hours, in which the reduction in positive revenue from overproduction to charge the battery is minimal. When comparing the charging strategy to the electricity prices in Figure 36, these hours correspond with the hours where downregulation prices are the most negative. The discharging in turn is focused on the hours with the largest forecast error and the highest

upregulation price. So, it is also optimal to discharge as much as possible when the forecast error and upregulation price is high, instead of discharging the battery over several hours at a time.

Even though the simulation period begins with an overproduction period, which is followed by three consecutive underproduction hours, the battery is not charged or discharged at all during the first nine hours. This is because the model is given information regarding the future imbalances and market prices in advance. It is not optimal to charge the battery if the subsequent underproduction period has negative upregulation prices. If the upregulation price during an underproduction hour is negative, the WFO is paid for the negative imbalance error. Consequently, utilizing the battery to compensate for the wind farm's underproduction would actually increase the imbalance costs and the battery would have needlessly charged the battery during the last overproduction period, decreasing the revenue from overproduction and incurring battery degradation costs and OPEX.

8.5.2 Scenario 2

In the second scenario, both the DA market price and the average forecast error are high. The most notable forecast errors occur at the end of the simulation period, where the wind farm overproduces significantly for several consecutive hours. In the baseline case, the wind farm generates revenue totalling 446 230 €. The high revenue is due to the high amount of overproduction, for which the WFO will be paid according to the downregulation price. The use of the battery increased the revenue by 3725.1 € to 449 955 €. If these conditions were to persist for a full year, the battery could potentially increase the annual revenues by 339 917 €. Similarly to Scenario 1, the battery usage is able to decrease the forecast error during the period, but the reduction is not significant. The average forecast error decreased by 3.5 percentage points from 59.7 % to 56.2 %. Figure 44 depicts the battery SOC level during the simulation period.

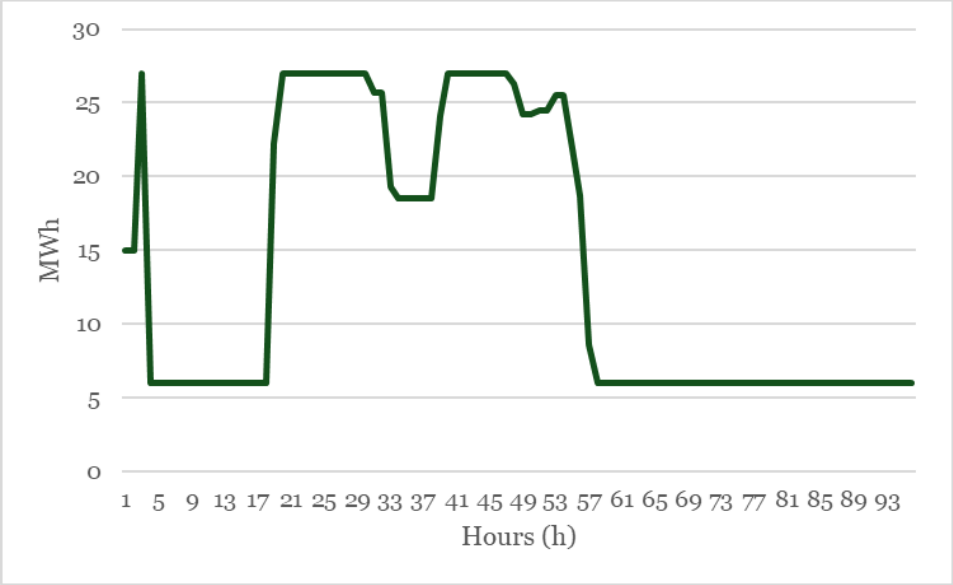

Figure 44: Battery SOC level during the simulation period.

In comparison to the first scenario, the battery is utilized more in this scenario, as indicated by the FEC count of 1.6. However, the usage is limited by the several consecutive hours of overproduction towards the end of the simulation period, resulting in overall low battery usage. The simulation period starts with three consecutive hours of overproduction from the wind farm, during which the battery is charged to its maximum SOC level to prepare for the following underproduction hours. The charging is scheduled for hour three, where the downregulation price is the lowest. The battery is then discharged to its minimum SOC level during the first hour of the underproduction period, where the upregulation price is the highest at 152 €/MWh.

Following the initial underproduction period, the battery is fully charged during the subsequent extended period of overproduction from the wind farm. At hours 31 and 33, the battery discharges as much as possible to counterbalance the wind farm's underproduction. Notably, at hour 34, the battery is not utilized to fully compensate for the remaining 10.7 MW of underproduction from the wind farm. Even though the battery has an available capacity of 19 MWh, it only discharges 0.65 MW during this hour. The upregulation price at hour 34 is 111.75 €/MWh, suggesting that there is an opportunity to reduce the imbalance costs by 1196 €. Instead of discharging the battery, the WFO accepts the higher imbalance costs at hour 34 to enhance the compensation from the subsequent overproduction period, as it has to charge the battery less during these hours.

Despite having full capacity, the battery is not utilized to decrease the imbalance costs between hours 41 and 46, when the upregulation prices range from

67.77 €/MWh to 24.23 €/MWh. Instead, the battery is discharged to balance the minor imbalances at hours 48 and 49, when the upregulation prices reach 178.20 €/MWh and 170.09 €/MWh, respectively. This ensures that the WFO captures the complete revenue from the overproduction during hour 47, when the downregulation price is at 169.87 €/MWh. The battery is not charged to its full capacity during hours 50, 51 and 53 before the longer underproduction period starting at hour 54. The battery discharges its remaining capacity between the hours 55 and 58, coinciding with the highest upregulation prices ranging from 167.28 €/MWh to 183.12 €/MWh. The battery remains unutilized during the last overproduction period to maximize the available revenue.

8.5.3 Scenario 3

In the third scenario, both the DA market price and the average wind forecast error are lower than the yearly averages. Furthermore, the over- and underproduction periods are more evenly distributed in this scenario. In the baseline case the WFO generates 5505.80 € of revenue throughout the entire four-day period. Using the battery, the revenue increased by 233.91 €, which means that if similar conditions persisted for an entire year, the battery would be able to generate 21 344.61 € of additional revenue. This is the smallest increase in annual revenue among all the scenarios examined. The battery is able to decrease the average forecast error by a small margin of 0.31 percentage points and the battery usage in this scenario is the lowest with a FEC count of 0.2. The battery is only discharged for three hours and charged during one, which further indicates that the utilization of the battery in these conditions is not warranted. Figure 45 depicts the change in battery SOC level throughout the simulation period.

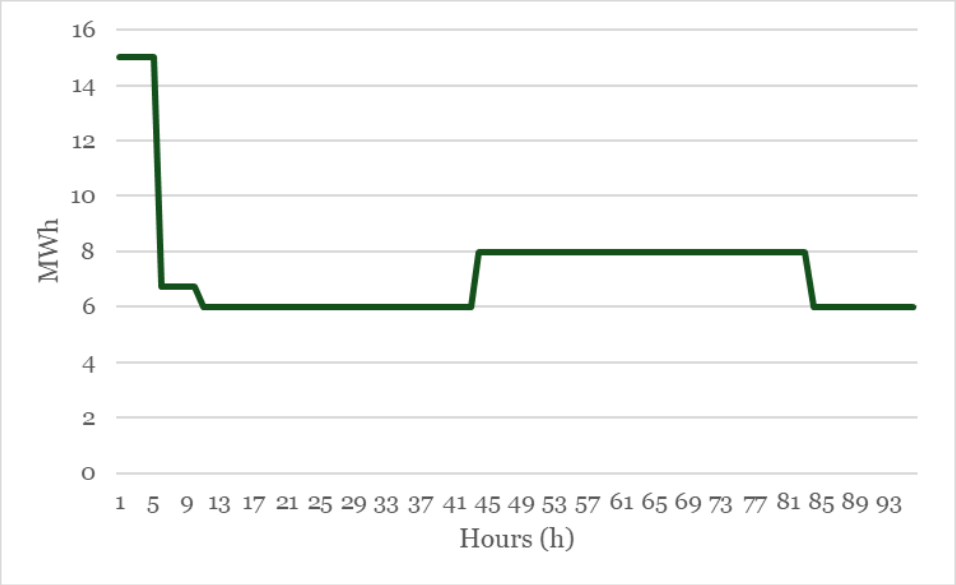

Figure 45: The change in battery SOC level throughout the simulation period in Scenario 3.

The battery is discharged at hour 6 when the wind farm underproduces 7.6 MW and the upregulation price is 46.1 €/MWh. The battery is the not charged during hours 8 or 9, indicating that its unable to compensate for the underproduction between hours 18 to 36. The upregulation prices during this period are negative, so the WFO is paid for the underproduction.

An extended overproduction period begins at hour 37 and continues until hour 48, during which downregulation prices are negative. Although charging the battery during these hours would reduce imbalance costs, the battery is not charged because the battery degradation costs and OPEX are higher. The battery is only charged at hour 44 for 1.9 MW, which is then discharged at hour 84 when the upregulation price peaks at 57.23 €/MWh. Hour 84 is the only underproduction hour following the extended overproduction period, where the upregulation price is higher than the combined battery degradation costs and OPEX. This suggests that charging the battery during overproduction periods with negative downregulation prices is only warranted if the subsequent underproduction periods have sufficiently high upregulation prices to offset the high operation costs.

8.5.4 Scenario 4

In the fourth scenario, the DA market price is higher than the yearly average and the average wind power forecast error is in turn smaller. Also, similarly to Scenario 3, the under- and overproduction periods are quite evenly distributed. In the baseline case the WFO generates 420 850.61 € of revenue

throughout the entire four-day period and using the battery the revenue is increased by 7322.25 € to 428 172.86 €. If the similar conditions had endured for the whole year, the WFO would have increased its revenue by 668 155.25 €, which is the highest increase in revenue between the scenarios. Also, the decrease in average forecast error is the highest in this scenario with 4.5 percentage points. The usage of the battery in this scenario is also the highest with a FEC count of 3.6, which is more than the combined FEC count of the other scenarios. Figure 46 depicts the battery SOC level during the simulation period.

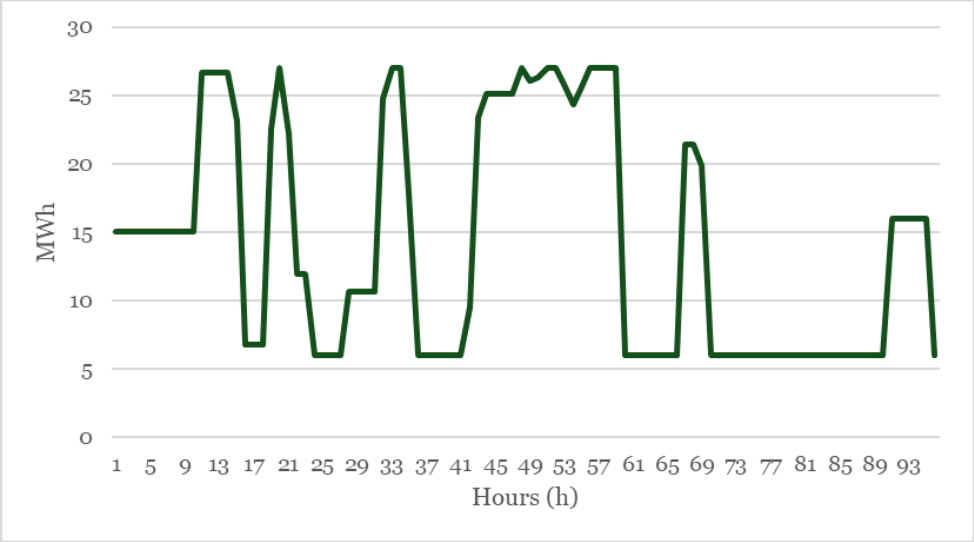

Figure 46: The change in battery SOC level in Scenario 4.

Figure 46 indicates that the battery is used actively throughout the whole simulation period. The longest period, in which the battery remains unutilized, occurs between hours 70 and 90. Figure 47 depicts the battery charge and discharge cycles during the simulation period.

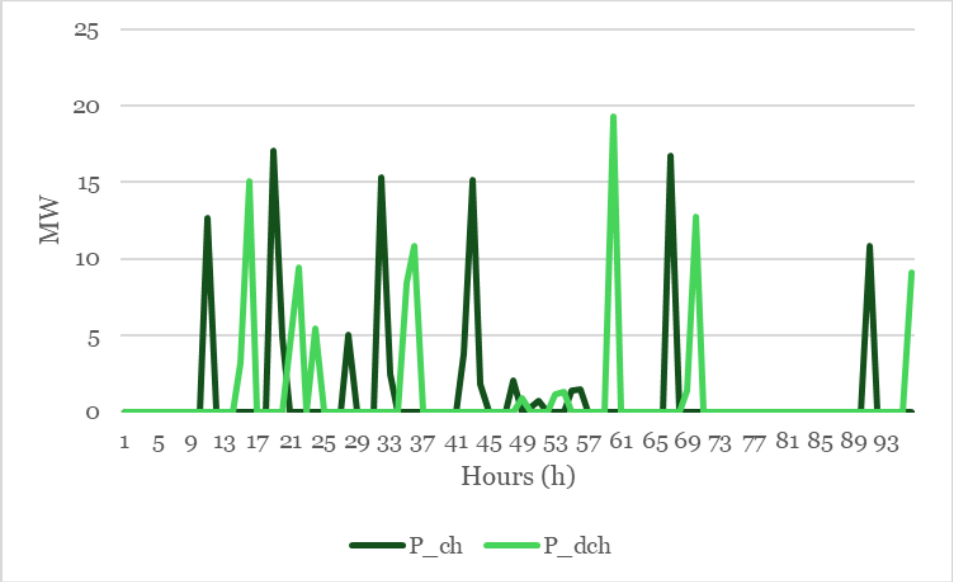

Figure 47: Realized battery charge and discharge cycles during the simulation period in Scenario 4.

The simulation period begins with an overproduction period, where the battery is charged to its maximum SOC level at hour 11, while the downregulation price is at its lowest at 66.04 €/MWh. The battery is then discharged at hours 15 and 16 to fully compensate for the wind farm's underproduction. The upregulation prices peak at 179 €/MWh and 131 €/MWh during these discharge cycles. In this scenario, the overproduction periods are used more actively to charge the battery to or close to the maximum SOC level, as the high upregulation prices force the WFO to use the battery to compensate for the wind farm's underproduction. This was not the case in Scenario 3, where the low upregulation prices did not support the charging of the battery with high degradation costs and OPEX.

Similarly to previous scenarios, the model schedules the charge and discharge cycles to minimize the imbalance and the battery degradation costs and the OPEX. The DODs of individual discharge cycles are consistently close to the 70 % maximum. This is also evident from Figure 47, where the individual discharge periods do not last more than two hours at a time. Similarly, during charging, the model prioritizes reaching the maximum SOC during the lowest downregulation price hours, thereby minimizing the lost revenue from overproduction. Since, the model has information regarding the amount of discharging that is required in the future to maximize the revenue, it can manage the SOC level of the battery to minimize both degradation costs and OPEX.

8.5.5 Annual operation in 2023

As in the previous scenarios, the operation of the wind farm in the electricity market without the battery is first simulated. The results from the baseline case are then compared with the results from the full model and the battery operation is analyzed in more detail. Figure 48 depicts the volume of the individual over- and underproduction hours throughout the entire year 2023.

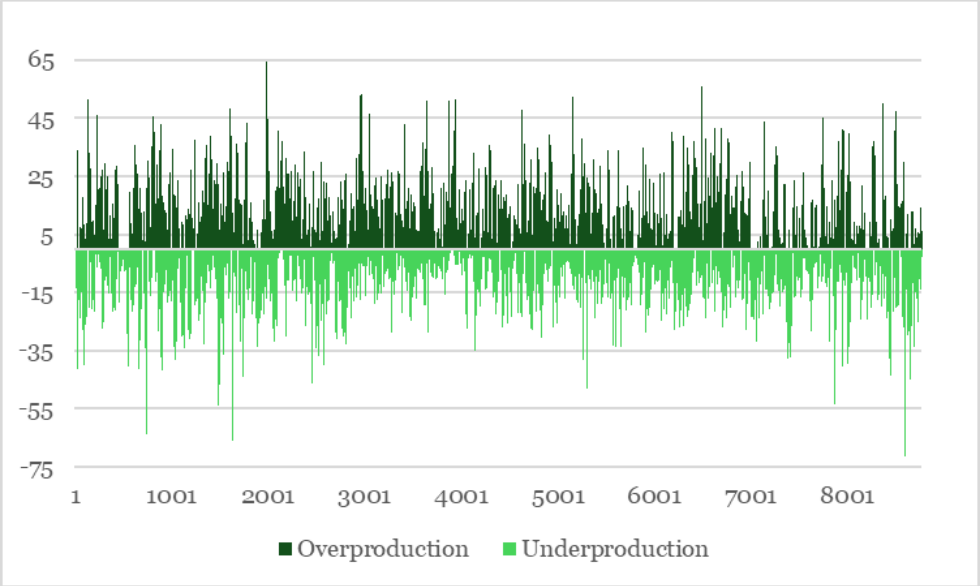

Figure 48: The volume of individual over- and underproduction hours throughout the entire year 2023.

The wind farm's highest overproduction for the year happen at hours 1982 and 6487, with an excess production of 64.5 MW and 55.8 MW respectively. These hours occur in March and September. The most significant underproduction occur at hours 8584 and 1627, where the output falls short by 71.5 MW and 66.1 MW from the forecasted amounts. These hours are in December and March. As indicated in Figure 48, significant forecast errors in both up- and downward directions are distributed evenly throughout the year. However, the number of significant overproduction hours is higher than the amount of large underproduction hours.

In the baseline case the WFO generated annual revenue of 13 520 810 € and the imbalance costs for the whole year amounted to –1 484 343 €. The battery is able to decrease the imbalance costs by 574 496 € to -909 847 €. Overall, the battery is able to increase the revenue by 491 661 € to 14 012 471 €. Table 9 contains some figures related to the operation of the battery and the profitability of the investment.

Table 9: Battery investment profitability analysis.

Average SOC level	16.77 MWh
FEC count	160.5
The ratio of imbalance costs to DA market revenue without the battery	9.76 %
The ratio of imbalance costs to DA market revenue with the battery	5.98 %
NPV	- 10 303 520.84 €
Payback period (years)	> 20
Discounted payback period (years)	> 20

Even though the battery is able to increase profitability through decreasing the imbalance costs, the increase in annual revenue is not enough to make the investment profitable in the long run. The NPV of the investment with a 5 % discount rate is -10.3 M€ (million euros) and both the payback and discounted payback periods were over 20 years. The annual FEC count of the battery is 160.5 cycles, meaning that the battery life, which is approximately 6600 cycles, would not be exceeded during the ten-year operation period.

8.6 Summary of results of the wind power balance error management model

The results from the four distinctive scenarios and the annual operation indicate that the battery is able to decrease the wind forecast error and the imbalance costs. However, the usage of the battery is relatively low in all the cases and the annual operation accumulated only 161 full equivalent cycles. Indicated by the results from Scenario 1 and Scenario 3, the usage of the battery is particularly low when also the electricity prices are low. In these scenarios the electricity prices remain largely negative, leading to charging of the battery to balance the wind farm's overproduction to reduce the imbalance costs. However, frequently during the following underproduction hours, the upregulation prices are also negative, resulting in the WFO generating profit from the wind farm's underproduction. These negative prices are rarely higher than the battery degradation costs and the OPEX, indicating it is often optimal not to use the battery at all. The scenario specific generated revenues and FEC counts have been depicted in Table 10.

Table 10: Scenario specific generated revenues and FEC counts.

	Scenario 1	Scenario 2	Scenario 3	Scenario 4
Revenue	1 105.9 €	3 725.1 €	233.9 €	7 322.3 €
Revenue given consistent conditions throughout the year 2023	100 918.6 €	339 917.0 €	21 344.6 €	668 155.3 €
FEC count	1.4	1.6	0.2	3.6

The battery's low usage in all scenarios is primarily due to its high operational costs. These costs make it unprofitable to charge and discharge the battery unless it can significantly reduce the wind farm's imbalance costs. The battery usage is also constrained by the potential earnings from the wind farm's overproduction during periods with positive downregulation prices, as charging the battery would decrease this overproduction. Given that the model is deterministic, it has prior knowledge of all electricity market prices and imbalances. Charging the battery is only beneficial if it can profitably compensate for the wind farm's future underproduction, when considering the battery degradation costs, OPEX and the potential loss of revenue from the wind farm's overproduction.

The results from the four different scenarios also indicate that the model attempted in all scenarios to discharge and charge the battery as much as possible during the specific hours when it was optimal to generate revenue. The discharging and charging periods are not divided between consecutive under- and overproduction hours and individual charge and discharge cycles are often close to the maximum DOD of 70 %.

Even though the battery is able to decrease the wind power forecast error, none of the investment calculations supported the investment solely for wind power balance error management. The annual operation of the battery in 2023 yielded an increase in revenue by 491 661 €. Using the same conditions for the next ten years and a 5 % discount rate led to an NPV of -10.3 M€ and a payback period of over 20 years.

Out of the four scenarios examined, the BESS is most successful in increasing the revenues of the wind farm in Scenario 4, where the DA market price is higher than the yearly average and the wind power forecast error is smaller. In this scenario, the battery is also used the most actively. The battery is able to decrease the balance error by 4.5 percentage points during the simulation period, and if similar conditions had endured for the entire year of 2023, the battery would have been able to increase the revenue by 668 155.25 €. Even

though the increase in revenue is notable compared to the annual operation scenario, the investment would not be profitable if the same conditions remained for the next ten years, as the NPV is still -8.9 M€ and the payback period is over 20 years.

The simulations utilize the hourly electricity prices from the DA and balancing markets in Finland for the year 2023. A comparison of the DA market prices in 2023 with those of the two previous years indicates a significant decrease in average DA market price. The average DA market price in 2023 was 56.45 €/MWh, while it was 154.03 €/MWh and 72.34 €/MWh in 2022 and 2021 respectively. Figure 49 depicts the behaviour of the DA market price in 2022.

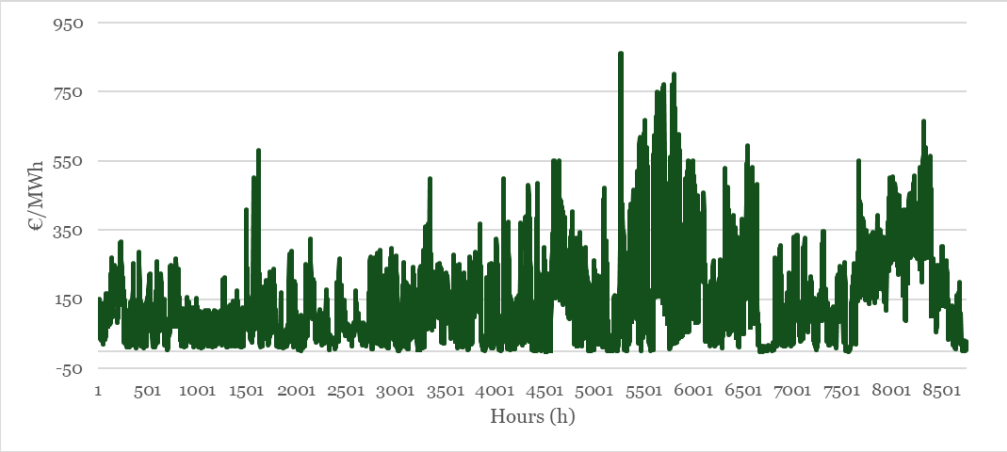

Figure 49: The DA market price in 2022.

As seen in Figure 49, the DA market price was much more volatile in 2022 than in 2023. The highest DA price in 2022 was significantly higher at 861.11 €/MWh compared to 777.18 €/MWh in 2023. 2022 had only 27 hours of negative DA prices, while in 2023 467 such hours occurred. During these 27 hours in 2022, the minimum price was only -2.08 €/MWh, whereas in 2023, the lowest DA price was -500 €/MWh. The simulations suggested that the battery usage is more profitable and it is used more actively to balance the wind farm's imbalances during periods of higher electricity prices. This implies that the battery usage might have been more profitable in 2022. A similar conclusion can be drawn for 2021, which also had a higher average electricity price than 2023. The behaviour of the DA market price in 2021 has been depicted in Figure 50.

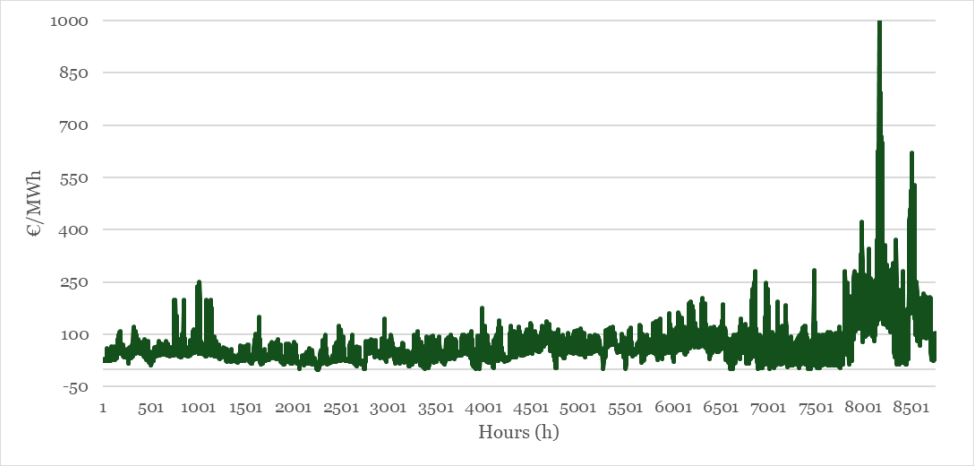

Figure 50: The DA market price in 2021.

Figure 50 shows that the DA market price volatility in 2021 was very similar to that in 2023. The maximum price in 2021 was 1000.07 €/MWh, while the minimum price was only -1.41 €/MWh. Also, 2021 had only 5 hours when the DA market price was negative. Considering the DA market price conditions, 2022 also seemed to be a more profitable year for managing wind power balance. However, this does not necessarily guarantee the long term profitability of the investment. The DA electricity market data has been obtained from Nord Pool.

8.7 Sensitivity analysis

The profitability of the battery in wind power balance error management is investigated further by performing a sensitivity analysis on the capacity and CAPEX of the battery and the annually generated revenue. As in previous sections, the annual revenue generated by the battery in 2023 is used to calculate the NPV of the investment using a holding period of 10 years and a discount rate of 5 %. It is assumed that similar conditions to 2023 prevail for the entire holding period.

The effect of BESS capacity on the investment profitability is investigated by adjusting the ratio of battery capacity to wind power plant rated power. Initially, the battery capacity is 10 % of the wind power plants nominal power and the ratio is increased by ten percentage points at a time until the battery capacity is the same as the rated power of the wind power plant. The rated power of the wind power plant is 100 MW, so the battery capacity starts at 10 MW and increases by 10 MW until the capacities are identical. For each BESS capacity, the CAPEX are estimated using data from Figure 29. Figure 51 depicts the relationship between the capacity and the profitability of the BESS in wind power balance error management.

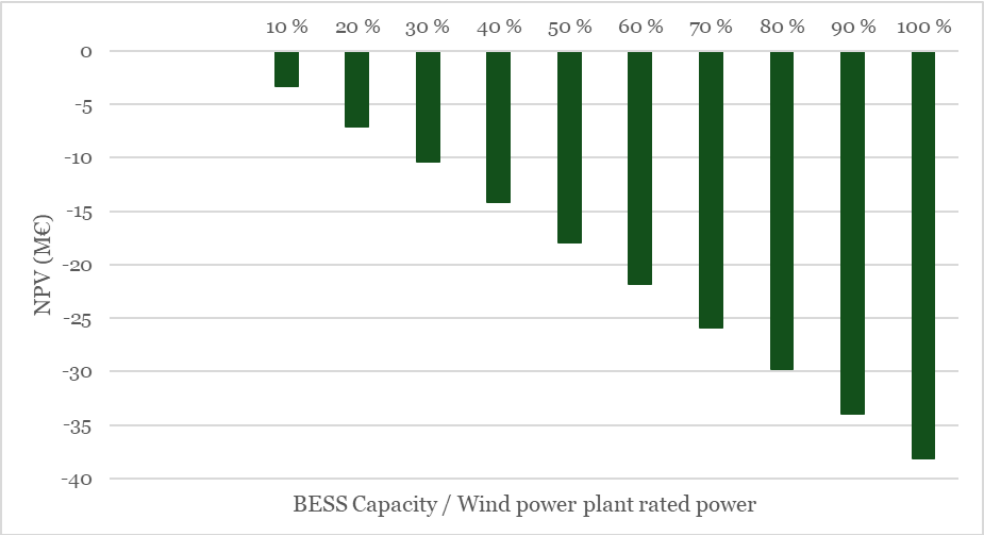

Figure 51: The relationship between the battery capacity and profitability.

Figure 51 indicates that increasing the ratio between the BESS and the wind power plant capacities decreases the profitability. None of the selected BESS capacities make the investment profitable. The highest NPV of -3.32 M€ is reached using a 10 MW/10 MWh BESS.

The effect of BESS CAPEX on the profitability is analyzed by decreasing the CAPEX for each BESS capacity by ten percentage points until the CAPEX are 10 % of the current estimate for each BESS capacity. The impact of BESS capacity on the investment profitability is depicted in Figure 52. The results are tableted in Appendix 1.

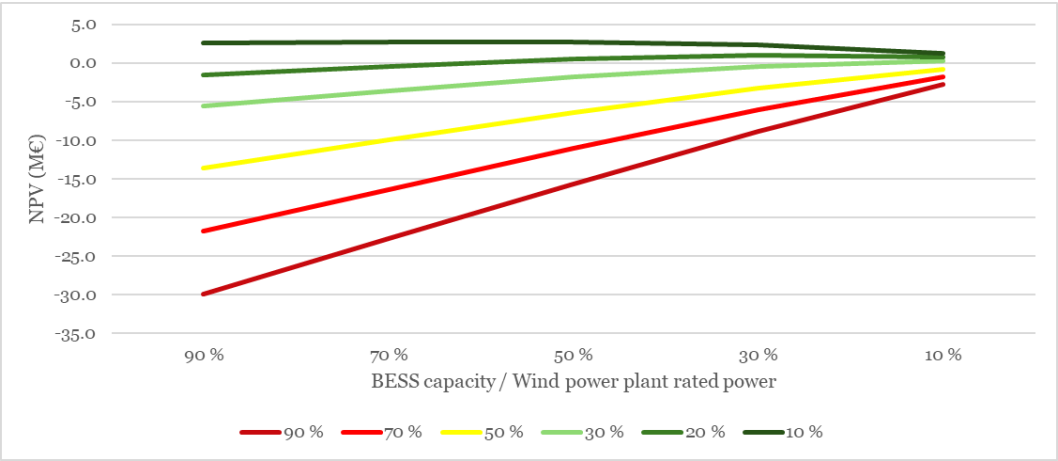

Figure 52: The effect of BESS CAPEX on the investment profitability.

In Figure 52, the curves describe the ratio of BESS CAPEX to the current estimates, so in the yellow curve the CAPEX is 50 % of the current estimate for each BESS capacity. Even if the BESS CAPEX decreased to 40 % of the initial value, none of the investments would be profitable. A 10 MW/10 MWh BESS becomes profitable if the CAPEX decreased to approximately 39.5 % of the current estimate and a 30 MW/30MWh BESS is profitable if the CAPEX decreased to approximately 29.7 % of the current estimate.

The effect of annually generated revenue on the investment profitability is analyzed by increasing the annually generated revenue in 2023 obtained in the simulation. For each BESS capacity the annual revenue in 2023 is increased by 10 percentage points at a time until the annual generated revenues are 90 % higher than in 2023 originally. Figure 53 depicts the impact of annually generated revenue on the profitability. The results are depicted in Appendix 2.

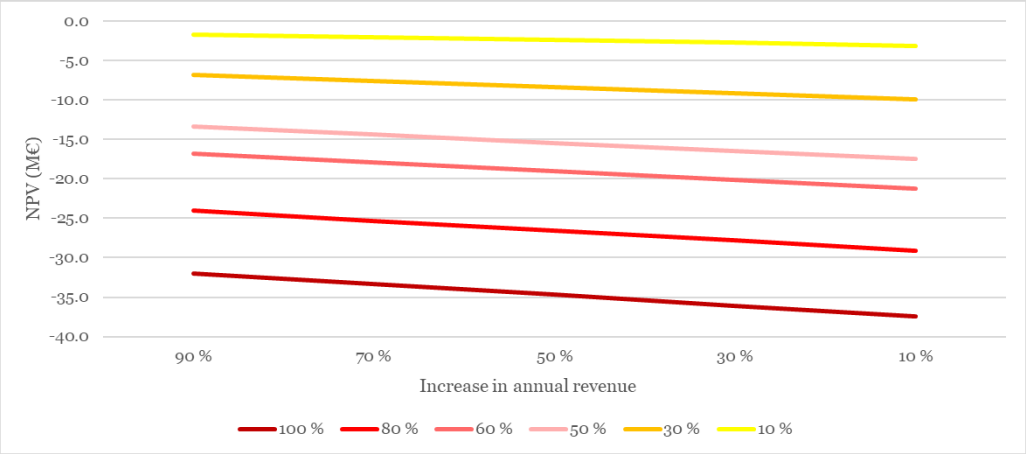

Figure 53: The effect of annually generated revenue on the investment profitability.

In Figure 53, the curves indicate the different ratios between the BESS capacity and the wind power plant rated power. Even though the revenues are increased by 90 %, none of the BESS configurations become profitable in wind power balance error management.

9 The operation of a standalone BESS in the FCR-N and FFR markets

The operation of a BESS in the FCR-N and FFR markets is researched in this chapter. The research methods, underlying assumptions and the data used in the simulation are presented. The mathematical formulation of the model is then given. This chapter concludes with an analysis of the obtained simulation results and a sensitivity analysis.

9.1 Research methods

In this section, the potential revenue streams for a standalone BESS in the Finnish reserve markets are modelled. The BESS owner bids simultaneously in the FCR-N and FFR markets and the optimal operation is achieved by maximizing the overall profit, also considering hourly battery degradation costs, battery OPEX and the network fees. The simulation is conducted using a similar LIB used in wind power balance error management in Section 8, modified to a capacity of 20 MW/20 MWh. The resulting model is a MINLP model, which is further recast into an equivalent MILP model in order to ease the solving process. The model is optimized on an hourly basis and the simulation is done for one year in GAMS using the CPLEX solver. In the simulation the electricity prices and real-time frequency data from 2023 are used. A flowchart of the model is shown in Figure 54.

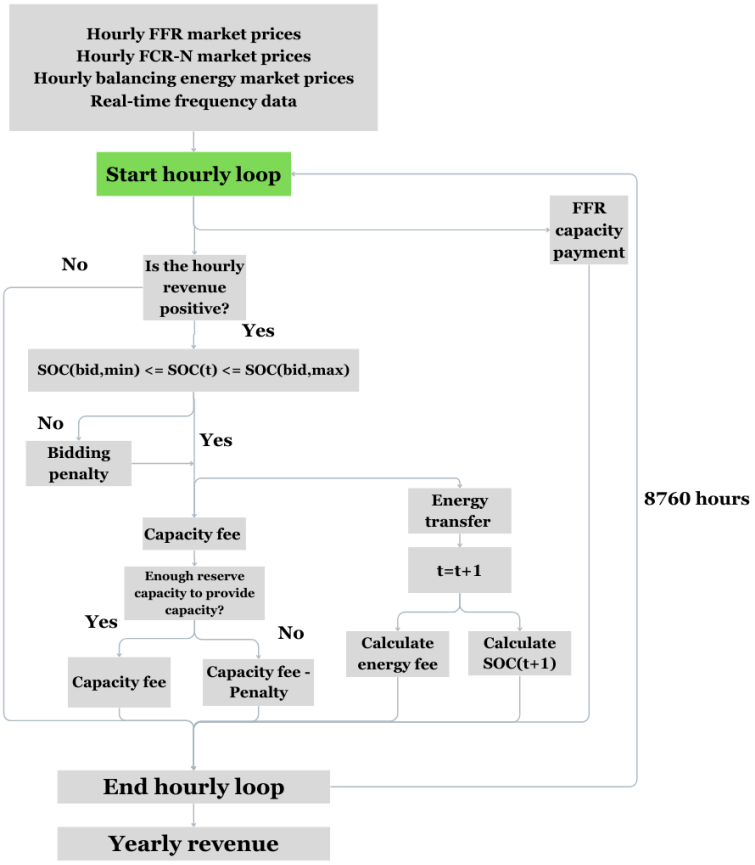

Figure 54: Yearly operation of a standalone BESS in the Finnish reserve markets.

The model is deterministic, indicating that the BESS owner has perfect information regarding the future market prices and required regulation power in the simulation. It is assumed that the BESS owner is a price taker and unable to influence the market prices. It is furthermore assumed that the bid of the owner is always accepted and the participation in the markets happens according to the hourly prices of the year. The response time of the battery is assumed to be immediate. The BESS participates in the FCR-N and FFR markets simultaneously which means that the overall capacity of the battery is divided hourly between the two markets. To simplify the simulation, it is assumed that the BESS owner bids a capacity of 10 MW every hour to the FFR market and the remaining 10 MW would be used in the FCR-N market. According to Section 4.4.1, an overall reserve capacity of 10 MW would allow a maximum bid capacity of 5 MW, as the endurance requirement for a BESS is 60 minutes for both up- and downregulation. Also, the maximum capacity for a single bid for FCR-N is 5 MW. The BESS owner decides how much FCR-

N provision to offer to the market at each hour, considering the maximum bid capacity.

For the FFR market, only the capacity payments for the reserve provision are considered and it is assumed that the FFR provision does not include any energy transfer. The used frequency data to simulate the BESS operation in the reserve markets did not include any required FFR provision. Hence the frequency data did not include any time interval, in which the frequency would have dropped below 49.7 Hz. This may be because the fast frequency reserves have been able to restore the frequency above 49.7 Hz before it is reflected in the real-time frequency data, updated at three-minute intervals. It can be thus assumed that the amount of transferred energy compared to FCR-N is negligible. A similar assumption is made in an article by Hameed et al. (2023), in which the revenue streams of a BESS were analyzed in the Danish reserve markets. As no energy is assumed to be transferred during FFR provision, participating in that market does not affect the BESS hourly SOC level or the battery degradation costs and OPEX, which are calculated based on the hourly transferred energy. In the FCR-N provision both the capacity and energy payments are considered, as energy payments form a more significant part of the overall FCR-N revenue stream.

After the simulation, the BESS operation is examined and the generated annual revenue is used to conduct a profitability analysis on the investment using the NPV and the payback period methods introduced in Section 6. This analysis examines the value of the investment over the entire investment holding period of 10 years. In the profitability analysis it is assumed that the 2023 conditions remain the same throughout the entire investment holding period. A more detailed profitability analysis would have required precise market analysis and accurate forecasting of electricity prices which is beyond the scope of this thesis.

9.2 Data and sources

The data used in this model is obtained through the Fingrid open data platform (Fingrid 2024b). To model the BESS operation in the FFR market, the hourly FFR price data for the year 2023 was used, as it represents the most recent FFR price data for a full year. To model the BESS operation in the FCR-N market, Fingrid's real-time frequency data with a three-minute resolution was used. Since the model uses one hour time resolution, the frequency data and thus the information about the required regulation energy must be also modified to one hour time resolution. This is done by calculating the hourly average up- or downregulation energy needed from the BESS, which corresponds to the bid capacity of 5 MW. First the average frequency deviation is calculated every hour using the three-minute frequency

measurements. The frequency deviation from the nominal system frequency of 50 Hz can be calculated using (44) (Fingrid 2023c):

$$\Delta f = f_n - f_{i_1}, \tag{44}$$

where Δf is the frequency deviation from the nominal system frequency, f_n is the nominal system frequency and f_{i_1} is the frequency measurement. After calculating the frequency deviation for every three-minute interval, the hourly average deviation can be obtained. The cumulative required up- or downregulation energy can be calculated using the average hourly frequency deviation using (45) (Fingrid 2023c, p. 12):

$$P_t^{reg} = \frac{P_t^{FCR} \cdot \Delta f_t^{avg} \cdot 1h}{0.1\ Hz}, \tag{45}$$

where P_t^{reg} is the required up- or downregulation energy from the BESS at hour t, Δf_t^{avg} is the hourly average frequency deviation in Hz, 0.1 Hz is the maximum frequency deviation at which the total prequalified FCR-N reserves must be activated in Finland. The variable P_t^{FCR} represents the BESS maximum power capacity for FCR-N, which is the bid capacity of 5 MW. In the data, negative required energy P_t^{reg} represents the required downregulation or charging energy from the BESS during hour *t* and positive P_t^{reg} represents the required upregulation or discharging energy.

The real-time frequency data contained some inconsistencies, which have been modified. The dataset contained two separate time periods of 10 and 11 hours, during which all the individual three-minute frequency measurements were identical. Since these time periods were relatively short compared to the entire simulation period, these measurements were left unmodified. The data also included a 26-hour period, during which individual frequency measurements were taken with a one-minute resolution instead of three-minute resolution. These measurement points were adjusted to match the three-minute resolution by calculating their three-minute averages.

Fingrid's open data platform was also used to obtain the hourly FCR-N market prices and the up- and downregulation prices in the balancing market (Fingrid 2024b). These prices were utilized to calculate the hourly capacity revenue and energy payments from charging and discharging, respectively. The battery parameters and other constant values used in this simulation are depicted in Table 11.

Table 11: Data for reserve market simulation.

Symbol	Value	Symbol	Value
λ^{output} (€/MWh)	0.92	$SOC^{bid,max}$ (MWh)	12
λ^{input} (€/MWh)	0.61	$SOC^{bid,min}$ (MWh)	8
c^{deg} (€/MWh)	8.08	SOC_0 (MWh)	10
OM^s (€/MWh)	0.913	η^c	0.92
P^{FFR} (MW)	10	η^d	0.92
SOC^{max} (MWh)	18	E^s (MWh)	20
SOC^{min} (MWh)	4	P_FCRU (MW)	5

In the investment calculations a discount factor of 5 % and the investment holding period of 10 years are used. The CAPEX for a 20 MW / 20 MWh battery are estimated to be 500 €/kWh. The CAPEX was estimated using Figure 29.

9.3 Optimization problem formulation

The goal of the model is to maximize the hourly profit from the FCR-N and FFR markets. This is done in the objective function (46). In (46) the variables $R_t^{FCR,CU}$ and $R_t^{FCR,CD}$ represent the hourly cash flow from the capacity payments for both up- and downregulation in the FCR-N market. $R_t^{FCR,E}$ represents the hourly energy payments. If the owner decides to bid to the FCR-N market even though the battery SOC level is not between the desired limits of $SOC^{bid,min}$ and $SOC^{bid,max}$, a penalty S_t^{FCR} is enforced. A penalty is used to encourage the battery owner to keep the SOC level as close to 50 % of the overall battery capacity as possible, which is a requirement for batteries providing FCR-N (ENTSO-E 2023, p. 38). The hourly battery degradation costs and OPEX have been calculated using coefficients c^{deg} and OM^s and the hourly energy transferred between the battery and the grid. The hourly capacity payment from the FFR market is calculated using the bidding capacity P^{FFR} and the hourly FFR price λ_t^{FFR}. The last two terms represent the fees for the energy transferred through the connection point by the BESS. λ^{output} is 0.92 €/MWh and λ^{input} is 0.61 €/MWh (Fingrid 2024j). The simulation period T is 8760 hours.

$$\max\left\{\sum_{t=1}^{T}\left[R_t^{FCR,CU}+R_t^{FCR,CD}+R_t^{FCR,E}-S_t^{FCR}-c^{deg}\cdot\left(-P_t^{down}+P_t^{up}\right)-OM^s\cdot\left(-P_t^{down}+P_t^{up}\right)+P^{FFR}\cdot\lambda_t^{FFR}+\lambda^{output}\cdot P_t^{down}-\lambda^{input}\cdot P_t^{up}\right]\right\} \quad (46)$$

$$v1_t = 1;\ \forall t, P_t^{reg} < 0 \tag{47}$$
$$v2_t = 1;\ \forall t, P_t^{reg} \geq 0 \tag{48}$$
$$v1_t + v2_t \leq 1; \forall t \tag{49}$$
$$P_t^{reg} \leq P_t^{down};\ \forall t, P_t^{reg} < 0 \tag{50}$$
$$P_t^{reg} \geq P_t^{up};\ \forall t, P_t^{reg} \geq 0 \tag{51}$$
$$P_t^{FCR} \leq P\_FCRU;\ \forall t \tag{52}$$
$$P_t^{down} \geq -P_t^{FCR} \cdot r2_t;\ \forall t, P_t^{reg} < 0 \tag{53}$$
$$P_t^{up} \leq P_t^{FCR} \cdot r1_t;\ \forall t, P_t^{reg} \geq 0 \tag{54}$$
$$r2_t + r1_t \leq 1;\ \forall t \tag{55}$$
$$SOC^{bid,min} - (1 - u1_t) \cdot SOC^{min} \leq SOC_t \leq SOC^{bid,max} + (1 - u1_t) \cdot 0.30 \cdot E^s;\ \forall t \tag{56}$$

$$SOC_t \leq SOC^{max} - u2_t \cdot 0.50 \cdot E^s;\ \forall t \tag{57}$$
$$SOC_t \geq SOC^{min} + u3_t \cdot SOC^{bid,min};\ \forall t \tag{58}$$
$$u1_t + u2_t + u3_t = 1;\ \forall t \tag{59}$$
$$\begin{cases} SOC_t = SOC_0 + \left(-P_t^{down} \cdot \eta^c - \dfrac{P_t^{up}}{\eta^d}\right);\ \forall t = 1 \\ SOC_t = SOC_{t-1} + \left(-P_t^{down} \cdot \eta^c - \dfrac{P_t^{up}}{\eta^d}\right);\ \forall t \backslash t = 1 \end{cases} \tag{60}$$
$$S_t^{FCR} = \lambda_t^+ \cdot u2_t \cdot \left(SOC^{bid,min} - SOC_t\right) + \lambda_t^+ \cdot u3_t \cdot (SOC_t - SOC^{bid,max});\ \forall t \tag{61}$$
$$R_t^{FCR,E} = \lambda_t^- \cdot P_t^{up} + \lambda_t^+ \cdot P_t^{down};\ \forall t \tag{62}$$
$$\left(P_t^{up} + M1 \cdot z_t\right) \cdot v2_t \geq P_t^{reg};\ \forall t, P_t^{reg} \geq 0 \tag{63}$$
$$P_t^{up} \cdot v2_t \leq P_t^{reg} + M2 \cdot (1 - z_t);\ \forall t, P_t^{reg} \geq 0 \tag{64}$$

$$R_t^{FCR,CU} = v2_t \cdot \left\{\lambda_t^{FCR} \cdot P_t^{FCR} \cdot (1 - z_t) + z_t \cdot \left[\lambda_t^{FCR} \cdot P_t^{up} - 3 \cdot \lambda_t^{FCR} \cdot P_t^{FCR}\right]\right\};\ \forall t \tag{65}$$

$$\left(P_t^{down} - M1 \cdot x_t\right) \cdot v1_t \leq P_t^{reg};\ \forall t, P_t^{reg} < 0 \tag{66}$$
$$P_t^{down} \cdot v1_t \geq P_t^{reg} - M2 \cdot (1 - x_t);\ \forall t, P_t^{reg} < 0 \tag{67}$$

$$R_t^{FCR,CD} = v1_t \cdot \left\{\lambda_t^{FCR} \cdot P_t^{FCR} \cdot (1 - x_t) + x_t \cdot \left[\lambda_t^{FCR} \cdot \left(-P_t^{down}\right) - 3 \cdot \lambda_t^{FCR} \cdot P_t^{FCR}\right]\right\};\ \forall t \tag{68}$$

Equations (47) and (48) define two binary variables $v1_t$ and $v2_t$ depending on if the operation hour is a down- or upregulation hour. These equations use conditional statements to check the direction of the required regulation power from the datafile. (49) ensures that up- and downregulation cannot occur simultaneously. (50) and (51) ensure that the provided up- or

downregulation power from the BESS does not exceed the required regulation power from the market, as the BESS cannot provide more regulation than what is needed. (52) sets the maximum hourly bid capacity in the FCR-N market which is 5 MW. The BESS owner can decide how much FCR-N provision to offer to the market at each hour. Equations (53) and (54) ensure that the provided regulation power at each hour does not exceed the maximum bid capacity of 5 MW and (55) ensures that the BESS cannot provide both up- and downregulation simultaneously by using two binary variables $r1_t$ and $r2_t$.

The desired battery SOC range when bidding for the FCR-N market has been defined in (57)– (59). The binary variables $u1_t$, $u2_t$ and $u3_t$ are used to define the battery SOC level in respect to the desired bidding range between $SOC^{bid,min}$ and $SOC^{bid,max}$. Variable E^s represents the energy capacity of the battery. If the owner bids to the FCR-N market even though the battery SOC level is either higher than 60 % or lower than 40 % of the overall capacity, a penalty S_t^{FCR} must be paid. S_t^{FCR} is calculated in (61) by comparing how much higher or lower the battery SOC level is compared to the maximum or minimum bidding SOC levels. This ensures that a larger deviation from the bidding SOC range incurs higher penalties for the owner.

In (60) the hourly SOC level SOC_t is calculated in two different ways based on which operation hour it is in. During the first operation hour, SOC_t is calculated based on the initial SOC level which has been set to 50 % of the overall capacity. After that SOC_t is calculated based on the SOC level of the previous hour. Charging the battery increases the SOC level, whereas discharging decreases it. Energy is lost during the charge and discharge cycles, which is represented by the efficiencies η^c and η^d. In the base datafile downregulation power is calculated as negative and upregulation power as positive, which is why both are set as negative when calculating the hourly energy transfer between the battery and the grid.

The generated cash flow from the energy transfer in the FCR-N market between the battery and the grid is calculated in (62). The generated cash flow can be either positive or negative depending on if the operation hour was an up- or downregulation hour. If the battery provides upregulation, the owner receives a payment for the discharged energy. If the battery provides downregulation, the owner must pay for the charged energy. The variables λ_t^- and λ_t^+ represent the up- and downregulation prices in the balancing energy market.

Equations (63)-(68) define the capacity fee for the owner providing the reserve capacity for that particular hour. Equations (63)-(65) define the

capacity fee for upregulation hours and (66)-(68) are used to calculate the capacity for downregulation hours. The binary variables $v1_t$ and $v2_t$ are used to control which set of equations to use based on the needed regulation. If the particular hour is an upregulation hour, (48) is activated, $v2_t$ is equal to one and $v1_t$ is zero. As $v1_t$ is zero, (68) is also zero and (66) and (67) are deactivated using the conditional statements. (63)-(65) are used to calculate the capacity fee. If the hour is a downregulation hour, (47) is active, $v1_t$ is equal to one and $v2_t$ is zero. (63) and (64) are deactivated using the conditional statements and (65) is zero. The capacity fee is then calculated using (66)-(68).

If the hour is an upregulation hour, (63)-(65) are active. The amount of reserve power that is needed from the battery is P_t^{reg} and the Big M method using binary variable z_t is used to define if the battery has provided the required regulation. If the battery has provided the required regulation, the variable P_t^{up} is equal to P_t^{reg} and the binary variable z_t is equal to zero. (64) is thus relaxed and (63) becomes the binding constraint. The capacity fee is calculated using the first term of (65), as the latter part of the equation is zero. If the battery is not able to provide the full required reserve capacity, z_t is one, (63) is relaxed and (64) becomes the binding constraint. The capacity payment is calculated using the latter term of (65) and the owner is paid for the provided capacity but sanctioned for the reserve that was left unprovided. The imposed sanction is three times the full capacity fee. Bidding to the FCR-N with an inadequate battery capacity can lead to significant negative cash flow from the capacity fee if the battery cannot provide the promised reserve power.

When an hour is a downregulation hour and $v1_t$ is one, (66)-(68) are active and P_t^{down} is the provided downregulation energy from the battery during that hour. The Big M method using binary variable x_t is used to check if the battery has provided the required downregulation. If the battery has provided the required regulation, x_t is equal to zero, (67) is relaxed and (66) becomes the binding constraint. The capacity fee is calculated using the first term of (68), as the latter part is zero due to x_t. If, the battery has not provided the entire required reserve capacity, x_t is equal to one, (66) is relaxed and (67) is the binding constraint. The capacity payment is calculated using the latter term of (68). The owner is paid for the capacity that was provided for that hour, but sanctioned for the reserve capacity left unprovided. Since the model is deterministic and the owner can decide how much BESS capacity to bid to the FCR-N market at each hour, the owner can also decide not to bid if the hourly conditions are unfavourable, leading to a non-optimal solution.

In this model, there are several nonlinear terms which need to be linearized in order to ease the solving process and find a global optimal solution via a linear-based solver such as CPLEX instead of using the LINDO solver. Equations (53), (54), (61), (63), (64), (65), (66), (67) and (68) contain bilinear terms due to the products of continuous and binary variables. (53) and (54) are linearized using the equations (18)-(21) presented in Section 7.2 and (61) and (63)-(68) have been linearized using equations (22)-(26). Equations (63), (65), (66) and (68) also contain products of two binary variables, which can be linearized using equations (27)-(30).

9.4 Simulation results of a standalone BESS operation in the FCR-N and FFR markets

The simulation was carried out in GAMS using the CPLEX solver. Due to the complexity and duration of the solving process, the results with a relative gap of 2.45 % were used. The relative gap represents the tolerance between the objective of the best node and the best integer objective (IBM 2022). The results from the annual operation of a standalone BESS in the Finnish FCR-N and FFR markets in 2023 are given in Table 12.

Table 12: Results from the annual operation of the BESS in the FCR-N and FFR markets.

Total annual revenue	2 413 135.0 €
NPV	8 633 588.8 €
Payback period (years)	< 5
Annual FCR-N market capacity revenue	1 921 120.0 €
Annual FCR-N market energy revenue	83 691.6 €
Annual FFR market revenue	393 868.2 €
Annual FEC count	280
Average SOC level	10.2 MWh

The results in Table 12 indicate that the simultaneous BESS operation in the FCR-N and FFR markets is profitable. The BESS generated an annual revenue of 2.4 M€ and assuming the same operating conditions for the next ten years, leading to an NPV of 8.6 M€ and a payback period of under 5 years. Approximately 80 % of the annual revenue came from the capacity payments in the FCR-N market, which are paid hourly to the reserve provider for the provided reserve capacity. The revenue from energy transmission was relatively small at 83 700 €, which is primarily because charging the battery

incurs costs for the reserve provider. When assessing the long-term profitability of a BESS in the reserve markets, it is crucial to analyze the development of FCR-N market prices, which dictate the amount of revenue obtained from the capacity fees.

The FFR market accounted for about 16 % of the total annual revenue. The revenue generated from the FFR market indicates that it is not profitable for the BESS to participate solely in this market. This is due to the market's smaller volume, which is also evident in Figure 17. However, the lower energy transmission volumes make it an attractive marketplace for BESSs when combined with other reserve markets. Figure 55 depicts the provided hourly up- and downregulation from the BESS throughout the entire year.

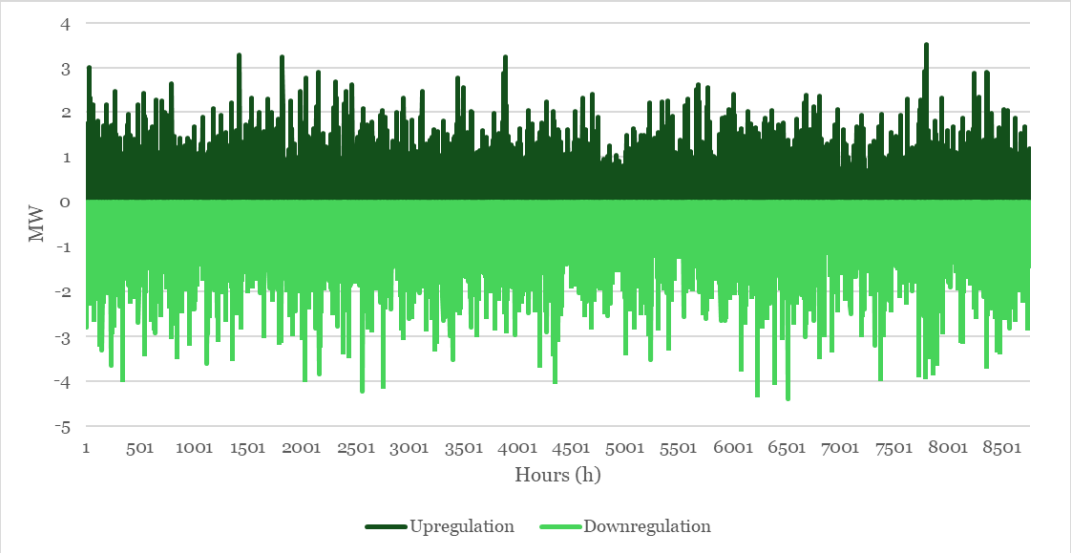

Figure 55: The hourly up- and downregulation from the BESS during the simulation period.

Figure 55 indicates that the BESS was active in the FCR-N market throughout the entire year. Despite the activity, the FEC count was only 280, which would mean around 2800 cycles over a ten-year period. Compared to the maximum cycle numbers for LFP batteries presented in literature, the battery could be used for a longer time and potentially be utilized in other markets as well, assuming that similar operating conditions prevail. Figure 56 depicts the battery SOC level throughout the simulation period.

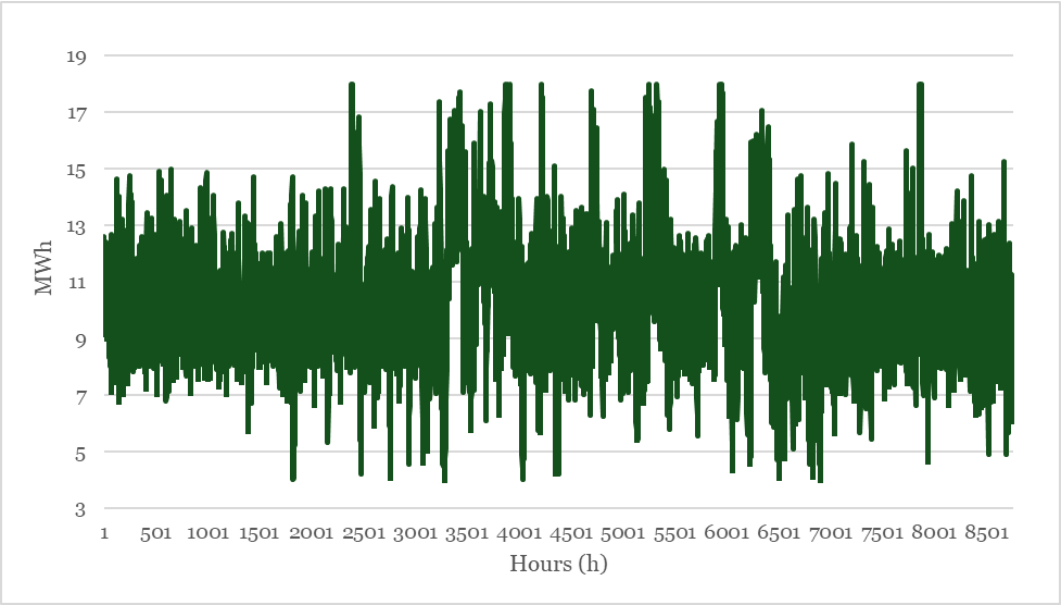

Figure 56: Battery SOC level throughout the simulation period.

The battery charge held between the desired bidding SOC limit of 8-12 MWh 69.4 % of the hours during the entire year. It reached the maximum SOC level of 18 MWh 26 times and the minimum SOC level of 4 MWh two times during the entire simulation period. Thus, the bidding penalty was successful in enforcing the battery owner to only bid to the FCR-N with an adequate capacity to curb the bidding sanctions. In the problem formulation the bidding sanction S_t^{FCR} was calculated using the downregulation prices in the balancing market. When the prices were negative, the battery owner was actually encouraged to bid to the market with a SOC level outside the desired bidding range.

9.5 Sensitivity analysis

The profitability of the BESS in the FCR-N and FFR markets is further investigated by performing a sensitivity analysis on three different parameters of BESS CAPEX, generated annual revenue and the discount rate. In the analysis each parameter is varied individually while keeping the others unchanged, with the lowest value being 50 % less than the initial value and the highest value being 50 % greater than the initial value. The parameters are changed in 10 % steps. Similar to previous sections, the total annual revenue in 2023 is used to calculate the NPV of the investment using a holding period of 10 years. It is also assumed that similar conditions to 2023 prevail for the entire holding period. Figure 57 depicts the results of the sensitivity analysis.

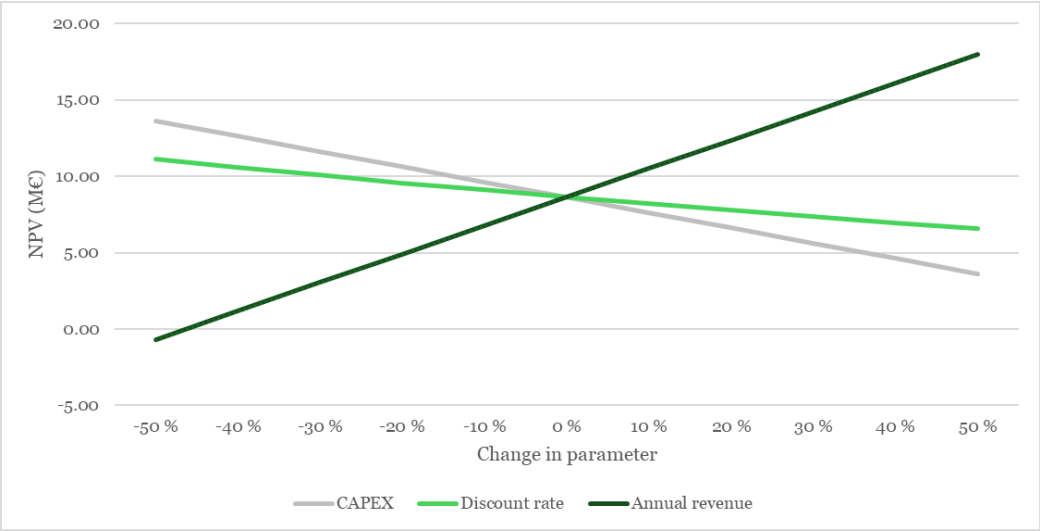

Figure 57: The effect of BESS CAPEX, discount rate and the annually generated revenue on the NPV of the BESS investment.

Figure 57 indicates that changes in the annually generated revenues affect the NPV outlook of the investment more than BESS CAPEX and the discount rate. The discount rate had the smallest impact on the investment's NPV, as the NPV changed by 4.6 M€, when the discount rate was changed from the highest to the lowest value. This same change in NPV was 10 M€, when the BESS CAPEX was varied. Varying the annual revenue from the lowest value to the highest resulted in a change of 18.6 M€ in the investment NPV.

Changes in the interest rate environment or the BESS CAPEX in the future do not significantly increase or decrease the overall profitability of the investment. However, the variation of annually generated revenues in the future can significantly transform an initially profitable investment into an unprofitable one and also an unprofitable one to be profitable. The majority of the annual revenue in 2023 came from the capacity payments in the FCR-N market. Since annually generated revenue affect the long-term profitability of the investment significantly, even small changes in reserve market prices can greatly affect the profitability outlook in different years. This result supports the findings in Section 9.4, where it was concluded that the development of FCR-N market prices play an important role in assessing the profitability of BESS investments. When analyzing the development of Finnish reserve markets, the possible market saturation and the resulting decline in market prices and how they affect the long-term profitability of the investment must be considered.

10 Conclusions and proposed further research

Reducing emissions from energy production is imperative to mitigate climate change and achieve carbon neutrality by 2050. A significant share of the overall renewable energy is produced by wind power. The poor predictability and instability of wind power production cause issues in the power system, which must balance energy generation and demand at all times. Additionally, inverter-coupled power plants do not inherently produce physical inertia in the system further increasing the need for faster reserve capacity. These problems can be addressed by utilizing battery energy storage systems (BESSs).

In this thesis the utilization of a BESS in wind power balance error management and in Finnish reserve markets was researched. The utilization of the BESS in wind power balance error management was analyzed using a MILP model. The operation of a standalone BESS in the Finnish reserve markets was researched using a MINLP model, which was recast into a MILP model to simplify the solving process. In this case the BESS owner bids simultaneously in the FCR-N and FFR markets and the operation is optimized by maximizing the overall annual profit. The long-term profitability of the investments in both cases was analyzed using the annual revenue from 2023.

The results indicate that a BESS is able to decrease the wind power balance error and the imbalance costs for the WFO. However, the low annually generated revenue combined with high CAPEX do not support the investment solely for wind power balance error management, with a payback period of over 20 years. The low profitability of the BESS is primarily due to its high OPEX and degradation costs, which makes it unprofitable to charge and discharge the battery unless it can significantly reduce the wind power plant's imbalance costs. Additionally, the potential revenues generated by the overproduction of the wind power plant limit the usage of the battery, as charging the battery decreases the positive balance error.

The results also show that the simultaneous operation of a standalone BESS in the FCR-N and FFR markets is profitable. The annual operation in 2023 generated 2.4 M€ in revenue leading to an NPV of 8.6 M€ over ten years. 80 % of the annual revenue for the BESS owner consisted of capacity payments from the FCR-N market, while the revenue from the energy transfer remained small. The FFR market represented 16 % of the total annual revenue. Since the capacity payments in the FCR-N represent majority of the total revenue, further analysis of the development of the FCR-N market is needed to fully evaluate the long-term profitability of BESSs in this market. The lower revenue obtained from the FFR market indicates that the market volume is not large enough to make the operation of the BESS profitable solely in this

market. However, the low energy transfer makes the market an attractive alternative for BESSs when combined with other reserve markets.

For the BESS wind power balance error management model, a further research opportunity is to model the BESS operation simultaneously in wind power balance error management and in other electricity markets such as the Intraday (ID) market. By utilizing the ID market, the WFO could more effectively decrease the imbalance costs by charging the BESS independently in the ID market without reducing the revenue from the wind power plant's overproduction. This would also enable the WFO to possibly sell the energy from the BESS in the ID market during longer overproduction periods from the wind power plant.

The MINLP model formulated in this thesis, representing the standalone operation of a BESS in the FCR-N and FFR markets, was successful in simulating the potential revenue streams for a BESS in the Finnish reserve markets. However, there are several ways to improve the model even further, for example by considering the Normal State Energy Management (NEM) and Alert State Energy Management (AEM) states for more detailed BESS charge management in the FCR-N market. A more precise modelling of battery charge management could give more accurate information on how the State of Charge (SOC) affects the battery operation.

This thesis focused on the FCR-N and FFR markets and further research could explore other markets such as FCR-D, aFRR, mFRR, DA and ID markets as possible operating areas for BESSs. Additionally, further investigation is needed on how the transition to the 15-minute imbalance settlement period could impact the battery operation in these different markets. These other markets can become more attractive for BESSs with shorter balancing resolution. Lastly, formulating a non-deterministic version of the model would give insight into the operation of a standalone BESS under electricity price uncertainty. This would give more accurate information on obtainable potential revenues and long-term profitability of the BESS investment. This could also enable the use of artificial intelligence to predict different market prices in advance and direct the battery operation to the most profitable markets.

References

Abdelghafar, I., Refaie, A.G., Kerikous, E., Thévenin, D., Hoerner, S. 2023. Optimum geometry of seashell-shaped wind turbine rotor: Maximizing output power and minimizing thrust. Energy Conversion and Management, 292, 117331. https://doi.org/10.1016/j.enconman.2023.117331

Abdelhady, S., Borello, D., Shaban, A. 2017. Assessment of levelized cost of electricity of offshore wind energy in Egypt. Wind Engineering, 41, 0309524X1770684. https://doi.org/10.1177/0309524X17706846

Abdi, H., Mohammadi-ivatloo, B., Javadi, S., Khodaei, A.R., Dehnavi, E. 2017. Chapter 7 - Energy Storage Systems, in: Gharehpetian, G.B. & Mousavi Agah, S.M. (Eds.), Distributed Generation Systems. Butterworth-Heinemann, 580 . https://doi.org/10.1016/B978-0-12-804208-3.00007-8

AES Indiana. 2022. 2022 Integrated Resource Plan. Volume 1. [Accessed 29.1.2024]. Available at: https://www.aesindiana.com/integrated-resource-plan

Ahlawat, A. & Das, D. 2023. Optimal sizing and scheduling of battery energy storage system with solar and wind DG under seasonal load variations considering uncertainties. Journal of Energy Storage, 74, 109377. https://doi.org/10.1016/j.est.2023.109377

Akpinar, K.N., Gundogdu, B., Ozgonenel, O. 2023. A novel cycle counting perspective for energy management of grid integrated battery energy storage systems. Energy Reports, 2022 9th International Conference on Power and Energy Systems Engineering 9, Kyoto, Japan, 9-11.9.2022, p. 123–131. https://doi.org/10.1016/j.egyr.2022.10.359

Al-Ani, M.K. 2015. A Strategic Framework to Use Payback Period in Evaluating the Capital Budgeting in Energy and Oil and Gas Sectors in Oman. International Journal of Economics and Financial Issues, 5(2), p. 469-475. ISSN: 2146-4138.

Albadi, M.H., El-Saadany, E.F. 2010. Overview of wind power intermittency impacts on power systems. Electric Power Systems Research, 80, p. 627–632. https://doi.org/10.1016/j.epsr.2009.10.035

Alcaide-Godinez, I., Bai, F., Saha, T.K., Castellanos, R. 2022. Contingency reserve estimation of fast frequency response for battery energy storage system. International Journal of Electrical Power & Energy Systems, 143, 108428. https://doi.org/10.1016/j.ijepes.2022.108428

Alizadeh, M. 2017. Multi-objective optimisation of community battery energy storage capacity exploitation. Master's thesis, Electrical Engineering, Lappeenranta University of Technology. Available at: https://urn.fi/URN:NBN:fi-fe2017121255754

Allamehzadeh, H. 2016. Wind energy history, technology and control. Presented at the 2016 IEEE Conference on Technologies for Sustainability (SusTech), p. 119–126. https://doi.org/10.1109/SusTech.2016.7897153

Alzubaidi, M., Hasan, K.N., Meegahapola, L. 2022. Identification of the Impact of Wind Speed and Load Uncertainties on Short-term Voltage Stability. 2022 IEEE PES 14th Asia-Pacific Power and Energy Engineering Conference (APPEEC), Melbourne, Australia, 20-23.11.2022, p. 1–7. https://doi.org/10.1109/APPEEC53445.2022.10072118

Arnold, T. 2014. How Net Present Value Is Implemented, in: Arnold, T. (Ed.) A Pragmatic Guide to Real Options. Palgrave Macmillan US, New York. https://doi.org/10.1057/9781137391162_1

Asealen. 2023. Technical and economic study of two energy storage technologies in Spain. [Accessed 29.1.2024]. Available at: https://www.asealen.es/wp-content/uploads/2023/02/20230217-Conclusions-Technical-and-economic-study-of-two-energy-storage-technologies-in-Spain_G-advisory-Simulyde.pdf

Aziz, A., Than Oo, A., Stojcevski, A. 2018. Frequency regulation capabilities in wind power plant. Sustainable Energy Technologies and Assessments, 26, p. 47–76. https://doi.org/10.1016/j.seta.2017.10.002

Belegundu, A. & Chandrupatla, T. 2011. Optimization concepts and applications in engineering. 2nd (ed). New York: Cambridge University Press. ISBN: 9780521878463.

Benzohra, O., Echcharqaouy, S.S., Fraija, F., Saifaoui, D. 2020. Integrating wind energy into the power grid: Impact and solutions. Materials Today: Proceedings, International Conference on Renewable Energy and Applications (ICREA 19), 30, p. 987–992. https://doi.org/10.1016/j.matpr.2020.04.363

Bera, A., Almasabi, S., Tian, Y., Byrne, R.H., Chalamala, B., Nguyen, T.A., Mitra, J. 2020. Maximising the investment returns of a grid-connected battery considering degradation cost. IET Generation, Transmission & Distribution, 14, p. 4711–4718. https://doi.org/10.1049/iet-gtd.2020.0403

Bin Abu Sofian, A.D.A., Imaduddin, I.S., Majid, S.R., Kurniawan, T.A., Chew, K.W., Lay, C.-H., Show, P.L. 2024. Nickel-rich nickel–cobalt–manganese and nickel–cobalt–aluminum cathodes in lithium-ion batteries: Pathways for performance optimization. Journal of Cleaner Production, 435, 140324. https://doi.org/10.1016/j.jclepro.2023.140324

BloombergNEF. 2023a. Lithium-ion Battery Pack Prices Hit Record Low of $139/kWh. [Accessed 29.1.2024]. Available at: https://about.bnef.com/blog/lithium-ion-battery-pack-prices-hit-record-low-of-139-kwh/

BloombergNEF. 2023b. Top 10 Energy Storage Trends in 2023. [Accessed 29.1.2024]. Available at: https://about.bnef.com/blog/top-10-energy-storage-trends-in-2023/

Bresser, D., Paillard, E., Passerini, S. 2015. Lithium-Ion Batteries (LIBs) for Medium- and Large-Scale Energy Storage: Current Cell Materials and Components. In: Menictas, C., Skyllas-Kazacos, M., Lim, T. M. (Eds.) Advances in batteries for medium- and large-scale energy storage, 607. ISBN: 9781782420132

Camuñas García-Miguel, P.L., Alonso-Martinez, J., Arnaltes Gómez, S., Rodríguez-Amenedo, J.L. 2024. Impact of risk measures and degradation cost on the optimal arbitrage schedule for battery energy storage systems. International Journal of Electrical Power & Energy Systems, 157, 109883. https://doi.org/10.1016/j.ijepes.2024.109883

Choi, D., Shamim, N., Crawford, A., Huang, Q., Vartanian, C.K., Viswanathan, V.V., Paiss, M.D., Alam, M.J.E., Reed, D.M., Sprenkle, V.L. 2021. Li-ion battery technology for grid application. Journal of Power Sources, 511, 230419. https://doi.org/10.1016/j.jpowsour.2021.230419

Chreim, B., Esseghir, M., Merghem-Boulahia, L. 2024. Recent sizing, placement, and management techniques for individual and shared battery energy storage systems in residential areas: A review. Energy Reports, 11, p. 250–260. https://doi.org/10.1016/j.egyr.2023.11.053

Cision. 2023. Sisäpiiritieto: Merus Powerille 20 miljoonan euron tilaus suuren sähkövaraston toimittamisesta Taaleri Energialle. [Finnish]. Merus Power. [Accessed 29.1.2024]. Available at: https://news.cision.com/fi/merus-power-oyj/r/sisapiiritieto--merus-powerille-20-miljoonan-euron-tilaus-suuren-sahkovaraston-toimittamisesta-taale,c3710997

Collath, N., Tepe, B., Englberger, S., Jossen, A., Hesse, H. 2022. Aging aware operation of lithium-ion battery energy storage systems: A review. Journal of Energy Storage, 55, 105634. https://doi.org/10.1016/j.est.2022.105634

da Silva Lima, L., Wu, J., Cadena, E., Groombridge, A.S., Dewulf, J. 2023. Towards environmentally sustainable battery anode materials: Life cycle assessment of mixed niobium oxide (XNO™) and lithium-titanium-oxide (LTO). Sustainable Materials and Technologies, 37, e00654. https://doi.org/10.1016/j.susmat.2023.e00654

Das, C.K., Bass, O., Kothapalli, G., Mahmoud, T.S., Habibi, D. 2018. Overview of energy storage systems in distribution networks: Placement, sizing, operation, and power quality. Renewable and Sustainable Energy Reviews, 91, p. 1205–1230. https://doi.org/10.1016/j.rser.2018.03.068

Davis, N.N., Byrkjedal, Ø., Hahmann, A.N., Clausen, N.-E., Žagar, M. 2016. Ice detection on wind turbines using the observed power curve. Wind Energy, 19, p. 999–1010. https://doi.org/10.1002/we.1878

De Lellis, M., Reginatto, R., Saraiva, R., Trofino, A. 2018. The Betz limit applied to Airborne Wind Energy. Renewable Energy, 127, p. 32–40. https://doi.org/10.1016/j.renene.2018.04.034

Díaz-González, F., Sumper, A., Gomis-Bellmunt, O., Villafáfila-Robles, R., 2012. A review of energy storage technologies for wind power applications. Renewable and Sustainable Energy Reviews, 16, p. 2154–2171. https://doi.org/10.1016/j.rser.2012.01.029

Dui, X., Zhu, G., Yao, L. 2017. Two-Stage Optimization of Battery Energy Storage Capacity to Decrease Wind Power Curtailment in Grid-Connected Wind Farms. IEEE Transactions on Power Systems, 33, p. 3296–3305. https://doi.org/10.1109/TPWRS.2017.2779134

Elkington, K. 2012. The Dynamic Impact of Large Wind Farms on Power System Stability. Doctoral Thesis, KTH School of Electrical Engineering. Available at: https://www.diva-portal.org/smash/get/diva2:516618/FULLTEXT01.pdf&sa=U&ei=PLRqU-79IaWK0AXM-oHAAw&ved=0CBsQFjAA&usg=AFQjCNGj5kwypvDhLQ4qKsAIXncB7IH6Ig

Electricity Market Act 386/1995. Issued 01.06.1995. Available at: https://www.finlex.fi/en/laki/kaannokset/1995/en19950386

Elovaara, J. & Haarla, L. 2011. Sähköverkot 1 – Järjestelmätekniikka ja sähköverkon laskenta. [Finnish]. Otatieto. ISBN 978-951-672-360-3

Empower. 2018. Enabling a Smooth Transition to 15 Minute Balance Settlement. [Accessed 21.1.2024]. Available at: https://energiavirasto.fi/documents/11120570/13026619/Final+Report+-+15+Minute+Balance+Settlement,+Delivered+version.pdf/b9d7ae4d-a0e0-ca4d-4d8e-748d382d5436/Final+Report+-+15+Minute+Balance+Settlement,+Delivered+version.pdf?t=1556278429000

ENTEC. 2023. Study on Energy Storage. European Commission. Available at: https://op.europa.eu/en/publication-detail/-/publication/a6eba083-932e-11ea-aac4-01aa75ed71a1

ENTSO-E. 2019. Fast Frequency Reserve – Solution to the Nordic inertia challenge. [Accessed 16.1.2024]. Available at: https://www.fingrid.fi/globalassets/dokumentit/en/electricity-market/reserves/fast-frequency-reserve-solution-to-the-nordic-inertia-challenge.pdf

ENTSO-E. 2021. Technical Requirements for Frequency Containment Reserve Provision in the Nordic Synchronous Area. [Accessed 11.1.2024]. Available at: https://www.fingrid.fi/globalassets/dokumentit/fi/sahkomarkkinat/reservit/fcr-technical-requirements-for-pilot-phase-v0.91.pdf

ENTSO-E. 2023. Technical Requirements for Frequency Containment Reserve Provision in the Nordic Synchronous Area. [Accessed 11.1.2024]. Available at: https://www.fingrid.fi/globalassets/dokumentit/fi/sahkomarkkinat/reservit/appendix-2-the-technical-requirements-and-the-prequalification-process-of-frequency-containment-reserves-fcr.pdf

eSett. 2023. Commissioning Plan – 15 min Imbalance Settlement Period. 2nd Ed. [Accessed 21.1.2024]. Available at: https://www.esett.com/app/uploads/2023/09/15_min_Commissioning_Plan.pdf

eSett. 2024. Nordic Imbalance Settlement Handbook – Instructions and Rules for Market Participants. [Accessed 5.1.2024]. Available at: https://www.esett.com/handbook/

Fallah, N. & Fitzpatrick, C. 2024. Exploring the state of health of electric vehicle batteries at end of use; hierarchical waste flow analysis to determine the recycling and reuse potential. Journal of Remanufacturing, 14, p. 155–168. https://doi.org/10.1007/s13243-024-00137-4

Fallahifar, R. & Kalantar, M. 2023. Optimal planning of lithium ion battery energy storage for microgrid applications: Considering capacity degradation. Journal of Energy Storage, 57, 106103. https://doi.org/10.1016/j.est.2022.106103

Fingrid. 2019. The technical requirements and the prequalification process of Automatic Frequency Restoration Reserve (aFRR). [Accessed 21.1.2024]. Available at: https://www.fingrid.fi/globalassets/dokumentit/en/electricity-market/reserves/automaattisen-taajuudenhallintareservin-afrr-teknisten-vaatimusten-todentaminen-ja-hyvaksyttamispr_en.pdf

Fingrid. 2023a. Electricity system vision 2023. [Accessed 20.12.2023]. Available at: https://www.fingrid.fi/en/grid/development/electricity-system-vision-2023/

Fingrid. 2023b. Reserve products and reserve market places. [Accessed 9.1.2024]. Available at: https://www.fingrid.fi/globalassets/dokumentit/en/electricity-market/reserves/reserve-products-and-reserve-market-places.pdf

Fingrid. 2023c. Terms and conditions for providers of Frequency Containment Reserves (FCR). [Accessed 11.1.2024]. Available at: https://www.fingrid.fi/globalassets/dokumentit/fi/sahkomarkkinat/reservit/terms-and-conditions-for-providers-of-frequency-containment-reserves-fcr-as-of-22-may-2023.pdf

Fingrid. 2023d. The technical requirements and the prequalification process of Fast Frequency Reserve (FFR). [Accessed 16.1.2024]. Available at: https://www.fingrid.fi/globalassets/dokumentit/fi/sahkomarkkinat/reservit/the-technical-requirements-and-the-prequalification-process-of-fast-frequency-reserve-ffr-as-of-22-may-2023.pdf

Fingrid. 2023e. Terms and conditions for providers of Fast Frequency Reserves (FFR). [Accessed 16.1.2024]. Available at: https://www.fingrid.fi/globalassets/dokumentit/fi/sahkomarkkinat/reservit/terms-and-conditions-for-providers-of-fast-frequency-reserves-ffr-as-of-22-may-2023.pdf

Fingrid. 2023f. Terms and conditions for providers of manual Frequency Restoration Reserves (mFRR). [Accessed 16.1.2024]. Available at: https://www.fingrid.fi/globalassets/dokumentit/fi/sahkomarkkinat/saatosahko/liite-1-mfrr-ehdot-4-2022-hyvaksytyt-ehdot-en.pdf

Fingrid. 2023g. Terms and conditions for providers of automatic Frequency Restoration Reserves (aFRR). [Accessed 21.1.2024]. Available at: https://www.fingrid.fi/globalassets/dokumentit/en/electricity-market/reserves/afrr-ehdot-toukokuu2023-muutospyynnon-mukainen_en.pdf

Fingrid. 2023h. Varttitaseen käyttöönotto 22.5.2023. [Finnish]. [Accessed 21.1.2024]. Available at: https://www.fingrid.fi/globalassets/dokumentit/fi/sahkomarkkinat/varttitase/varttitaseen-kayttoonotto-suomessa-22.5.2023--paivitetty-17.3.2023.pdf

Fingrid. 2024a. Reserves and balancing power. [Accessed 3.1.2024]. Available at: https://www.fingrid.fi/en/electricity-market/reserves_and_balancing/#reserve-products

Fingrid. 2024b. Open data. [Accessed 11.1.2024]. Available at: https://data.fingrid.fi/en/

Fingrid. 2024c. Description of balance model. [Accessed 5.1.2024]. Available at: https://www.fingrid.fi/en/electricity-market/balance-service/description-of-balance-model/

Fingrid. 2024d. Balancing energy and balancing capacity markets (mFRR). [Accessed 7.1.2024]. Available at: https://www.fingrid.fi/en/electricity-market/reserves_and_balancing/balancing-energy-and-balancing-capacity-markets/#balancing-energy-bids

Fingrid. 2024e. Markkinapaikat. [Finnish]. [Accessed 8.1.2024]. Available at: https://www.fingrid.fi/sahkomarkkinat/markkinoiden-yhtenaisyys/johdanto-sahkomarkkinoihin/

Fingrid. 2024f. Frequency containment reserves (FCR products). [Accessed 11.1.2024]. Available at: https://www.fingrid.fi/en/electricity-market/reserves_and_balancing/frequency-containment-reserves/#procurement

Fingrid. 2024g. Fast Frequency Reserve (FFR). [Accessed 16.1.2024]. Available at: https://www.fingrid.fi/en/electricity-market/reserves_and_balancing/fast-frequency-reserve/#technical-requirements

Fingrid. 2024h. Automatic frequency restoration reserve (aFRR). [Accessed 21.1.2024]. Available at: https://www.fingrid.fi/en/electricity-market/reserves_and_balancing/automatic-frequency-restoration-reserve/

Fingrid. 2024i. Fees. [Accessed 18.3.2024]. Available at: https://www.fingrid.fi/en/electricity-market/balance-service/fees/

Fingrid. 2024j. Kantaverkkosopimus ja kantaverkkopalvelumaksut. [Finnish]. [Accessed 19.3.2024]. Available at: https://www.fingrid.fi/kantaverkko/liitynta-kantaverkkoon/kantaverkkosopimus-ja--palvelumaksut/#kantaverkkopalvelumaksut

Finnish Energy. 2023. Energy Year 2022 – Electricity. Available at: https://energia.fi/en/statistics/energy-year-2022-electricity/

Finnish Wind Power Association. 2023a. Tuulivoimatekniikka. [Finnish]. [Accessed 21.12.2023]. Available at: https://tuulivoimayhdistys.fi/tietoa-tuulivoimasta-2/tietoa-tuulivoimasta/tuulivoimatekniikka/tuulivoimatekniikka-2

Finnish Wind Power Association. 2023b. Tuulivoimatilastot 2022. [Accessed 20.12.2023]. Available at: https://tuulivoimayhdistys.fi/ajankohtaista/tilastot-2/tuulivoimatilastot-2022

Finnish Wind Power Association. 2023c. Wind power projects in Finland 05/2023. [Accessed 3.1.2023]. Available at: https://tuulivoimayhdistys.fi/en/wind-power-in-finland/projects-under-planning

Frade, P.M.S., Pereira, J.P., Santana, J.J.E., Catalão, J.P.S. 2019. Wind balancing costs in a power system with high wind penetration – Evidence from Portugal. Energy Policy, 132, p. 702–713. https://doi.org/10.1016/j.enpol.2019.06.006

Gailani, A., Al-Greer, M., Short, M., Crosbie, T. 2020. Degradation Cost Analysis of Li-Ion Batteries in the Capacity Market with Different Degradation Models. Electronics, 9, 90. https://doi.org/10.3390/electronics9010090

GAMS. 2023. System overview. [Accessed 4.3.2024]. Available at: https://www.gams.com/products/gams/gams-language/

García-Miguel, P.L.C., Alonso-Martínez, J., Arnaltes Gómez, S., García Plaza, M., Asensio, A.P. 2022. A Review on the Degradation Implementation for the Operation of Battery Energy Storage Systems. Batteries, 8, 110. https://doi.org/10.3390/batteries8090110

Glavic, M. & Greene, S. 2022. Voltage stability in future power systems. In: Garcia, J. (Ed.) Encyclopedia of Electrical and Electronic Power Engineering, p. 209-223. https://doi.org/10.1016/B978-0-12-821204-2.00141-0

Global Wind Energy Council. 2023. Global Wind Report 2023. [Accessed 15.4.2024]. Available at: https://gwec.net/globalwindreport2023/

Gundogdu, B. & Gladwin, D.T. 2018. A Fast Battery Cycle Counting Method for Grid-Tied Battery Energy Storage System Subjected to Microcycles, 2018 International Electrical Engineering Congress (iEECON), Krabi, Thailand, 7-9.5.2019, p. 1–4. https://doi.org/10.1109/IEECON.2018.8712263

Hameed, Z., Træholt, C., Hashemi, S. 2023. Investigating the participation of battery energy storage systems in the Nordic ancillary services markets from a business perspective. Journal of Energy Storage, 58, 106464. https://doi.org/10.1016/j.est.2022.106464

Hannan, M.A., Wali, S.B., Ker, P.J., Rahman, M.S.A., Mansor, M., Ramachandaramurthy, V.K., Muttaqi, K.M., Mahlia, T.M.I., Dong, Z.Y. 2021. Battery energy-storage system: A review of technologies, optimization objectives, constraints, approaches, and outstanding issues. Journal of Energy Storage, 42, 103023. https://doi.org/10.1016/j.est.2021.103023

He, G., Chen, Q., Kang, C., Xia, Q., Poolla, K. 2016. Cooperation of Wind Power and Battery Storage to Provide Frequency Regulation in Power Markets. IEEE Transactions on Power Systems, 32, p. 3559–3568. https://doi.org/10.1109/TPWRS.2016.2644642

Hesse, H.C., Schimpe, M., Kucevic, D., Jossen, A. 2017. Lithium-Ion Battery Storage for the Grid—A Review of Stationary Battery Storage System Design Tailored for Applications in Modern Power Grids. Energies, 10, 2107. https://doi.org/10.3390/en10122107

Hodge, B.-M., Brancucci Martinez-Anido, C., Wang, Q., Chartan, E., Florita, A., Kiviluoma, J. 2018. The combined value of wind and solar power forecasting improvements and electricity storage. Applied Energy, 214, p. 1–15. https://doi.org/10.1016/j.apenergy.2017.12.120

Holttinen, H., Miettinen, J., Sillanpää, S. 2013. Wind power forecasting accuracy and uncertainty in Finland. VTT Technology 95. Available at: https://publications.vtt.fi/pdf/technology/2013/T95.pdf

Hu, X., Jaraitė, J., Kažukauskas, A. 2021. The effects of wind power on electricity markets: A case study of the Swedish intraday market. Energy Economics, 96, 105159. https://doi.org/10.1016/j.eneco.2021.105159

Huang, J., Tong, J., Wang, P., Zheng, X. 2022. Application and Comparison of NPV and IRR Methods in the Company Investment Decision. The 2022

7th International Conference on Financial Innovation and Economic Development (ICFIED 2022), Atlantis Press, p. 71–78. https://doi.org/10.2991/aebmr.k.220307.012

IBM. 2022. Relative MIP gap tolerance. [Accessed 20.6.2024]. Available at: https://www.ibm.com/docs/en/icos/22.1.1?topic=parameters-relative-mip-gap-tolerance

IEA. 2017. Getting Wind and Sun onto the Grid. Available at: https://www.iea.org/reports/getting-wind-and-solar-onto-the-grid

IEA. 2023a. World Energy Outlook 2023. [Accessed 29.1.2024]. Available at: https://www.iea.org/reports/world-energy-outlook-2023

IEA. 2023b. Wind. [Accessed 15.4.2024]. Available at: https://www.iea.org/energy-system/renewables/wind

Ikäheimo, S., Malmi, T., Walden, R. 2019. Yrityksen laskentatoimi. [Finnish]. 8. Helsinki: Alma Talent Oy.

Ilmatar. 2023. Ilmatar builds its second hybrid solution: An energy storage facility at the Piiparinmäki wind farm. [Accessed 25.1.2024]. Available at: https://ilmatar.fi/en/ilmatar-builds-its-second-hybrid-solution-an-energy-storage-facility-at-the-piiparinmaki-wind-farm/

IRENA. 2017. Electricity storage and renewables: Costs and markets to 2030. International Renewable Energy Agency. Abu Dhabi. Available at: https://www.irena.org/-/media/Files/IRENA/Agency/Publication/2017/Oct/IRENA_Electricity_Storage_Costs_2017.pdf?rev=a264707cb8034a52b6f6123d5f1b1148

Johnson, A., Escobar, A., Balda, J.C., Barnes, A.K. 2012. Wind farm layout for mitigating output power intermittency. 2012 3rd IEEE International Symposium on Power Electronics for Distributed Generation Systems (PEDG), Aalborg, Denmark, 25-28.6.2012, p. 883–889. https://doi.org/10.1109/PEDG.2012.6254105

Jyrinsalo, J. 2023. Tulevaisuuden investointitarpeet. Fingrid. [Finnish]. [Accessed 20.12.2023]. Available at: https://www.fingrid.fi/globalassets/dokumentit/fi/yhtio/toimikunnat/neuvottelukunta/tulevaisuuden-investointitarpeet_neuvottelukunta.pdf

Jääskeläinen, J., Huhta, K., Syri, S. 2022. The Anatomy of Unaffordable Electricity in Northern Europe in 2021. Energies, 15, 7504. https://doi.org/10.3390/en15207504

Kambanou, M.L. & Lindahl, M. 2016. A Literature Review of Life Cycle Costing in the Product-Service System Context. Procedia CIRP, Product-Service Systems across Life Cycle, 47, p. 186–191. https://doi.org/10.1016/j.procir.2016.03.054

Kauniskangas, M. 2009. What you should know about the electricity market. Finnish Energy Industries and Fingrid Oyj. Available at: https://www.fingrid.fi/globalassets/dokumentit/en/publications/uusin_versio_sahkomark_en.pdf

Kebede, A.A., Kalogiannis, T., Van Mierlo, J., Berecibar, M. 2022. A comprehensive review of stationary energy storage devices for large scale renewable energy sources grid integration. Renewable and Sustainable Energy Reviews, 159, 112213. https://doi.org/10.1016/j.rser.2022.112213

Khajeh, H., Parthasarathy, C., Doroudchi, E., Laaksonen, H. 2023. Optimized siting and sizing of distribution-network-connected battery energy storage system providing flexibility services for system operators. Energy, 285, 129490. https://doi.org/10.1016/j.energy.2023.129490

Khojasteh, M., Faria, P., Vale, Z. 2022. A robust model for aggregated bidding of energy storages and wind resources in the joint energy and reserve markets. Energy, 238, 121735. https://doi.org/10.1016/j.energy.2021.121735

Kim, S.H. & Shin, Y.-J. 2023. Optimize the operating range for improving the cycle life of battery energy storage systems under uncertainty by managing the depth of discharge. Journal of Energy Storage, 73, 109144. https://doi.org/10.1016/j.est.2023.109144

Klyve, Ø.S., Klæboe, G., Nygård, M.M., Marstein, E.S. 2023. Limiting imbalance settlement costs from variable renewable energy sources in the Nordics: Internal balancing vs. balancing market participation. Applied Energy, 350, 121696. https://doi.org/10.1016/j.apenergy.2023.121696

Koniak, M. & Czerepicki, A. 2017. Selection of the battery pack parameters for an electric vehicle based on performance requirements. IOP Conference Series: Materials Science and Engineering, International Conference on Aerospace, Mechanical and Mechatronic Engineering, Bangkok, Thailand, 21-23.4.2017, 211, 012005. https://doi.org/10.1088/1757-899X/211/1/012005

Kordkheili, Ramin Ahmadi, Pourakbari-Kasmaei, M., Lehtonen, M., Kordkheili, Reza Ahmadi, Pouresmaeil, E. 2021. Multi-Alternative Operation-Planning Problem of Wind Farms Participating in Gas and Electricity Markets, IEEE Access, 9, p. 166. https://doi.org/10.1109/ACCESS.2021.3135702

Korhonen, J-P. 2022. Teollisen kokoluokan aurinkovoimalan ja akkuvaraston kannattavuus ja hyödyntäminen sähkömarkkinoilla. Master's thesis, Electrical Engineering, Lappeenranta University of Technology. Available at: https://urn.fi/URN:NBN:fi-fe2022102062629

Krause, L.J., Jensen, L.D., Chevrier, V.L. 2017. Measurement of Li-Ion Battery Electrolyte Stability by Electrochemical Calorimetry. J. Electrochemical Society, 164, A889. https://doi.org/10.1149/2.1651704jes

Krismanto, A., Sulistiawati, I., Limpraptono, Y., Priyadi, A., Setiadi, H., Abdillah, M. 2021. Impact of Large-Scale Wind Power Penetration on Dynamic Voltage Stability of Interconnected Power System: An Indonesia Case Study. International Journal of Intelligent Engineering and Systems, 14. https://doi.org/10.22266/ijies2021.0831.23

Kurzweil, P. 2015. Lithium Battery Energy Storage: State of the Art Including Lithium-Air and Lithium-Sulfur Systems. In: Moseley, P. & Garche, J. (Eds.) Electrochemical Energy Storage for Renewable Sources and Grid Balancing. Elsevier, Oxford, Netherlands, 493. ISBN : 9780444626103

Lam, D.H.C., Lim, Y.S., Wong, J., Sapihie, S.N.M. 2023. Life-cycle assessment of batteries for peak demand reduction. Journal of Electronic Science and Technology, 21, 100226. https://doi.org/10.1016/j.jnlest.2023.100226

Lavoie, Y., Danet, F., Lombard, B. 2017. Lithium-ion batteries for industrial applications. 2017 Petroleum and Chemical Industry Technical Conference (PCIC), Calgary, Canada, 18-20.9.2017, p. 283–290. https://doi.org/10.1109/PCICON.2017.8188747

Lazard. 2023. LCOE+. [Accessed 30.1.2024]. Available at: https://www.lazard.com/research-insights/levelized-cost-of-energyplus/

Li, J., Wang, C., Wang, H. 2023a. Deep reinforcement learning for wind and energy storage coordination in wholesale energy and ancillary service markets. Energy and AI, 14, 100280. https://doi.org/10.1016/j.egyai.2023.100280

Li, S., Xu, Q., Huang, J. 2023b. Research on the integrated application of battery energy storage systems in grid peak and frequency regulation. Journal of Energy Storage, 59, 106459. https://doi.org/10.1016/j.est.2022.106459

Li, Y. & Chengxin, L. 2018. Overview of Maximum Power Point Tracking Control Method for Wind Power Generation System. IOP Conference Series: Materials Science and Engineering, 428, 012007. https://doi.org/10.1088/1757-899X/428/1/012007

Lim, S., Kim, T., Yoon, K., Choi, D., Park, J.-W. 2022. A Study on Frequency Stability and Primary Frequency Response of the Korean Electric Power System Considering the High Penetration of Wind Power. Energies, 15, 1784. https://doi.org/10.3390/en15051784

Lindo Systems Inc. 2024. Solver Suite – our introductory bundle for Mathematical Optimization. [Accessed 24.6.2024]. Available at: https://www.lindo.com/index.php/products/solver-suite

Londero, R.R., de Mattos Affonso, C., Vieira, J.P.A. 2014. Long-Term Voltage Stability Analysis of Variable Speed Wind Generators. IEEE Transactions on Power Systems, 30, p. 439–447. https://doi.org/10.1109/TPWRS.2014.2322258

Lundgren, J. 2012. Market Liberization and Market Integration. Doctoral thesis, Department of Economics, Umeå School of Business and Economics. Available at: https://www.diva-portal.org/smash/get/diva2:570731/FULLTEXT01.pdf

Ma, D. & Qin, X. 2022. Residual Life Prediction of Lithium Batteries Based on Data Mining. Computational Intelligence and Neuroscience 2022, e4520160. https://doi.org/10.1155/2022/4520160

Ma, Z., Jia, M., Koltermann, L., Blömeke, A., De Doncker, R.W., Li, W., Sauer, D.U. 2023. Review on grid-tied modular battery energy storage systems: Configuration classifications, control advances, and performance evaluations. Journal of Energy Storage, 74, 109272. https://doi.org/10.1016/j.est.2023.109272

Mahesh, M., Bhaskar, D.V., Jisha, R.K., Krishan, R., Gnanadass, R. 2022. Lifetime estimation of grid connected LiFePO4 battery energy storage systems. Electrical Engineering, 104, p. 67–81. https://doi.org/10.1007/s00202-021-01371-w

Marzewski, S. 2023. Periodic Review of Default Gross CONE and Gross ACR Values. [Accessed 29.1.2024]. Available at: https://www.pjm.com/-/media/committees-groups/committees/mic/2022/20221006/item-13a---periodic-review-of-default-cone-and-acr-values.ashx

Mathew, S. & Philip, G.S. 2012. 2.05 - Wind Turbines: Evolution, Basic Principles, and Classifications, in: Sayigh, A. (Ed.), Comprehensive Renewable Energy. Elsevier, Oxford, p. 93–111. https://doi.org/10.1016/B978-0-08-087872-0.00205-5

Miao, Y., Hynan, P., von Jouanne, A., Yokochi, A. 2019. Current Li-Ion Battery Technologies in Electric Vehicles and Opportunities for Advancements. Energies, 12, 1074. https://doi.org/10.3390/en12061074

Milligan, M., Porter, K., DeMeo, E., Denholm, P., Holttinen, H., Kirby, B., Miller, N., Mills, A., O'Malley, M., Schuerger, M., Soder, L. 2009. Wind power myths debunked. IEEE Power and Energy Magazine, 7, p. 89–99. https://doi.org/10.1109/MPE.2009.934268

Mitali, J., Dhinakaran, S., Mohamad, A.A. 2022. Energy storage systems: a review. Energy Storage and Saving, 1, p. 166–216. https://doi.org/10.1016/j.enss.2022.07.002

Moghaddam, I.N., Chowdhury, B., Doostan, M. 2018. Optimal Sizing and Operation of Battery Energy Storage Systems Connected to Wind Farms Participating in Electricity Markets. IEEE Transactions on Sustainable Energy, 10, p. 1184–1193. https://doi.org/10.1109/TSTE.2018.2863272

Mohamed, A., Rigo-Mariani, R., Debusschere, V., Pin, L. 2023. Stacked revenues for energy storage participating in energy and reserve markets with an optimal frequency regulation modeling. Applied Energy, 350, 121721. https://doi.org/10.1016/j.apenergy.2023.121721

Naemi, M., Davis, D., Brear, M.J. 2022. Optimisation and analysis of battery storage integrated into a wind power plant participating in a wholesale electricity market with energy and ancillary services. Journal of Cleaner Production, 373, 133909. https://doi.org/10.1016/j.jclepro.2022.133909

Nemeth, T., Schröer, P., Kuipers, M., Sauer, D.U. 2020. Lithium titanate oxide battery cells for high-power automotive applications – Electro-thermal properties, aging behavior and cost considerations. Journal of Energy Storage, 31, 101656. https://doi.org/10.1016/j.est.2020.101656

Neoen. 2020. Neoen builds in Finalnd the Nordic's largest battery storage unit. Media release. [Accessed 25.1.2024]. Available at: https://neoen.com/app/uploads/2020/06/20200609-neoen-media-release-ypr.pdf

Newell, S., Hagerty, J.M., Pfeifenberger, J., Zhou, B., Carless, T., Janakiraman, R., Gang, S., Daou, J., Junge, J. 2022. PJM Cone 2026/2027 Report. PJM Interconnection. Available at: https://www.brattle.com/insights-events/publications/pjm-cone-2026-27-report/

Nord Pool. 2023a. Price calculation. [Accessed 9.1.2024]. Available at: https://www.nordpoolgroup.com/en/trading/Day-ahead-trading/Price-calculation/

Nord Pool. 2023b. Nord Pool Announces 2022 Trading Figures. [Accessed 9.1.2024]. Available at: https://www.nordpoolgroup.com/en/message-center-container/newsroom/exchange-message-list/2023/q1/nord-pool-announces-2022-trading-figures/

Nord Pool. 2024a. Day-ahead prices. [Accessed 7.1.2024]. Available at: https://www.nordpoolgroup.com/en/Market-data1/Dayahead/Area-Prices/ALL1/Hourly/?view=table

Nord Pool. 2024b. Day-ahead market. [Accessed 9.1.2024]. Available at: https://www.nordpoolgroup.com/en/the-power-market/Day-ahead-market/

Nord Pool. 2024c. Intraday trading. [Accessed 9.1.2024]. Available at: https://www.nordpoolgroup.com/en/trading/intraday-trading/

Nouriani, A. & Moradi, H. 2020. Smooth switching in power control of wind turbines using a combination strategy of hysteresis and modified middle regions. Sustainable Energy Technologies and Assessments, 37, 100585. https://doi.org/10.1016/j.seta.2019.100585

NREL. 2023. Utility-Scale Battery Storage. National Renewable Energy Laboratory. [Accessed 29.1.2024]. Available at: https://atb.nrel.gov/electricity/2023/utility-scale_battery_storage

Paasolainen, V. 2023. Sähkövaraston hyödyntäminen tuuli- ja aurinkovoimapuistossa. [Finnish]. Master's thesis, Electrical Engineering, Lappeenranta University of Technology. Available at: https://urn.fi/URN:NBN:fi-fe2023062157422

Paul, S., Nath, A.P., Rather, Z.H. 2019. A Multi-Objective Planning Framework for Coordinated Generation From Offshore Wind Farm and Battery Energy Storage System. IEEE Transactions on Sustainable Energy, 11, p. 2087–2097. https://doi.org/10.1109/TSTE.2019.2950310

Power Technology. 2021. Whitelee Wind Farms – Battery Energy Storage System, UK. [Accessed 25.1.2024]. Available at: https://www.power-technology.com/marketdata/whitelee-wind-farm-battery-energy-storage-system-uk/

Pusceddu, E., Zakeri, B., Castagneto Gissey, G. 2021. Synergies between energy arbitrage and fast frequency response for battery energy storage systems. Applied Energy, 283, 116274. https://doi.org/10.1016/j.apenergy.2020.116274

Ramasamy, V., Zuboy, J., Woodhause, M., O'Shaughnessy, E., Feldman, E., Desai, J., Walker, A., Margolis, R., Basore, P. 2023. U.S. Solar Photovoltaic System and Energy Storage Cost Benchmarks, With Minimum Sustainable Price Analysis: Q1 2023. Available. NREL. Available at: https://www.nrel.gov/docs/fy23osti/87303.pdf

Rao, S. 2020. Engineering optimization: theory and practice, 5th (ed). John Wiley & Sons, USA. ISBN: 1-5231-5497-7

Ren, G., Liu, J., Wan, J., Guo, Y., Yu, D. 2017. Overview of wind power intermittency: Impacts, measurements, and mitigation solutions. Applied Energy, 204, p. 47–65. https://doi.org/10.1016/j.apenergy.2017.06.098

Roberson, D., Ellison, J., Bhatnagar, D., Schoenwald, D. 2014. Performance Assessment of the PNM Prosperity Electricity Storage Project: A Study for the DOE Energy Storage Systems Program PNM Prosperity Electricity Storage Project Evaluation. SANDIA Report. Available at: https://www.sandia.gov/ess-ssl/publications/SAND2014-2883.pdf

Rouhi, H., Karola, E., Serna-Guerrero, R., Santasalo-Aarnio, A. 2021. Voltage behavior in lithium-ion batteries after electrochemical discharge and its implications on the safety of recycling processes. Journal of Energy Storage, 35, 102323. https://doi.org/10.1016/j.est.2021.102323

Ruegg, R.T. & Marshall, H.E. 1990. Internal Rate-of-Return (IRR), in: Ruegg, R.T. & Marshall, H.E. (Eds.), Building Economics: Theory and Practice. Springer US, Boston, MA, p. 232. https://doi.org/10.1007/978-1-4757-4688-4_5

Rystad Energy. 2023. Five key parameters of BESS capex. Whitepaper. [Accessed 29.1.2024]. Available at: https://www.rystadenergy.com/insights/five-key-parameters-of-bess-capex

Sandia National Laboratories. 2023. Statistics. DOE Global Energy Database. [Accessed 23.1.2024]. Available at: https://sandia.gov/ess-ssl/gesdb/public/statistics.html

Sarasketa-Zabala, E., Gandiaga, I., Martinez-Laserna, E., Rodriguez-Martinez, L.M., Villarreal, I. 2015. Cycle ageing analysis of a LiFePO4/graphite cell with dynamic model validations: Towards realistic lifetime predictions. Journal of Power Sources, 275, p. 573–587. https://doi.org/10.1016/j.jpowsour.2014.10.153

Sarkar, M., Altin, M., Hansen, A., Sørensen, P. 2017. Impact of Wind Power Plants on Voltage Control of Power System. Available at: https://backend.orbit.dtu.dk/ws/portalfiles/portal/137265691/10C_3_GIZ17_088_paper_Moumita_Sarkar.pdf

Sauer, D.U., Fuchs, G., Lunz, B., Leuthold, M. 2012. Technology Overview on Electricity Storage - Overview on the potential and on the deployment perspectives of electricity storage technologies. https://doi.org/10.13140/RG.2.1.5191.5925

Sayfutdinov, T., Patsios, C., Vorobev, P., Gryazina, E., Greenwood, D.M., Bialek, J.W., Taylor, P.C. 2020. Degradation and Operation-Aware Framework for the Optimal Siting, Sizing, and Technology Selection of Battery Storage. IEEE Transactions on Sustainable Energy, 11, p. 2130–2140. https://doi.org/10.1109/TSTE.2019.2950723

Sekine. 2024. Energy Storage: 10 Things to Watch in 2024. BloombergNEF. [Accessed 29.1.2024]. Available at: https://about.bnef.com/blog/energy-storage-10-things-to-watch-in-2024/

Setiawan, A., Arifin, Z., Jufri, F.H., Sudiarto, B., Garniwa, I., Setiabudy, R. 2023. Economic analysis of cost-based load shifting implementation on large utility systems using battery energy storage system. International Journal of Sustainable Energy, 42, p. 1182–1201. https://doi.org/10.1080/14786451.2023.2248503

Shair, J., Li, H., Hu, J., Xie, X. 2021. Power system stability issues, classifications and research prospects in the context of high-penetration of renewables and power electronics. Renewable and Sustainable Energy Reviews, 145, 111111. https://doi.org/10.1016/j.rser.2021.111111

Sioshansi, R. & Conejo, A.J. 2017. Optimization in Engineering, Springer Optimization and Its Applications. Springer International Publishing, Springer Cham, 412. https://doi.org/10.1007/978-3-319-56769-3

Soysal, E.R., Olsen, O.J., Skytte, K., Sekamane, J.K. 2017. Intraday market asymmetries — A Nordic example. 2017 14th International Conference on the European Energy Market (EEM), Dresden, Germany, 6-9.6.2017, p. 1–6. https://doi.org/10.1109/EEM.2017.7981920

Spodniak, P., Ollikka, K., Honkapuro, S. 2019. The Relevance of Wholesale Electricity Market Places: The Nordic Case. VATT Workinh Papers 126. Available at: https://urn.fi/URN:ISBN:978-952-274-245-2

Statnett. 2022. Fast Frequency Reserves. [Accessed 14.1.2024]. Available at: https://www.statnett.no/globalassets/for-aktorer-i-kraftsystemet/marked/reservemarkeder/ffr/ffr_brochure_2022.pdf

Statnett. 2024. Data from the power system. [Accessed 9.1.2024]. Available at: https://www.statnett.no/en/for-stakeholders-in-the-power-industry/data-from-the-power-system/

Stecca, M., Elizondo, L.R., Soeiro, T.B., Bauer, P., Palensky, P. 2020. A Comprehensive Review of the Integration of Battery Energy Storage Systems Into Distribution Networks. IEEE Open Journal of the Industrial Electronics Society, 1, p. 46–65. https://doi.org/10.1109/OJIES.2020.2981832

Stenberg, A., & Holttinen, H. 2011. Tuulivoiman tuotantotilastot: Vuosiraportti 2010. [Finnish]. VTT Technical Research Centre of Finland. VTT Working Papers No. 178 https://publications.vtt.fi/pdf/workingpapers/2011/W178.pdf

Stroe, D.-I., Knap, V., Swierczynski, M., Stroe, A.-I., Teodorescu, R. 2017. Operation of a Grid-Connected Lithium-Ion Battery Energy Storage System for Primary Frequency Regulation: A Battery Lifetime Perspective. IEEE Transactions on Industry Applications, 53, p. 430–438. https://doi.org/10.1109/TIA.2016.2616319

Su, W., Xu, K., Zhong, G., Wei, Z., Wang, C., Meng, Y. 2017. Enhanced Electrochemical Performance of LiFePO4 as Cathode for Lithium Ion Battery by Codoping with Titanium and Nitrogen. International Journal of Electrochemical Science, 12, p. 6930–6939. https://doi.org/10.20964/2017.08.13

Taaleri Oyj. 2023. Finland's larget wind power producer Taaleri expands its business to energy storage systems. Investor news. [Accessed 25.1.2024]. Available at: https://www.taaleri.com/en/news/finlands-largest-wind-power-producer-taaleri-expands-its-business-energy-storage-systems
Tsai, W.-C., Hong, C.-M., Tu, C.-S., Lin, W.-M., Chen, C.-H. 2023. A Review of Modern Wind Power Generation Forecasting Technologies. Sustainability, 15, 10757. https://doi.org/10.3390/su151410757

Turkia, V., Huttunen, S., Wallenius, T. 2013. Method for estimating wind turbine production losses due to icing. VTT Technology 114. Available at: https://www.vttresearch.com/sites/default/files/pdf/technology/2013/T114.pdf

Urquizo, J. & Singh, P. 2024. Partial cycling aging of Li-ion batteries in frequency regulation applications. Journal of Power Sources, 592, 233908. https://doi.org/10.1016/j.jpowsour.2023.233908

Viswanathan, V., Mongird, K., Franks, R., Li, X., Sprenkle, V., Baxter, R. 2022. 2022 Grid Energy Storage Technology Cost and Performance Assessment. U.S. Department of Energy. Available at: https://www.pnnl.gov/sites/default/files/media/file/ESGC%20Cost%20Performance%20Report%202022%20PNNL-33283.pdf

Wang, A., Kadam, S., Li, H., Shi, S., Qi, Y. 2018. Review on modeling of the anode solid electrolyte interphase (SEI) for lithium-ion batteries. npj Computational Materials, 4, p. 1–26. https://doi.org/10.1038/s41524-018-0064-0

Wang, B., Zhang, F., Zhou, X., Wang, P., Wang, J., Ding, H., Dong, H., Liang, W., Zhang, N., Li, S. 2021. Which of the nickel-rich NCM and NCA is structurally superior as a cathode material for lithium-ion batteries? Journal of Materials Chemistry A, 9, p. 13540–13551. https://doi.org/10.1039/D1TA01128F

WSP. 2020. Making Batteries Work. Thought Piece. [Accessed 29.1.2024]. Available at: https://www.wsp.com/en-au/sectors/battery-storage

Xiaoming, W., Yuguang, X., Bo, G., Yuanjie, Z., Fan, C. 2018. Analysis of Factors Affecting Wind Farm Output Power. 2018 2nd IEEE Conference on Energy Internet and Energy System Integration (EI2), Beijing, China, 20-22.10.2018, p. 1–5. https://doi.org/10.1109/EI2.2018.8582379

Yaldız, A., Gökçek, T., Şengör, İ., Erdinç, O. 2021. Optimal sizing and economic analysis of Photovoltaic distributed generation with Battery Energy Storage System considering peer-to-peer energy trading. Sustainable Energy, Grids and Networks, 28, 100540. https://doi.org/10.1016/j.segan.2021.100540

Yang, Z., Zhang, J., Kintner-Meyer, M.C.W., Lu, X., Choi, D., Lemmon, J.P., Liu, J. 2011. Electrochemical Energy Storage for Green Grid. Chemical Reviews, 111, p. 3577–3613. https://doi.org/10.1021/cr100290v

Appendix 1. The effect of CAPEX on the BESS investment profitability in wind power balance error management

NPV (M€)

Decrease in CAPEX compared to base simulation

BESS capacity / wind power plant rated power	100 %	90 %	80 %	70 %	60 %	50 %	40 %	30 %	20 %	10 %
100 %	-38.1	-33.6	-29.1	-24.6	-20.1	-15.6	-11.1	-6.6	-2.1	2.4
90 %	-33.9	-29.9	-25.8	-21.8	-17.7	-13.7	-9.6	-5.6	-1.5	2.5
80 %	-29.7	-26.1	-22.5	-18.9	-15.3	-11.7	-8.1	-4.5	-0.9	2.7
70 %	-25.9	-22.7	-19.6	-16.4	-13.2	-10.0	-6.8	-3.6	-0.4	2.7
60 %	-21.8	-19.1	-16.3	-13.6	-10.9	-8.1	-5.4	-2.7	0.1	2.8
50 %	-18.0	-15.7	-13.4	-11.1	-8.8	-6.5	-4.2	-1.9	0.4	2.7
40 %	-14.1	-12.3	-10.4	-8.5	-6.7	-4.8	-3.0	-1.1	0.8	2.6
30 %	-10.3	-8.9	-7.5	-6.1	-4.7	-3.3	-1.8	-0.4	1.0	2.4
20 %	-7.1	-6.1	-5.1	-4.1	-3.1	-2.1	-1.1	-0.1	0.9	1.9
10 %	-3.3	-2.8	-2.3	-1.8	-1.3	-0.8	-0.3	0.2	0.8	1.3

Appendix 2. The effect of annual revenue on the BESS investment profitability in wind power balance error management

NPV (M€)

Increase in annual revenue compared to the base simulation

BESS capacity / wind power plant rated power	90 %	80 %	70 %	60 %	50 %	40 %	30 %	20 %	10 %	0 %
100 %	-32.0	-32.7	-33.3	-34.0	-34.7	-35.4	-36.1	-36.8	-37.5	-38.1
90 %	-28.0	-28.6	-29.3	-30.0	-30.6	-31.3	-31.9	-32.6	-33.3	-33.9
80 %	-24.1	-24.7	-25.3	-26.0	-26.6	-27.2	-27.8	-28.5	-29.1	-29.7
70 %	-20.6	-21.2	-21.8	-22.4	-23.0	-23.6	-24.1	-24.7	-25.3	-25.9
60 %	-16.8	-17.4	-17.9	-18.5	-19.0	-19.6	-20.1	-20.7	-21.2	-21.8
50 %	-13.4	-13.9	-14.4	-14.9	-15.4	-15.9	-16.4	-16.9	-17.4	-18.0
40 %	-10.1	-10.5	-11.0	-11.4	-11.9	-12.3	-12.8	-13.2	-13.7	-14.1
30 %	-6.9	-7.3	-7.6	-8.0	-8.4	-8.8	-9.2	-9.5	-9.9	-10.3
20 %	-4.4	-4.7	-5.0	-5.3	-5.6	-5.9	-6.2	-6.5	-6.8	-7.1
10 %	-1.7	-1.9	-2.1	-2.3	-2.4	-2.6	-2.8	-3.0	-3.1	-3.3